1-1-2012

Intricate dynamics and hydrodynamic frictional losses of the piston-ring assembly in internal combustion engines

Mohannad Hakeem
Wayne State University,

INTRICATE DYNAMICS AND HYDRODYNAMIC FRICTIONAL LOSSES OF THE PISTON-RING ASSEMBLY IN INTERNAL COMBUSTION ENGINES

by

MOHANNAD ABDULLAH HAKEEM

DISSERTATION

Submitted to the Graduate School

of Wayne State University,

Detroit, Michigan

in partial fulfillment of the requirements

for the degree of

DOCTOR OF PHILOSOPHY

2011

MAJOR: MECHANICAL ENGINEERING

Approved by:

_____

Advisor Date

_____

_____

_____

_____

DEDICATION

In the Name of God, Most Gracious, Most Merciful…

To my Lord, I can't but thank you and praise you for all the blessings you bestowed upon me, with the greatest one being that of knowledge, as revealed in Your Holy Book (The Quran):

Read! In the Name of your Lord, Who has created (all that exists) [96-1]….

Has created man from a clot (a piece of thick coagulated blood) [96-2]…

Read! And your Lord is the Most Generous [96-3]…

Who has taught (the writing) by the pen [96-4]…

Has taught man that which he knew not [96-5]…

ACKNOWLEDGMENTS

"Give thanks to Me and to your parents, unto Me is the final destination" [Quran, 31:14].

After thanking and praising God, I would like to thank my parents, Dr. Abdullah Hakeem and Mrs. Mona Khatib, for their unconditional and unwavering support. I would like to also thank my advisor and mentor, Dr. Nabil Chalhoub, for all the support, knowledge, and patience he showed during the past years. His methodology shaped my personality as an engineer and as a researcher. I also want to recognize the selfless assistance of Dr. Naeim Henein, who was always a source of inspiration to me and to the team. I would like to extend my gratitude to the committee members, Dr. Walter Bryzik, Dr. Trilochan Singh, and Dr. Pete Schihl, for their valuable input and expert contribution. Special thanks and appreciation to my colleagues, Dr. Nassim Khaled and Mr. Tamer Badawi, for all of their help at different stages of my PhD work.

None of this work would have been possible without the moral and emotional support of my beloved wife, Mrs. Ghina Ghazzawi. She was always there, and stood by me through the easy and difficult times. In addition, I thank my brothers, Engineers Mohammad Said, Bahaa-Eddine, and Bilal Hakeem, for all their support and help throughout the years.

Last but not least, I want to acknowledge the financial and technical support of the Center for Automotive Research at Wayne State University and the Automotive Research Center (consortium of eight universities directed by the University of Michigan) sponsored by the National Automotive Center, located

within the US Army Tank-Automotive Research, Development, and Engineering Center (TARDEC), Warren, Michigan.

TABLE OF CONTENTS

LIST OF TABLES

LIST OF FIGURES

NOMENCLATURE

A	Area
m	Mass
g	Gravitational acceleration
ρ	Mass density
E	Modulus of elasticity
G	Shear modulus of elasticity
k	Shear factor
M	Mass matrix
$\underset{\sim}{Q}^{NC}$	Generalized forces of the non-conservative external forces
$\underset{\sim}{\lambda}$	Lagrange multiplier vector
P	Gas pressure
h	Oil film thickness
η	Oil dynamic viscosity
I	Mass moment of inertia
J	Area moment of inertia
R	Radius
$\underset{\sim}{\omega}$	Angular velocity vector
$\underset{\sim}{r}_j^b$	Position vector of object j at point b
Θ_n	Central angle defining an element on the n^{th} ring.
e	Coefficient of restitution.
$\underset{\sim}{I}, \underset{\sim}{J}, \underset{\sim}{K}$	Unit vectors corresponding to the inertial frame.

k_{cstr}	Stiffness of the local spring whose force is applied on one of the equally spaced seven points on the ring beam element.
$\underset{\sim}{n}$	Equal to $-\underset{\sim}{i}_7$ and $\underset{\sim}{i}_7$ for contact with the top and bottom surfaces of the piston groove, respectively.
T_{load}	Load torque.
t^-, t^+	Instant of time before and after the impact between the piston and the ring.
T_k^j	Transformation matrix defining the origin and orientation of the j^{th} frame with respect to the k^{th} frame.
$F^{imp}_{(P-L)}$	Impact force between the piston and the cylinder liner
$F^{imp}_{(P-R)_{n_j}}$	Impact force between the piston and the nth ring
$\theta_{cs}, \beta, \gamma$	Generalized coordinates describing the rigid body motion of the crankshaft, connecting rod, and the piston, respectively.
X_{r_n}, ϕ_n, ψ_n	Generalized coordinates describing the rigid body motion of ring *n*.
u_j, v_j, θ_j	Longitudinal, in-plane transverse deformation, and rotation of the cross section of the beam around the z_j-axis, respectively.

SUBSCRIPTS/SUPERSCRIPTS

cr	Connecting rod
p	Piston
r_n	Ring *n*, *n*=1-3
$cs^{(i)}$	Crank shaft element (*i*), *i*=1-5
fl	Flywheel
cw_1, cw_2	Counterweights 1 and 2
cg	Crank gear
ck	Crank case
cyl	Cylinder
CL	Center line of the cylinder
$P-L$	Piston-liner contact point
$R-L$	Ring-liner contact point
$P-R$	Piston-ring contact point
$cstr$	Constraint force
*	Center of gravity

CHAPTER 1

INTRODUCTION

The present study addresses the research issues and challenges associated with the intricate dynamics of the piston-assembly of high power density Diesel engines. It also provides a tool for determining its instantaneous hydrodynamic frictional losses during the entire engine cycle under various operating conditions.

The motivation and objectives of the current study are discussed in the next Section. A literature survey on the relevant work that has been reported in the open literature will be presented. Subsequently, an overview of the current work is provided.

1.1 Motivation and Objectives

The dynamic behavior of the piston-assembly has a direct effect on the performance of internal combustion (IC) engines. It is widely recognized that the piston-assembly is a major contributor to the frictional losses, which have a significant and adverse effect on the engine fuel efficiency. Figure 1-1 shows the distribution of expenditure in the fuel energy between the brake horsepower (BHP) and other power losses for a Diesel engine operating at part load (20%). This figure, generated based on data from Ref. [1], demonstrates that the total frictional losses account approximately for about 10% of the total fuel energy [1]. Moreover, forty percent of these losses are attributed to the reciprocating motion of the piston-ring assembly as shown in Fig. 1-2.

Furthermore, during an engine cycle, the piston-assembly may experience boundary, mixed, and hydrodynamic lubrication regimes. In boundary lubrication, the interaction between the rubbing surfaces is handled by metal-to-metal contact. In mixed lubrication, the interaction is handled by both metal-to-metal contact and the oil film between the rubbing surfaces. However, in a hydrodynamic lubrication regime, the surfaces will be completely separated by the oil film. It should be pointed out that the lubrication regimes involving metal-to-metal contact lead to wear, which ultimately affect the engine durability.

Moreover, the ring-pack acts as a dynamic seal preventing the cylinder gases from leaking into the crankcase and vice versa. This is done in order to improve the engine thermal efficiency by reducing the blow-by gases, which can occur through the ring end gaps, ring-groove dynamic clearance, and ring-bore dynamic conformability. The sealing capability of the rings is dictated by their intricate dynamics and the pressure differentials between the control volumes that are defined in the clearances between the rings, piston grooves, and the liner. Furthermore, the elasticity of the rings strongly influences the ring-liner conformability, which can worsen the blowby problem. Moreover, the interaction between the rings and the gas flows can cause the rings to flutter in the axial direction and/or collapse in the radial direction, which can create more opening through which gases can leak into the crankcase [2, 3].

Furthermore, the ring-pack serves to control the oil film along the cylinder liner. Forty to eighty percent of the engine oil consumption has been attributed to

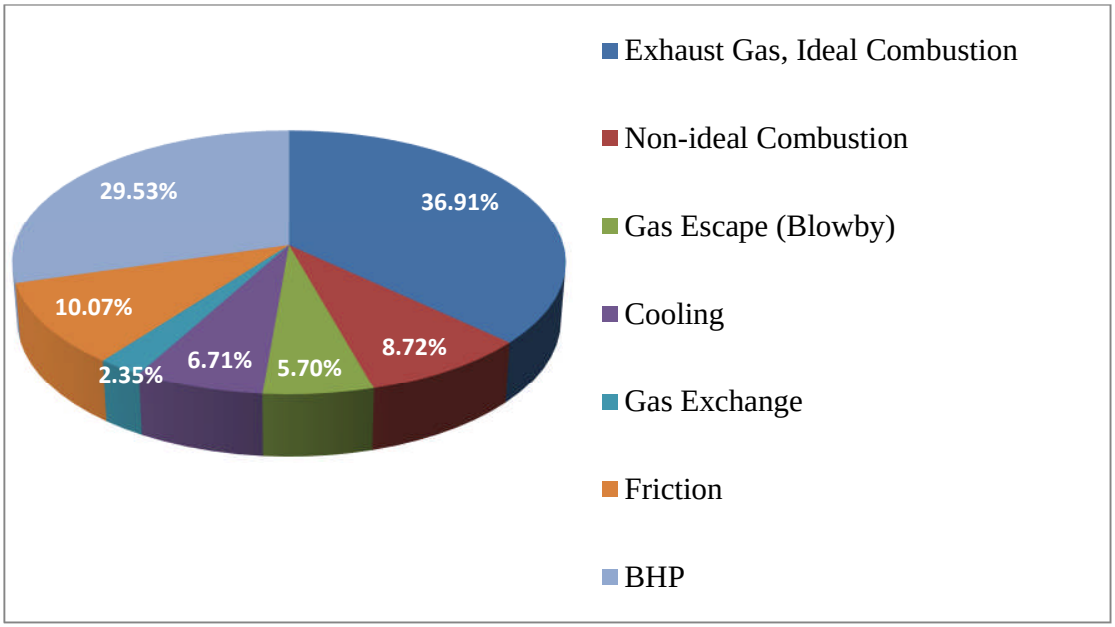

Fig. 1- 1 Percentage distribution of the fuel energy between BHP and other sources of power losses for Diesel engine operating at 20% load (data taken from Ref. [1])

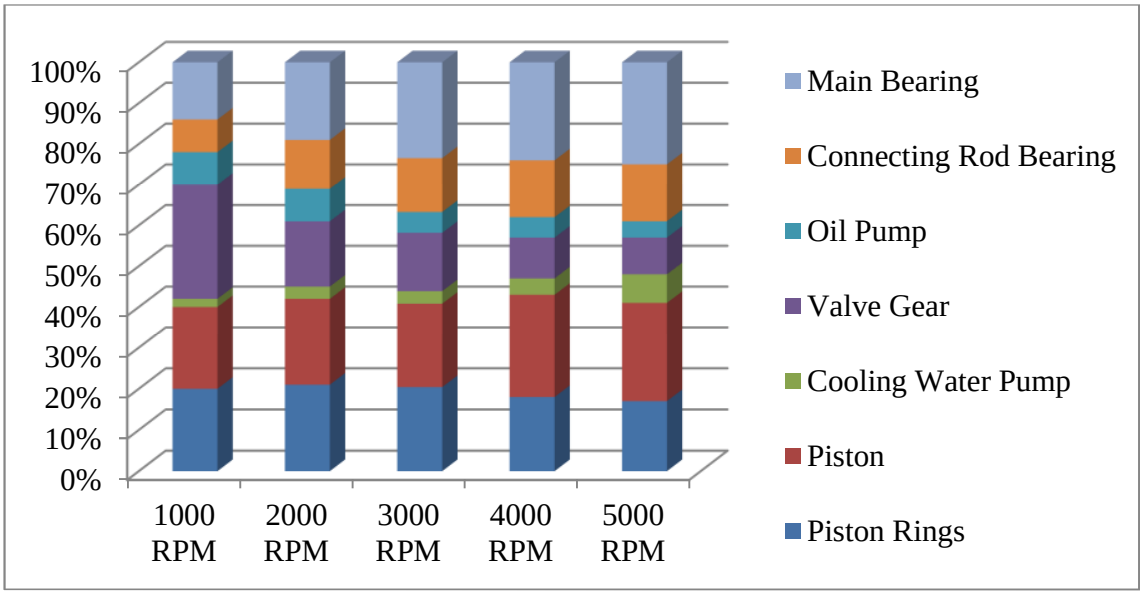

Fig. 1- 2 Percentage distribution of power losses between different engine components and accessories (data taken from Ref. [1])

ring-pack dynamics [4-6]. Oil mixes with the gases of the combustion chamber through evaporation from the oil film, oil entrainment in the reverse blowby where gases flow from the crankcase to the cylinder, and oil throw-off. The latter refers to the oil that accumulates on the top surface of the first compression or top ring and gets thrown off into the combustion chamber due to the inertia effects. It should be noted that any reduction in the oil consumption will ultimately result in lowering the tail-pipe emissions. It seems that an effective and relatively simple procedure for reducing the oil consumption is to increase the tension in the oil control ring. However, such an approach would have a significant adverse effect on both frictional losses and engine wear [1, 7].

In addition, the ring-pack facilitates the transfer of heat from the piston to the cylinder liner [8]. Moreover, a careful assessment of the piston secondary motions can provide useful design insights into the reduction of piston-slap, and ultimately, engine noise [9, 10]. Note that the piston secondary motions are most severe during the engine cold-start where the piston-liner clearance is at its maximum value [11].

The objective of the present study is to develop a reliable tool for predicting the intricate dynamics and the hydrodynamic frictional losses of the piston-assembly under various engine operating conditions. Such a tool will be instrumental in aiding both engine designers and manufacturers to optimize the the piston-assembly design as well as to investigate the impact of their design refinements on the overall engine performance [12, 13].

A reliable tool that can fully address the intricate dynamics of the piston-assembly along with its lubrication regimes, under actual engine operating conditions, must consider the following factors:

- The coupled dynamics of the crankshaft, connecting-rod, and the piston.
- The secondary motions of the piston, namely, piston-slap and piston-tilt.
- The deformation of the piston-skirt due to high thermal and dynamic loading conditions.
- The rigid and flexible motions of the rings within the piston grooves, including axial, radial, and rotational (twist) deformations.
- Gas flows through the ring end-gap, the ring-groove, and the ring-liner clearances.
- The lubrication regimes that may occur during an engine cycle such as boundary, mixed, hydrodynamic, and elasto-hydrodynamic lubrication regimes.
- Oil transport mechanism.
- Thermal distortion of the piston, bore, and rings due to high cyclic variations in the combustion chamber temperature.

Given the limited scope of the current work, the proposed tool will account for the coupled motions of the crankshaft, the connecting-rod, and the piston primary and secondary motions, which involve piston-slap and piston-tilting. Furthermore, each ring of the ring-pack will be treated as an independent deformable structure with a special attention given to the ring-liner-groove interactions. In addition, both the hydrodynamic lubrication regime of the piston-

skirt and the elasto-hydrodynamic lubrication regime of the rings will be considered in the formulation. The current work will preserve all coupling terms between the various factors of the piston-assembly that will be considered in the present work.

1.2 Literature Survey

Piston rings are classified into three categories according to their functionalities. First, the compression ring is used to minimize blow-by gases by sealing the combustion chamber from the crankcase. Moreover, it transfers heat from the piston to the cylinder wall and plays an important role in controlling the lube oil consumption (LOC) [1]. The compression ring free-shape and the geometry of its cross section are carefully designed in order to enhance the ring-liner conformability [11].

The second category consists of the second compression ring. Its function is to further improve on the sealing provided by the first compression ring and to scrape the excess oil on the cylinder liner in order to prevent it from penetrating into the combustion chamber. Most rings in this category are designed with a step recessed into the bottom outer surface of the ring to enhance their scraping capability [1].

The third category involves oil-control rings whose main purpose is to distribute the oil evenly onto the cylinder liner. This can be achieved by increasing the pre-tension of the ring, which improves ring-liner conformability and contact pressure. In addition, the geometry of the ring running surface is usually designed to have a scraping edge at the bottom for down-strokes and

avoid scraping edges at the top for up-strokes. However, these guidelines may reduce the oil availability at critical locations on the cylinder liner near top-dead-center (TDC) under engine firing condition, which may cause wear and increase frictional losses due to metal-to-metal contact [11]. Furthermore, it is worth noting that the current trend of designing lightweight engines has resulted in the bore undergoing significant distortions. A possible solution is to design very flexible oil rings in order to maintain contact with the liner [11].

There is a great deal of work that has been reported in the open-literature pertaining to ring-pack dynamics, lubrication regimes, and inter-ring gas flows [12, 13]. Much of the reported work has focused on various aspects of the piston-assembly dynamics with varying levels of simplifying assumptions in their formulations. However, recent studies have relaxed many of these assumptions to render the work closer to real engine operating conditions.

Jeng [14-16] focused on the ring frictional losses by solving a quasi-steady-state problem whereby the net resultant force, induced by the fluid film pressure, is balanced by the applied loads on the ring. The latter is considered to be axi-symmetric and in equilibrium. Both primary and secondary motions of the piston-assembly have been ignored along with all inertial forces/moments. The external ring forces stem from the gas pressure applied on the back surface of the ring as well as the ring elastic pressure due to the inherent ring elasticity. This work considered a 1-D Reynolds equation to examine the interaction between the piston ring and the lubricating oil film. In the first part of this study [15], a fully flooded inlet condition was considered. Whereas, in the second part [16], a

starved ring lubrication condition along with the lubricant transport on the cylinder liner were considered. Reynolds cavitation boundary conditions were used to detect the rupture of the lubricant oil film due to cavitation.

Herbst and Priebsch [17, 18] developed a software package – GLIDE – to simulate the dynamics of piston rings and their effect on oil consumption. They expanded the ring lubrication analysis by considering the piston secondary motions, a lumped mass model for the ring-pack, the effects of inertial forces and moments and a simplified blow-by model, based on ideal gas and convergent nozzle assumptions, to predict the oil transport and evaporation [19].

Priest et al [20] presented a simplified axi-symmetric dynamic model for a single compression ring. The twisting of the ring is ignored by assuming that it will always remain perpendicular to the liner. The axial motion of the ring is considered to be dominated by inertial and gas forces while the hydrodynamic friction force and the effect of gravity are neglected. The radial motion is assumed to be governed by an equilibrium equation with all inertial forces and friction force at the piston groove contact ignored. This model employs Greenwood and Tripp [21] formulation to account for the forces induced by the interactions between the asperities on the rubbing surfaces [22, 23].

Ruddy et al. [23] focused solely on the operating characteristics of a twin-land oil control ring. Their study neglects the effects of inertial forces and only considers the radial, axial, and torsional equilibrium equations. The effects of the inherent ring elasticity are accounted for in both the radial and torsional equations by using a single lumped parameter term in each of these equations.

The interaction between the ring and the piston groove is handled by a concentrated force applied on the ring. This force is assumed to have no effect on the ring twisting. Both hydrodynamic and mixed lubrication regimes were considered by implementing the average 1-D Reynolds equation [24]. The asperity interaction model is that of Greenwood and Tripp [21]. The added features of this work stem from the use of the torsional equilibrium equation and the computation of the oil flow rates between the lands and the liner as well as through the leakage slots in the oil ring.

Keribar et al [25] focused on developing an integrated model for the ring dynamics, hydrodynamic and mixed lubrications regimes along with blowby and inter-ring gas dynamics. Their methodology extends the work of Ruddy et al. [23] by considering the effects of inertial forces in the radial, axial, and torsional equations of motion. They used a similar lumped parameter approach for representing the effects of the inherent ring elasticity in the radial and torsion equations of motion. Note that this approach only accounts for the ring stiffness and ignores the inertia terms associated with the structural flexibility of the ring. In addition, the concentrated force, representing the interaction between the ring and the piston groove, is defined to be the product of the ring mass and the piston acceleration. Moreover, when the film thickness between the ring and the groove becomes of the same order as the composite roughness of the rubbing surfaces, a normal nonlinear spring force is applied in the axial direction to reflect the asperity interaction.

A 1-D Reynolds equation is used for modeling the hydrodynamic lubrication regime between the ring and the liner. In addition, the model developed by Greenwood and Tripp [21] was implemented to model the asperity interaction in the radial direction. Moreover, they used a similar approach as in Ref. [23] to model the ring-pack gas dynamics with the exception that the volumes in grooves and lands are computed based on the piston-groove and ring geometries and motions. Furthermore, they allowed the gas flows to occur due to ring end-gaps, space between rings and grooves induced by ring motions within the groove, and space between the ring and the liner due to ring non-conformability with the liner or ring "lift". This work represents a significant extension to the work of Ruddy et al [23].

Other studies [26, 27] have also developed an integrated model of ring dynamics and inter-ring gas flows. They considered only the dynamics of the two compression rings in a three ring-pack along with the gas flows in the regions above the oil control ring. The linear and angular momentum balance were implemented to derive the axial and torsional/twisting equations of motion of each ring. They used a similar approach as in Refs. [23, 25] in order to represent the effects of ring elasticity on the twisting behavior of the ring, in addition to effect of the piston motion on the ring dynamics. A special attention has also been given to the ring-groove interaction because it plays an important role in the ring dynamic twist [2, 3]. The asperity contact pressure and the oil squeezing pressure, between the ring and its groove, are accounted for in the ring equations of motion. It should be mentioned that the oil film thickness and

surface roughness of the ring and groove surfaces are prescribed in this work. The asperity contact pressure is determined by employing the formulation of Greenwood and Tripp's theory [21]. Whereas, the oil squeezing pressure is calculated by using simplified 1-D Reynolds equation whose sole forcing function is the oil squeeze film effect. In addition, the radial and torsion equations do consider the friction force on the ring running surface along with the moment induced by the radial pressure on the ring running surface. Note that all moments were computed with respect to the centroid of the ring cross section. The inter-ring gas flows are modeled as flows with low Reynolds number. Their approach for the gas dynamics is similar in concept to that of Refs. [23, 25], which determines the volumes of the spaces between the rings and the grooves based on the piston and groove geometries and their relative motions. Tian [2, 3] considered the local flow through the ring-groove clearance to be fully-developed viscous flow between parallel plates.

The coupled ring dynamics and inter-ring gas flows sub-models have been used to investigate ring radial collapse [2, 28, 29] and ring flutter inside the groove [2, 3, 27, 30-33]. The ring flutter is attributed to the strong coupling between the ring dynamics and inter-ring gas flows [2]. It can occur when the inertial forces on the ring are comparable in magnitude to that of the gas pressure. Moreover, Tian [3] used such an integrated model to examine the oil transport phenomenon, friction and wear. He highlighted the importance of ring-pack mechanical design on the blow-by and oil consumption [2, 3].

Thus far, all the described work has dealt with simplified lumped parameter terms to approximate the radial and torsional deformations of the ring. Liu et al. [34-36] developed a 3-D finite element model to approximate the static radial, axial, and torsional deformations of piston rings with either symmetric or asymmetric cross sections. The model accounts for ring-bore and ring-groove interactions by implementing the simplified asperity contact model of Ref. [19]. The latter was derived by curve fitting data generated through the implementation of the general theory of Greenwood and Tripp [21] for contact between two rough plane surfaces.

The model incorporates 2-node straight beam finite elements with 3 displacement and 3 rotational coordinates per node. The deformed profile of the ring, which is being constrained by the bore and the piston groove, is determined by solving the static equation relating the ring stiffness, static deformations, and nodal loads. This was done by implementing a step-by-step procedure, commonly used in finite element analysis, to handle large displacement problems without violating the small displacement assumption of the finite element formulation of this study. It should be noted that the large displacement problem arises from the large deformations incurred by the ring during its insertion into the cylinder.

This study was limited to static analysis of the ring because its main focus was on the ring-bore conformability problem. Its objective was to develop a reliable tool that yields free-shape design parameters of the ring, which produce the desired static twist profile after the insertion of the ring into the cylinder under

different ring-bore and ring-groove constraints. The desired static twist profile yields a ring-bore contact pressure distribution deemed to be necessary for controlling blow-by and oil transport phenomenon. The work in Ref. [37] has demonstrated that a variable wall thickness is required to produce a uniform contact pressure distribution between a circular bore and a circular ring with a rectangular cross section. Such a uniform contact pressure profile is not achievable with a constant cross sectional ring [38]. Dunaevsky and Alexandrov [39] presented formulae for determining the conformability of rings, with arbitrary cross-sections, to a bore whose lateral profile is described by selected Fourier harmonics [40, 41]. The equations for the three-dimensional deformation of the ring were based on the linear theory of elasticity. They were used to determine the twist of a compression ring and to compute the ring-bore contact pressure distribution. This work does not account for the ring-groove interaction.

Sun [42] addressed the ring-bore conformability problem by considering arbitrary bore and free-ring shapes along with thermal ring deformations and gas pressure effects. The bore distortion due to bolt-up stresses and uneven thermal expansion has been described by an empirical formula. A constant rectangular cross-section of the ring was considered in the analysis. The ring deflection is assumed to only occur in the plane perpendicular to the cylinder axis. It is modeled as a curved beam subjected to in-plane loads at steady-state. All friction related forces have been ignored.

Mittler et al [43] aimed at developing a model for understanding the fundamentals of ring dynamic behavior. This work accounts for the coupled

torsion (twist) and out-of-plane transverse (bending) deformations of the ring in the axial direction. However, it ignores the piston secondary motions. Moreover, it does not consider the longitudinal and the in-plane (radial) bending of the ring, which precludes the inclusion of a squeeze film effect. Only hydrodynamic pressure of the lube oil film is considered but the frictional losses due to the solid-fluid interaction are ignored. The structural elasticity problem of the ring is based on the Euler-Bernoulli beam theory and formulated independently from the rigid body motion of the ring. Axial constraint forces are applied on the ring when it comes in contact with either the upper or lower surfaces of the groove. The gas flows around the ring are determined by using the convergent nozzle assumption.

Keribar and Dursunkaya [44] developed a model for the piston-assembly that considers piston secondary motions and accounts for the hydrodynamic lubrication regime of the piston-skirt. In addition, the frictional losses induced by the hydrodynamic and mixed lubrication regimes of the wristpin bearings were determined by interpolating a pre-determined non-dimensional bearing impedance map. Dursunkaya et al [45] extended the work of Ref. [44] to consider the radial deformations of the piston-skirt for both conventional and articulated (two-piece) pistons. The axial and tangential deformations of the skirt are ignored. The radial deformation of the skirt was determined by employing an area corrected compliance matrix, which was extracted from a finite element model of the piston. This procedure only allows for the computation of the static deformation of the piston-skirt. To enhance the viability of this approach, the skirt

radial deformation was re-computed at every iteration. The oil film thickness is determined from the skirt radial deformation and the skirt-liner clearance. The elasto-hydrodynamic lubrication regime also accounted for the cavitation in the skirt oil film where the oil viscosity was varied in time based on the average temperature of the piston-skirt and liner surfaces. The piston-skirt elasto-hydrodynamic frictional losses and oil contact pressure are determined by incorporating a 3-D Reynolds' equation. The mixed lubrication regime is modeled based on the theory of contact-pressure between the asperities of flat surfaces using the Greenwood and Tripp formulation [21]. The hydrodynamic pressures and the frictional forces and moments are then used in a lumped model for determining the piston secondary motions.

Duyar et al [46, 47] extended the Ricardo commercial software PISDYN to handle partially lubricated piston-skirt. Unlike all the above studies that rely on the finite difference method to solve the Reynolds' equation, this work implements the finite volume method to overcome the shortcomings of the finite difference method in handling the continuity equation. In addition, they used the Reynolds boundary condition for the film rupture detection and the Jakobsson-Floberg-Olsson (JFO) boundary conditions for determining the re-attachment points of the oil film. Elrod [48] presented a computational scheme to systematically handle cavitated regions in hydrodynamic lubrication of bearings.

Perchanok [49] considered the effect of bore deformation on the piston-skirt lubrication regime. His model used a compliance matrix to determine the bore deformation. Moreover, the instantaneous piston-skirt structural deformation was

computed by scaling a skirt deformation distribution, which was pre-determined based on reference cylinder pressure and piston acceleration.

All the work that has been discussed in this Section focused on the ring with a prescribed motion of the piston or through the implementation of a simplified lumped mass model of the piston. Richard et al. [50] developed a lumped-mass model of the crankshaft/connecting-rod/piston-assembly, which considers the piston offset, to determine the piston speed. This allows for the computation of the frictional losses of the piston-assembly under more realistic engine operating conditions. Their formulation ignored the twisting of the rings, the piston secondary motions along with the elastic deformations of the ring-pack and the piston-skirt. A 1-D Reynolds' equation along with a simplistic Stribeck curve-based model were used in the formulation of the hydrodynamic and mixed lubrication regimes of the rings. A 3-D Reynolds' equation was implemented in the formulation of the hydrodynamic lubrication regime of the piston skirt. This work included both theoretical and experimental results.

The work of Ting and Mayer [51, 52] fits in the area of integrated modeling of ring-pack phenomena by considering the combined effects of ring lubrication, blow-by, and wear. However, they used a rigid body model of the crank-slider mechanism and considered the effect of the piston side thrust. The model provides the reciprocating motion of the ring and ignores the ring tilting inside the groove. Moreover, this study treats the ring as a thin-walled cylinder moving as a unit in the radial direction under the effects of the mean oil film pressure and the gas pressure applied on its back surface. It should be noted that the radial

motion is determined by ignoring the inertia of the ring. A 1-D Reynolds equation was used for the hydrodynamic lubrication regime of the ring. The inter-ring pressure variations are accounted for by considering the gas blowby through the ring-pack, which was considered to be an unsteady adiabatic flow satisfying the ideal gas law [53, 54]. This was done by incorporating a series of control volumes, representing the inter-ring spaces, connected through orifices. The Archard's wear relation is also included in their formulation. The main objective of this model was to predict the cylinder wear.

All the above studies have focused on specific aspects of the intricate dynamic behavior of the piston-assembly and/or frictional losses. The piston motion was determined independently from that of the ring. In the current study, the aim is on developing a comprehensive tool that will account for the integrated motion of the crankshaft, connecting-rod, primary and secondary motions of the piston along with the rigid and flexible motions of the ring-pack. Moreover, it will consider the solid-fluid interaction that occurs at the interface between the piston-assembly and the lubricating oil film.

1.3 Overview of the Current Study

The focus of the present study is on the development of a reliable tool to predict the intricate dynamics and the lubrication regimes of the piston-assembly under various engine operating conditions. The tool has been developed in modular form with three main modules. The first one provides the rigid body motion of the crankshaft/connecting-rod/piston mechanism excluding the ring-pack. It treats the crank-slider mechanism as an open-kinematic chain consisting

of multi-rigid bodies connected in series with the piston motion confined to the bounding wall of the cylinder. This module captures the piston secondary motions, namely, piston-slap and piston-tilting. Its formulation is covered in details in the first part of Chapter 2.

The second module focuses on the intricate dynamics of the ring-pack, which is considered herein to be made up of two compression rings and one oil control ring. Each ring has been modeled herein as a shear deformable structure undergoing two angular and one translational (axial) rigid body degrees of freedom within its respective piston groove. The longitudinal and in-plane transverse deformations of the ring are handled by employing two-node shear deformable curved beam elements, which are derived based on the Timoshenko beam theory and account for the inherent coupling between the longitudinal and transverse deformations of curved structures [55-57]. The rigid and flexible motions of the rings are formulated in the later portion of Chapter 2.

The third module aims at predicting the normal and friction forces exerted on the piston-assembly by the lubricating oil film. It accounts for the hydrodynamic lubrication regime of the piston-skirt and the elasto-hydrodynamic lubrication regime of the ring-pack. The module captures the solid-fluid interaction between the piston-assembly and the oil film. This is done by having the piston secondary motions dictate the instantaneous oil film thickness along the piston-skirt and the ring-pack running surfaces. While the effects of the lubricating oil film on the dynamics of the piston-assembly are accounted for through the instantaneous normal and tangential forces (friction forces) exerted

on the running surfaces of the piston-assembly. A 3-D and 1-D Reynolds' equations have been implemented to determine the oil film pressure distributions along the running surfaces of the piston-skirt and the ring-pack. The shear stresses, used in the computation of the friction forces, were calculated based on the Newton's law of viscous flow. The details of the third module are included in Chapter 3.

In Chapter 4, the three modules are integrated to form the proposed tool. The latter is used extensively to predict the intricate dynamics and the hydrodynamic frictional losses of the piston-assembly under different operating conditions. Finally, the work is summarized and the main contributions of the current work are outlined in Chapter 5.

CHAPTER 2

DYNAMIC MODEL OF THE PISTON-ASSEMBLY

A dynamic model for the piston-assembly of a four-stroke, single cylinder, internal combustion engine (IC) is presented in this Chapter. The formulation of this Chapter will only address the structural aspect of the problem, while the solid-fluid interaction between the piston-assembly and the lubricating oil film will be discussed in the subsequent Chapter.

The model treats the crankshaft, the connecting-rod, and the various components of the piston-assembly as a nonlinear multi-body system. The interaction between the various elements of this system is handled by a variable number of constraint equations whose number is dictated by the instantaneous configuration of the system. Consequently, the model will have a variable structure where the number of degrees of freedom fluctuates with the varying number of constraint equations.

The crank-slider mechanism structural equations of motion, presented in this Chapter, will later on be coupled with the oil film formulation, covered in Chapter 3, in order to develop a fully-integrated model that is suitable for investigating the intricate dynamics of the piston-assembly under realistic engine operating conditions.

2.1 Derivation of the Dynamic Model

A dynamic model for the crankshaft/connecting-rod/piston-assembly mechanism of a single cylinder internal combustion (IC) engine is discussed in this Section. In order to account for the piston secondary motions, the crank-

slider mechanism has been treated as an open-kinematic chain of rigid bodies. This will allow the piston, without the ring-pack, to undergo free or constrained motions whereby the piston may have a single-point, double-point, or surface contact with the liner [58]. The various piston configurations during an engine cycle cause the number of constraint equations to vary with the instantaneous position and orientation of the piston within the cylinder. Thus, the present model will have a variable structure in order to handle the piston-liner interaction. The current formulation builds on the crank-slider mechanism model that was presented in Refs. [58, 59]. This model will be described in the next Subsection and the modifications to its formulation will be discussed in detail.

Subsequently, the ring-pack model, which represents a significant contribution of the current work, will be covered. Its formulation considers each ring to be a shear deformable structure with inherently coupled longitudinal and in-plane transverse deformations. Moreover, the translational (axial) and rotational rigid body motions of the ring within the piston groove are accounted for in the derivation of the model. Both ring-liner and ring-groove interactions are considered in the formulations of the ring model. Depending on its location within the piston groove, the ring may have single-point, two-point, or surface contact with the top and bottom surfaces of the piston groove. In the event of no contact between the ring and the groove, the ring motion is considered to be free. Moreover, the current model accounts for the impact forces induced by the ring-groove and piston-liner collisions, which occur at their moments of contact.

2.1.1 Crank-Slider Mechanism Formulation

To consider the piston secondary motions such as the piston-slap and piston-tilting, the crank-slider mechanism has been modeled herein as an open-kinematic chain (see Fig. 2-1). The reference inertial frame, $\{X,Y,Z\}$, is assigned at point O. In addition, seven non-inertial body-fixed frames, $\{x_i, y_i, z_i\}$ with $i=1,\ldots,7$, have been defined in the rigid body configuration of the crank-slider mechanism.

The extended position vectors of arbitrary points in the rigid body configuration of the crankshaft, the connecting-rod, and the mass center of the piston, excluding the ring-pack, are expressed as

$$\left\{ \begin{matrix} r^T \\ \sim cs^{(i)} \end{matrix} \; | 1 \right\}^T = \left[\prod_{j=1}^{i} T_{j-1}^{j} \right] \{ x_i \;\; y_i \;\; z_i \; | 1 \}^T \quad i = 1, \; \cdots, \; 5 \tag{2-1}$$

$$\left\{ \begin{matrix} r^T \\ \sim cr \end{matrix} \; | 1 \right\}^T = T_0^3 T_3^{\bar{3}} T_{\bar{3}}^6 \{ x_6 \;\; y_6 \;\; z_6 \; | 1 \}^T \tag{2-2}$$

$$\left\{ \begin{matrix} r^T \\ \sim p \end{matrix} \; | 1 \right\}^T = T_0^3 T_3^{\bar{3}} T_{\bar{3}}^6 T_6^{6_e} T_{6_e}^7 \left\{ x_7^* \;\; y_7^* \;\; z_7^* \; | 1 \right\}^T \tag{2-3}$$

The reader is referred to Ref.[59] for the derivation of the above transformation matrices. The kinetic and potential energy expressions of the crank-slider mechanism, excluding the ring-pack, can be written as

$$T_1 = \frac{1}{2} \sum_{i=1}^{5} \int_{m_{cs^{(i)}}} \dot{\underset{\sim}{r}}_{cs^{(i)}} \cdot \dot{\underset{\sim}{r}}_{cs^{(i)}} dm_{cs^{(i)}} + \frac{1}{2} \sum_j \left(m_j \, \dot{\underset{\sim}{r}}_j \cdot \dot{\underset{\sim}{r}}_j + \bar{\underset{\sim}{\omega}}_j^T \bar{I}_j \, \bar{\underset{\sim}{\omega}}_j \right) + \frac{1}{2} \int_{m_{cr}} \dot{\underset{\sim}{r}}_{cr} \cdot \dot{\underset{\sim}{r}}_{cr} dm_{cr} \tag{2-4}$$

$$j = fl, \; cw1, \; cw2, \; cg, \; p$$

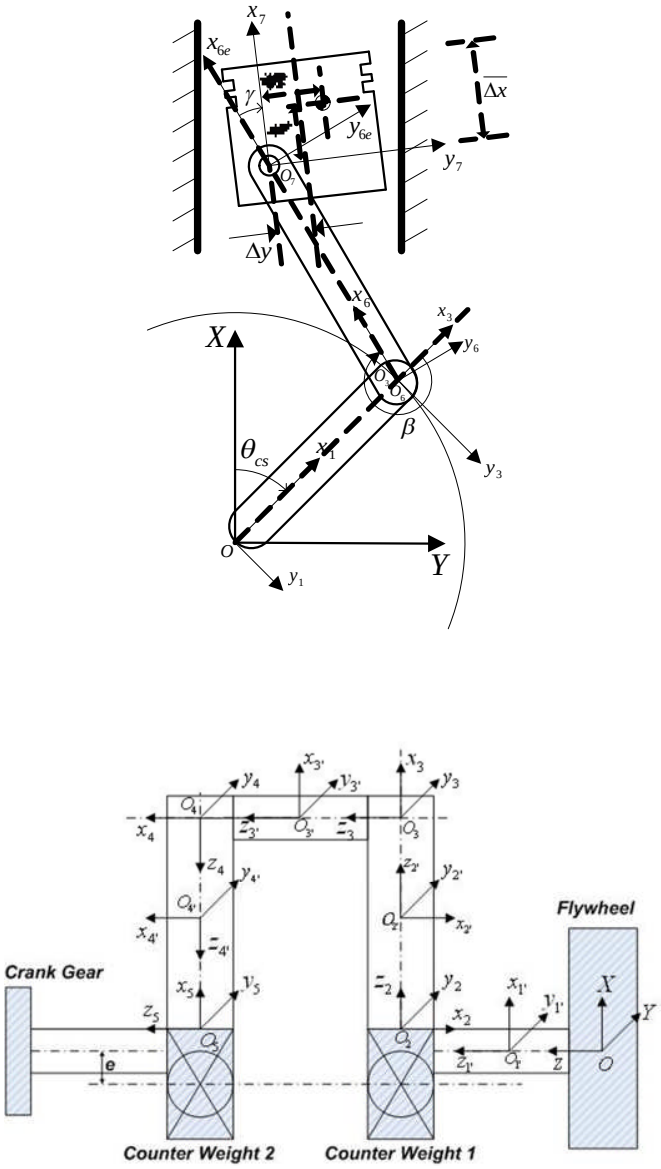

Fig. 2- 1 Schematics of the crankshaft, connecting-rod, and piston.

where j refers to the piston, the counterweights, the flywheel, and the crank gear. All these elements have been treated as rigid bodies undergoing both translations and rotations.

$$V_1 = \sum_{i=1}^{5} \int_0^{L_i} \rho A_i \, g \, \underset{\sim}{I} \cdot \underset{\sim}{r}_{cs^{(i)}} \, dz_i + \int_0^{L_6} \rho A_6 \, g \, \underset{\sim}{I} \cdot \underset{\sim}{r}_{cr} dx_6 + \sum_j m_j g \underset{\sim}{I} \cdot \underset{\sim}{r}_j \qquad (2\text{-}5)$$
$$j = fl, cw1, cw2, gr, p$$

The following expression for the virtual work serves to highlight the non-conservative forces and torques governing the dynamic response of the crank-slider mechanism:

$$\delta W_p^{NC} = \left(P_{ck} - P_{cyl}\right) A_p^{top} \underset{\sim}{I} . \delta \underset{\sim}{r}_{p^*} - T_{load} \underset{\sim}{K} . \left(\delta\theta_{cs}\right) \underset{\sim}{k}_5 + \sum_{i=1}^{2} \left(F^{imp}_{(P-L)_i} \underset{\sim}{J} \right) \cdot \delta \underset{\sim}{r}^{P-\mathrm{L}}_{p_i} + \sum_{n=1}^{3} \sum_{j_n=1}^{8} \left(-F^{imp}_{(P-R)_{n_j}} \underset{\sim}{\bar{n}}_n \right) \cdot \delta \underset{\sim}{r}^{P-R}_{p_{j_n}} + \delta W_p^{Oil} \qquad (2\text{-}6)$$

The third and the fourth terms in the above equation account for the impact forces induced by the piston-liner and ring-groove collisions at their moments of contact. Their magnitudes are determined by considering the impact problem between two rigid bodies, which entails the implementation of linear and angular momentum balances for each body and their substitution in the definition of the coefficient of restitution [60, 61]. Moreover, the δW_p^{Oil} term in the above equation refers to the virtual work done by the oil film pressure and the friction forces associated with the hydrodynamic lubrication regime of the piston skirt. The expression of this term will be provided in Chapter 3.

The crank-slider mechanism model has a variable structure due to the fact that its degrees of freedom fluctuate with the varying number of constraint

equations. For a single point contact between the piston and the liner (see Fig. 2-2), only one of the following constraint equation will be imposed [58]:

Case 1-a: $$\underset{\sim}{r}_p^{TR} \cdot \underset{\sim}{J} = R_{cyl} \qquad (2-7a)$$

Case 1-b: $$\underset{\sim}{r}_p^{BR} \cdot \underset{\sim}{J} = R_{cyl} \qquad (2-7b)$$

Case 1-c: $$\underset{\sim}{r}_p^{BL} \cdot \underset{\sim}{J} = -R_{cyl} \qquad (2-7c)$$

Case 1-d: $$\underset{\sim}{r}_p^{TL} \cdot \underset{\sim}{J} = -R_{cyl} \qquad (2-7d)$$

For a double-point contact between the piston and the liner, one of the following sets of constraint equations will be imposed [58], (refer to Fig. 2-3):

Case 2-a: $$\underset{\sim}{r}_p^{TR} \cdot \underset{\sim}{J} = R_{cyl} \;;\; \underset{\sim}{r}_p^{BL} \cdot \underset{\sim}{J} = -R_{cyl} \qquad (2-8a)$$

Case 2-b: $$\underset{\sim}{r}_p^{BR} \cdot \underset{\sim}{J} = R_{cyl} \;;\; \underset{\sim}{r}_p^{TL} \cdot \underset{\sim}{J} = -R_{cyl} \qquad (2-8b)$$

Whereas, for a line-contact between the piston and the liner, one would apply one of the following sets of constraint equations [58]:

Case 3-a: $$\underset{\sim}{r}_p^{TR} \cdot \underset{\sim}{J} = R_{cyl} \;;\; \underset{\sim}{r}_p^{BR} \cdot \underset{\sim}{J} = R_{cyl} \qquad (2-9a)$$

Case 3-b: $$\underset{\sim}{r}_p^{BL} \cdot \underset{\sim}{J} = -R_{cyl} \;;\; \underset{\sim}{r}_p^{TL} \cdot \underset{\sim}{J} = -R_{cyl} \qquad (2-9b)$$

However, if the piston motion is constrained then the number of degrees of freedom of the system will be reduced by the number of constraint equations. To deal with the superfluous coordinates, the algorithm developed by Glocker and Pfeiffer [62, 63] has been implemented in this study.

Three degrees of freedom, θ_{cs}, β and γ, are used to describe the unconstrained rigid body motion of the crankshaft/connecting-rod/piston mechanism (without the ring-pack). On the other hand, in the constrained configuration of the piston, the number of degrees of freedom of the system is reduced by the number of active constraint equations. The presence of constraint equations results in differential- algebraic (D-A) equations of motion for the crankshaft/connecting-rod/piston (without the ring-pack) mechanism.

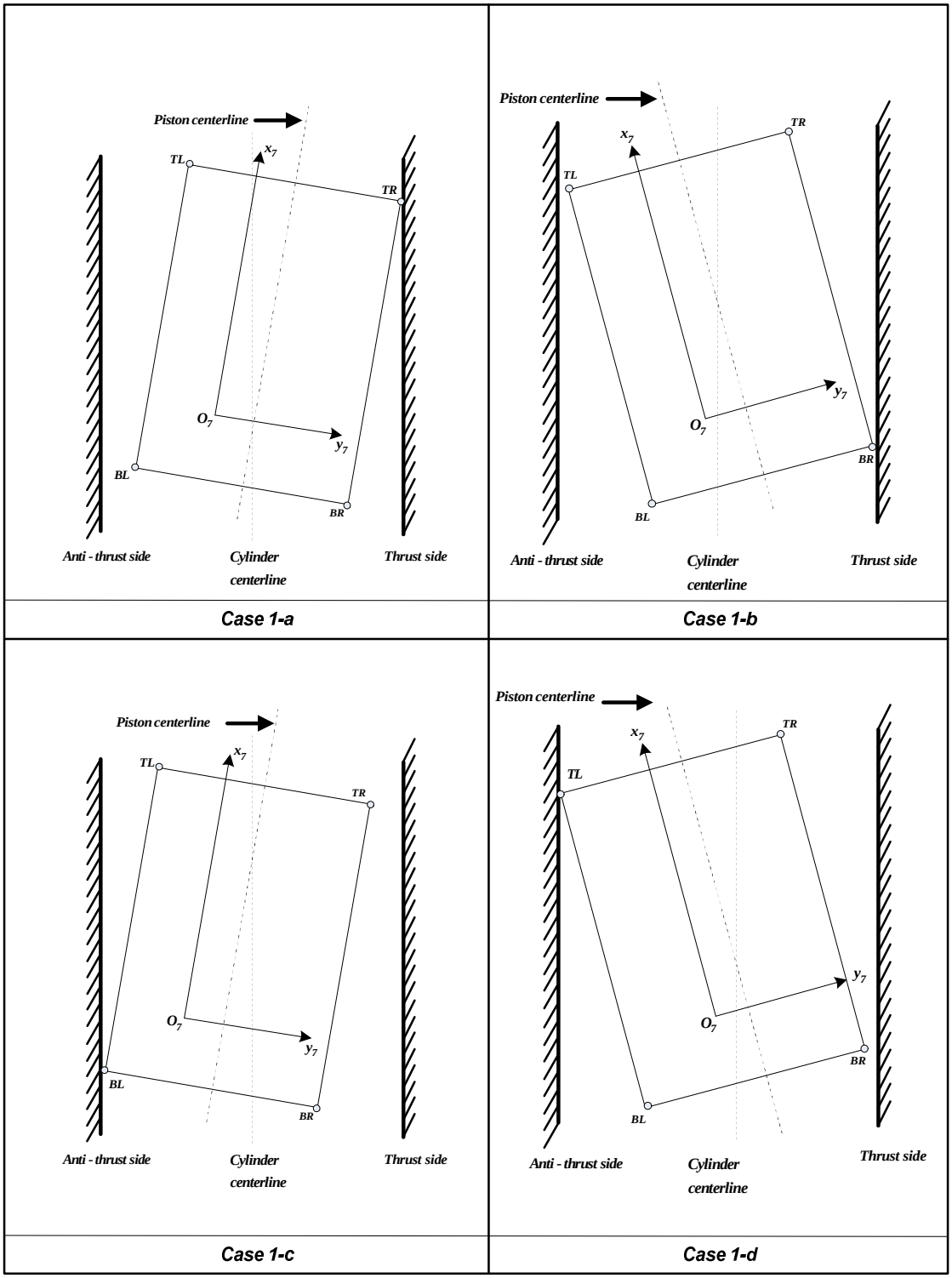

Fig. 2- 2 Piston-liner interactions through a single point contact [58].

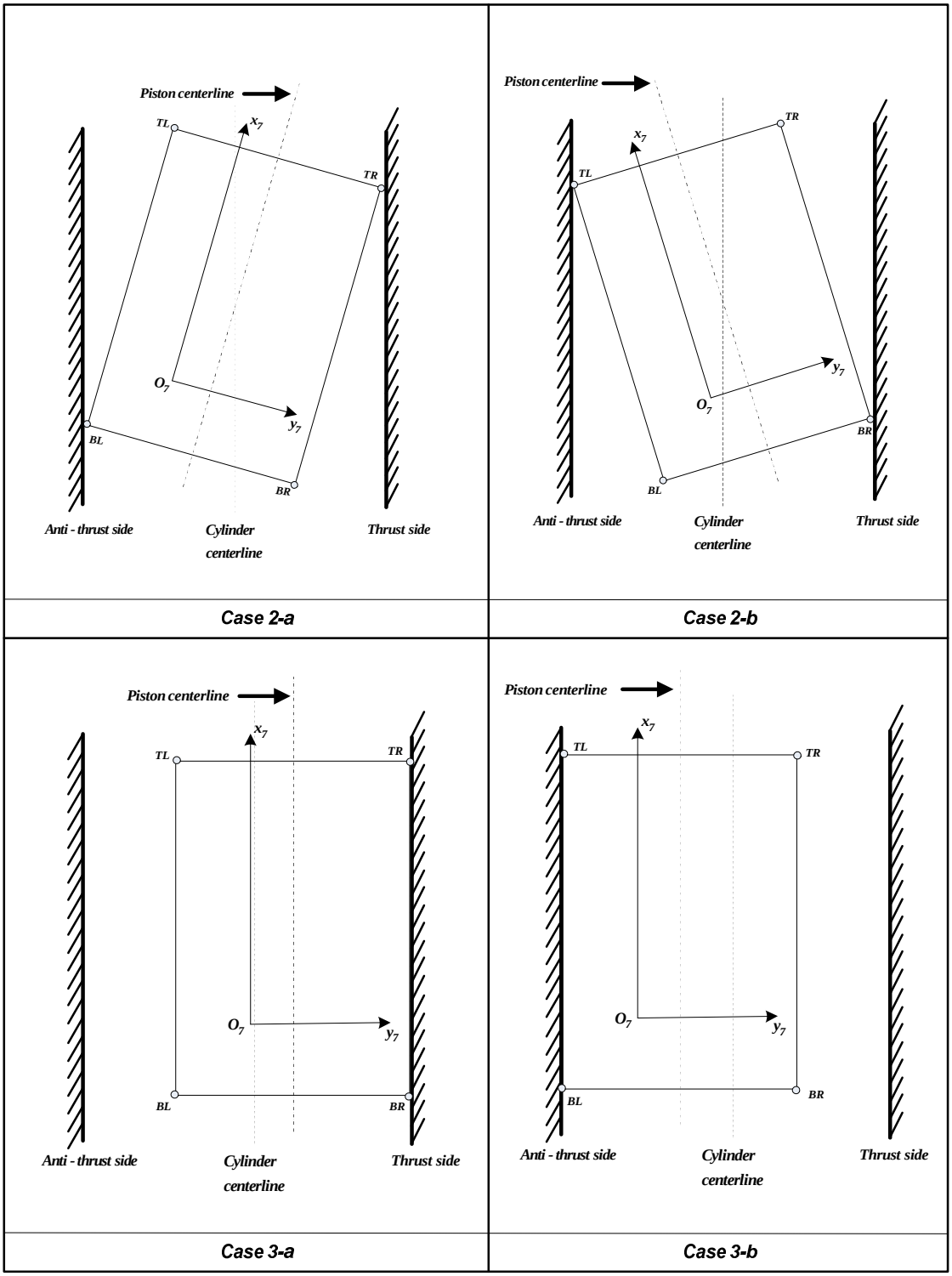

Fig. 2- 3 Piston-liner interactions through a double point or surface contact [58].

2.1.2 Piston Ring Formulation

In the current study, a ring-pack consisting of two compression rings and one oil control ring is employed. In the un-deformed configuration, the radius of each ring is larger than that of the cylinder. Therefore, the rings must be compressed in order to be inserted inside the cylinder. Each ring has been modeled herein as a shear deformable structure with two angular and one translational (axial) rigid body degrees of freedom.

In approximating the structural flexibility terms of the ring, the assumed modes method was initially implemented. Such a global approximation method is computationally efficient and uses eigenfunctions as admissible functions. However, it was found to be unsuitable for capturing the localized effects associated with the ring-groove and ring-liner interactions. As a consequence, the finite element method, using straight beam elements, was then employed. Usually, a large number of straight beam elements are required to accurately approximate the structural deformations of a curved structure. However, the large error at the midpoint of the element renders the implementation of straight beams to be inapplicable for solid-fluid problems associated with the interactions between the ring and its lubricating oil film. This is because the required accuracies for such problems are in the order of microns.

To deal with this issue, two-node shear deformable curved beam elements, derived based on the Timoshenko beam theory and account for the inherent

coupling between the longitudinal and transverse deformations of curved structures, have been implemented in this work [55-57].

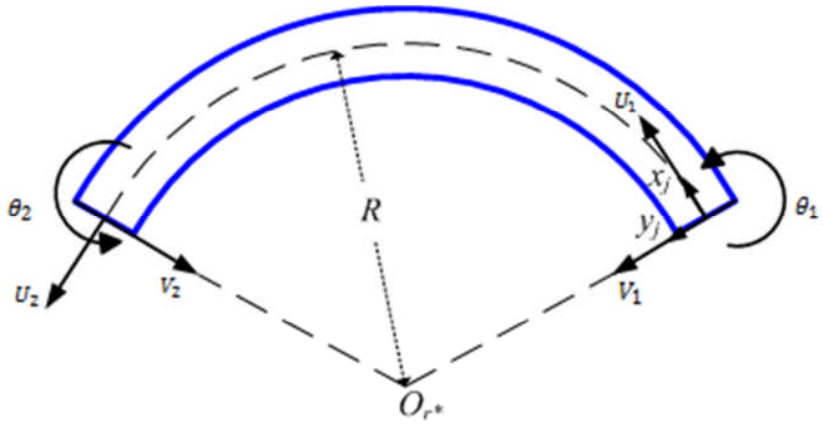

Fig. 2- 4 Curved beam Finite element with nodal coordinates

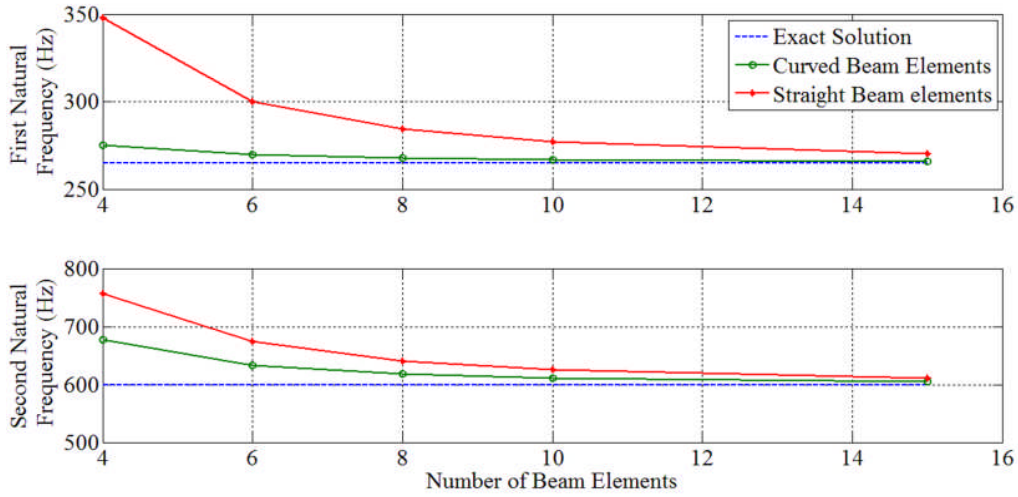

Fig. 2- 5 Convergence rate of the curved beam finite element model of the ring.

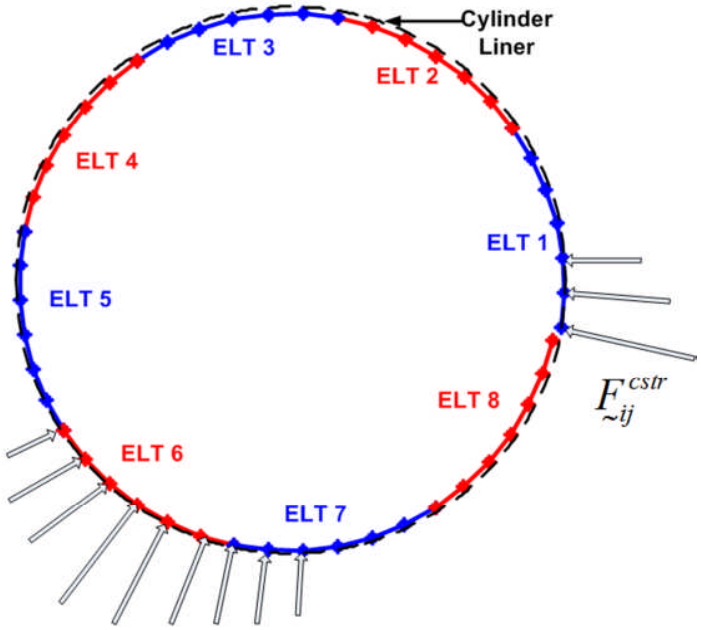

Fig. 2- 6 Ring-liner contact and the ensuing discretized constraint forces.

This is illustrated in Fig. 2-4. The shape functions of such an element are defined as [55]:

$$N = \left[1 \quad x \quad \cos\left(\frac{x}{R}\right) \quad x\cos\left(\frac{x}{R}\right) \quad \sin\left(\frac{x}{R}\right) \quad x\sin\left(\frac{x}{R}\right) \right] \tag{2-10}$$

Due to their efficiency, only six curved beam elements are actually needed to achieve the desired accuracy in the approximation of the longitudinal and in-plane transverse deformations of the ring. This is illustrated in Fig. 2-5.

In this document, the ring formulation is presented in a generic form so that it can be applied to any ring of the ring-pack. The index denoting the ring is assumed to be n is this documentation.

Eight beam elements have been used in this work in order to enhance the representation of the discretized constraint forces associated with the ring-liner

metal-to-metal contact. These forces are applied at seven equally spaced points along the curved beam element (see Fig. 2-6). They assume non-zero values whenever the radial distance between the point of application of the constraint force on the ring and the liner becomes smaller than a certain threshold. The constraint force is considered to increase linearly with the reduction of the radial distance between the ring and the liner. They are expressed as follows

$$\underset{\sim}{F}^{cstr}_{(R-L)_{n_{ij}}} = k_{cstr}\left(R_{cyl} - \left\| \underset{\sim}{r}^{n_{ij}}_{(R-L)_{(Y,Z)}} - \underset{\sim}{r}_{CL_{(Y,Z)}} \right\|\right) \underset{\sim}{j}_{\bar{j}_n'} \tag{2-11}$$

In this work, the ring is considered to have three rigid body degrees of freedom. Its vertical or axial translational motion is described by $X_{r_n}(t)$ along the $\underset{\sim}{I}$ – direction while its rigid body rotations are accounted for in the following expression for the ring angular velocity vector:

$$\underset{\sim}{\omega}_{r_n} = -\dot{\phi}_n \sin(\psi_n)\underset{\sim}{I} + \dot{\phi}_n \cos(\psi_n)\underset{\sim}{J} + \dot{\psi}_n \underset{\sim}{K} \tag{2-12}$$

The extended position vector of an arbitrary point B_n on the cross sectional area of the j^{th} beam element on the n^{th} ring can be written as (see Fig. 2-7)

$$\left\{ \underset{\sim}{r}^T_{B_n} \; | 1 \right\}^T = T^{r_n^*}_{\{X,Y,Z\}} T^{8_n}_{r_n^*} \left[T^{j_n}_{j_n - 1} \right]^{j_n - 1} T^{\bar{j}_n}_{j_n} T^{\bar{j}_n'}_{\bar{j}_n} \{0 \; y_{B_n} \; z_{B_n} \; | 1\}^T \tag{2-13}$$

where y_{B_n} and z_{B_n} are the coordinates of point B_n relative to $O_{\bar{j}_n'}$ defined in the $\left\{ x_{\bar{j}_n'}, y_{\bar{j}_n'}, z_{\bar{j}_n'} \right\}$ frame. $\left\{ x_{r_n^*}, y_{r_n^*}, z_{r_n^*} \right\}$ represents a body-fixed coordinate system attached at the mass center of the ring. Its location and orientation with respect

to the inertial reference frame is given by the following transformation matrix, $T^{r_n^*}_{\{X,Y,Z\}}$:

$$T^{r_n^*}_{\{X,Y,Z\}} = \begin{bmatrix} \cos\phi_n \cos\psi_n & -\sin\psi_n & \sin\phi_n \cos\psi_n & X_{r_n}(t) \\ \cos\phi_n \sin\psi_n & \cos\psi_n & \sin\phi_n \sin\psi_n & 0 \\ -\sin\phi_n & 0 & \cos\phi_n & Z_{CL} \\ 0 & 0 & 0 & 1 \end{bmatrix} \quad (2\text{-}14)$$

Moreover, the transformation matrix, $T^{8}_{r_n^*}$, representing the location and orientation of $\{x_{8_n}, y_{8_n}, z_{8_n}\}$ with respect to $\{x_{r_n^*}, y_{r_n^*}, z_{r_n^*}\}$ can be written as

$$T^{8_n}_{r_n^*} = \begin{bmatrix} 0 & 0 & 1 & 0 \\ 0 & -1 & 0 & R \\ 1 & 0 & 0 & 0 \\ 0 & 0 & 0 & 1 \end{bmatrix} \quad (2\text{-}15)$$

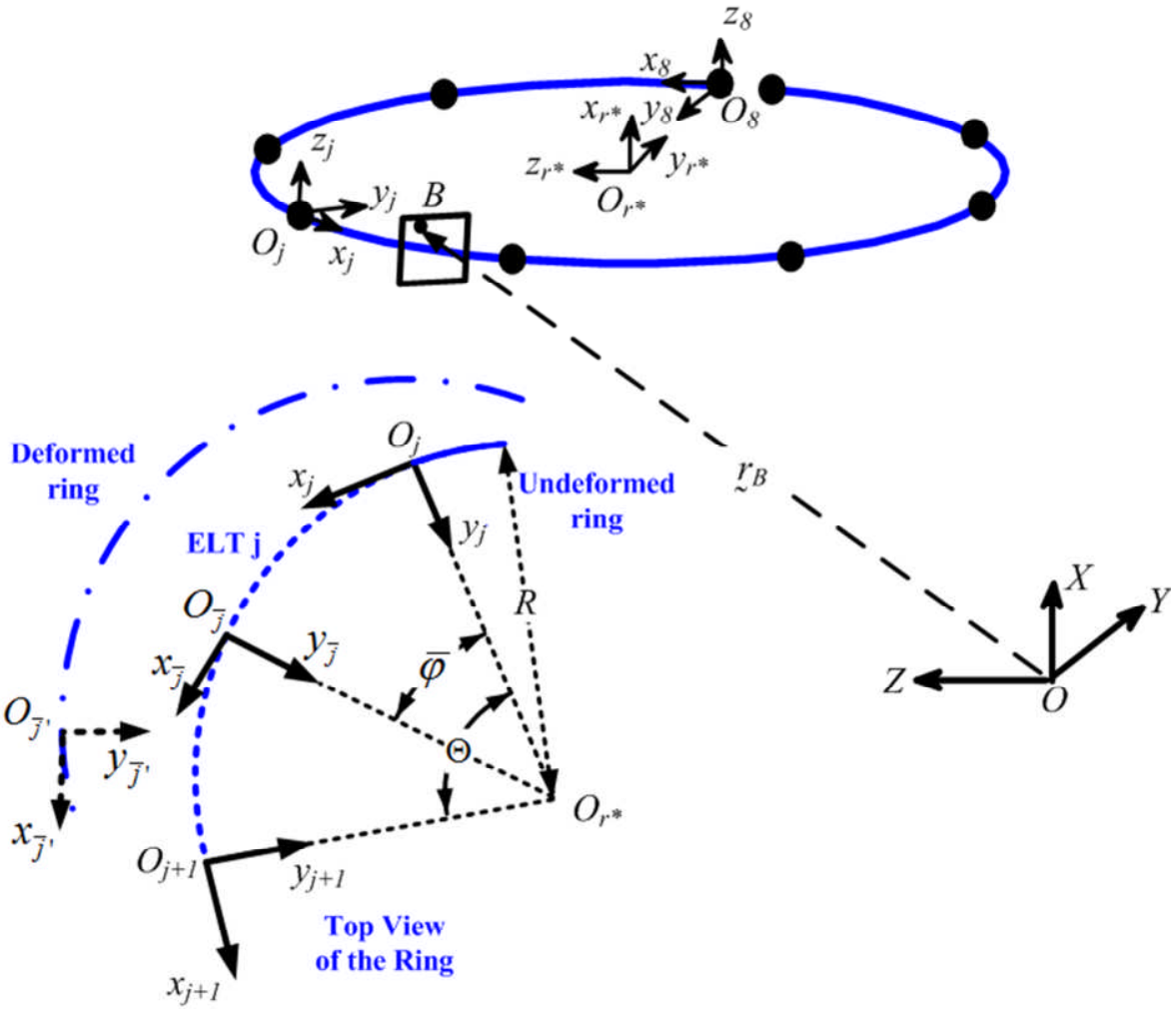

Fig. 2- 7 Curved beam finite element model of the ring.

Similarly, the $T_{j_n-1}^{j_n}$ matrix, defining the location and orientation of $\{x_{j_n}, y_{j_n}, z_{j_n}\}$ with respect to $\{x_{j_n-1}, y_{j_n-1}, z_{j_n-1}\}$, can be given by

$$T_{j_n-1}^{j_n} = \begin{bmatrix} \cos\Theta_n & -\sin\Theta_n & 0 & R\sin\Theta_n \\ \sin\Theta_n & \cos\Theta_n & 0 & R(1-\cos\Theta_n) \\ 0 & 0 & 1 & 0 \\ 0 & 0 & 0 & 1 \end{bmatrix} \tag{2-16}$$

The $\{x_{\bar{j}_n}, y_{\bar{j}_n}, z_{\bar{j}_n}\}$ frame is a floating one attached at a point located at a circumferential distance $R\bar{\varphi}$ from O_{j_n} along the neutral axis of the j^{th} beam element. Its location and orientation with respect to $\{x_{j_n}, y_{j_n}, z_{j_n}\}$ are expressed as

$$T_{j_n}^{\bar{j}_n} = \begin{bmatrix} \cos\bar{\varphi}_n & -\sin\bar{\varphi}_n & 0 & R\sin\bar{\varphi}_n \\ \sin\bar{\varphi}_n & \cos\bar{\varphi}_n & 0 & R(1-\cos\bar{\varphi}_n) \\ 0 & 0 & 1 & 0 \\ 0 & 0 & 0 & 1 \end{bmatrix} \tag{2-17}$$

Note that the expression for $T_{j_n}^{\bar{j}_n}$ is obtained from that of $T_{j_n-1}^{j_n}$ by substituting Θ_n with $\bar{\varphi}_n$ (see Fig. 2-7). The $\{x_{\bar{j}_n'}, y_{\bar{j}_n'}, z_{\bar{j}_n'}\}$ frame represents the $\{x_{\bar{j}_n}, y_{\bar{j}_n}, z_{\bar{j}_n}\}$ coordinate system in the deformed configuration of the ring. Its location and orientation with respect to $\{x_{\bar{j}_n}, y_{\bar{j}_n}, z_{\bar{j}_n}\}$ are described in the following structural flexibility transformation matrix, $T_{j_n}^{\bar{j}_n}$ [64]:

$$T_{\bar{j}_n}^{\bar{j}'_n} = \begin{bmatrix} 1 & -\bar{\theta}_{j_n} & 0 & \bar{u}_{j_n} \\ \bar{\theta}_{j_n} & 1 & 0 & \bar{v}_{j_n} \\ 0 & 0 & 1 & 0 \\ 0 & 0 & 0 & 1 \end{bmatrix} \tag{2-18}$$

The total kinetic energy of the ring-pack can be written as

$$T_2 = \frac{1}{2}\sum_{n=1}^{3}\sum_{j_n=1}^{8}\int_{m_{j_n}} \left(\dot{\underset{\sim}{r}}_{B_n}^{(j_n)} \cdot \dot{\underset{\sim}{r}}_{B_n}^{(j_n)} \right) dm_{j_n} \tag{2-19}$$

The total potential and strain energy of the ring-pack is determined from

$$\begin{aligned} V_2 = \frac{1}{2}\sum_{n=1}^{3}\Bigg\{ \sum_{j_n=1}^{8}\int_{0}^{R\Theta}\Bigg\{ & E_n A_{r_n}\left(\frac{\partial u_{j_n}}{\partial x_{j_n}} - \frac{v_{j_n}}{R}\right)^2 + E_n J_n \left(\frac{\partial \theta_{j_n}}{\partial x_{j_n}}\right)^2 \\ & + k_n A_n G_n \left(\frac{\partial v_{j_n}}{\partial x_{j_n}} - \theta_{j_n} + \frac{u_{j_n}}{R}\right)^2 + 2\rho_n A_n g \left(\underset{\sim}{r}_{p_{j_n}} \cdot \underset{\sim}{I}\right)\Bigg\} dx_{j_n} \Bigg\} \end{aligned} \tag{2-20}$$

The total virtual work of the ring-pack done by the non-conservative forces is given by

$$\begin{aligned} \delta W_r^{NC} = \sum_{n=1}^{3}\Bigg\{ & \sum_{j=1}^{8}\left(P_{2_n} - P_{1_n}\right) A_{r_n}^{top}\left(\underset{\sim}{k}_{\bar{j}'_n} \cdot \delta \underset{\sim}{r}^{*}_{r_{n_j}}\right) \\ & - \sum_{j=1}^{8}\left[P_{1_n}\delta_{r_n} + P_{2_n}\left(1-\delta_{r_n}\right)\right] A_{r_n}^{in}\left(\underset{\sim}{j}_{\bar{j}'_n} \cdot \delta \underset{\sim}{r}^{*}_{r_{n_j}}\right) \\ & + \sum_{j=1}^{8}\sum_{i=1}^{6} \underset{\sim}{F}^{cstr}_{n_{ij}} \cdot \delta \underset{\sim}{r}^{(L-R)}_{r_{n_{ij}}} + \sum_{j=1}^{8}\left(F^{imp}_{(P-R)_{n_j}} \underset{\sim}{\bar{n}}_n \right) \cdot \delta \underset{\sim}{r}^{*(P-R)}_{r_{n_j}} + \delta W_{r_n}^{Oil} \Bigg\} \end{aligned} \tag{2-21}$$

where δ_{r_n} is either 1 or 0 depending on whether the n^{th} ring is in contact with the lower or upper surfaces of its corresponding piston groove, respectively. P_{i_n} is the pressure in the i^{th} control volume surrounding the n^{th} ring (see Fig. 2-8).

Since the motion of the rings within their corresponding piston grooves can either be free or constrained then the ring-pack dynamic equations must satisfy constraint equations of the following form (see Fig. 2-9):

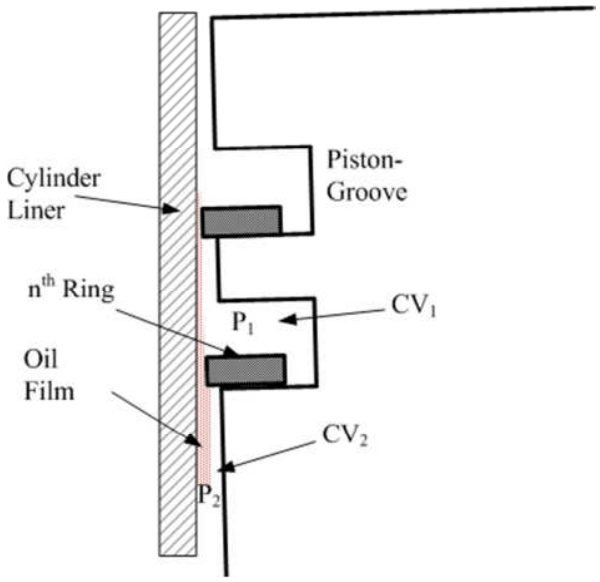

Fig. 2- 8 Schematic illustrating pressure notations for control volumes surrounding the rings.

$$\left(\delta \underset{\sim}{r}_{p_j}^{(P-R)} - \underset{\sim}{r}_{r_{n_j}}^{*(P-R)} \right) . \underset{\sim}{\bar{n}}_n = 0 \qquad (2\text{-}22)$$

where the number of the above constraint equations can range from 1 to three per ring depending on whether the ring has a single-point, double-point, or surface contact with the surfaces of its corresponding piston-groove, respectively.

The $\delta W_{r_n}^{Oil}$ term in Eq. (2-21) is the virtual work done by the oil film pressure and the friction forces associated with the elasto-hydrodynamic lubrication regime of the piston ring. This term will be derived in Chapter 3.

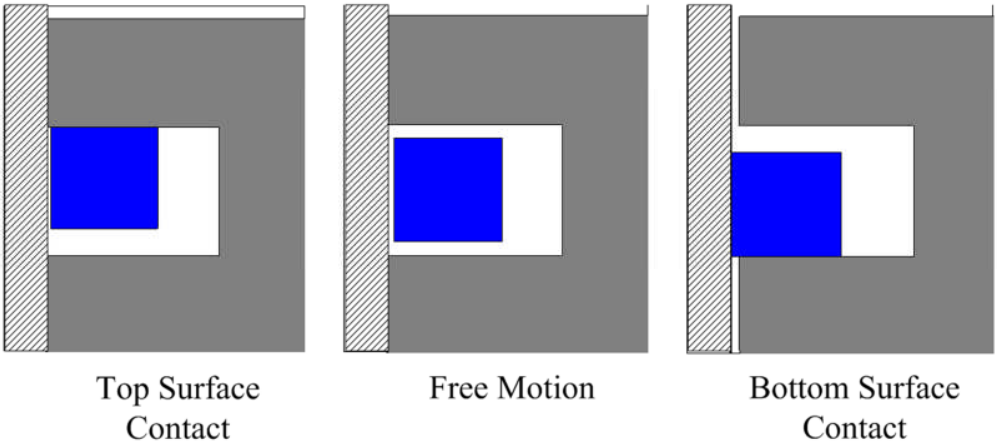

Fig. 2- 9 Free and constrained configuration of the ring within the groove.

2.1.3 Equations of Motion

The total kinetic energy of the crankshaft/connecting-rod/piston-assembly is obtained by adding Eqs. (2-4) and (2-19). Similarly, the total expression for the potential and strain energy of the system along with the total virtual work expressions are determined by adding Eqs. (2-5) to (2-20) and Eqs. (2-6) to (2-21), respectively. The equations of motion, derived by implementing the Lagrange principle, consists of 93 coupled, nonlinear, second order differential equations. Depending on the piston-liner, ring-liner and ring-groove interactions, a maximum of eleven constraint equations may be applied on the system. This

will result in a set of differential-algebraic (D-A) equations with a variable number of constraint equations. They can be written as

$$M\left(\underset{\sim}{q}\right)\ddot{\underset{\sim}{q}} + \underset{\sim}{F}\left(\underset{\sim}{q},\dot{\underset{\sim}{q}}\right) = \underset{\sim}{Q}^{NC} + p_1^T\left(\underset{\sim}{q}\right)\underset{\sim}{\lambda} \tag{2-23}$$

where $\underset{\sim}{\lambda}$ is the Lagrange multiplier vector. It is handled by implementing the numerical algorithm in Ref.[62] as follows

$$\underset{\sim}{\lambda} = -\left(s_1 M^{-1} s_1^T\right)^{-1}\left[\underset{\sim}{s}_2 + s_1 M^{-1}\left(\underset{\sim}{Q}^{NC} - \underset{\sim}{F}\right)\right] \tag{2-24}$$

where s_1 and $\underset{\sim}{s}_2$ are obtained by expressing the active constraint equations in the following differential form:

$$s_1\ddot{\underset{\sim}{q}} + \underset{\sim}{s}_2 = \underset{\sim}{0} \tag{2-25}$$

It should be pointed out that the number of entries of $\underset{\sim}{\lambda}$ is equal to the number of active constraint equations. The equations of motion are then converted to a set of first order nonlinear differential equations and solved numerically by implementing the Gear method [65].

2.2 Impact Formulation

In the impact formulation, the surfaces of the rings and the piston grooves are assumed to be smooth. It considers that the impact between the n^{th} ring and its respective piston groove occurs along the direction of the unit vector $\underset{\sim}{\bar{n}}_n$ (see Fig. 2-10). The latter is defined to be equal to $-\underset{\sim}{i}_7$ and $\underset{\sim}{i}_7$ when the ring collides with the top and the lower surfaces of the groove, respectively. By separately applying the equation of

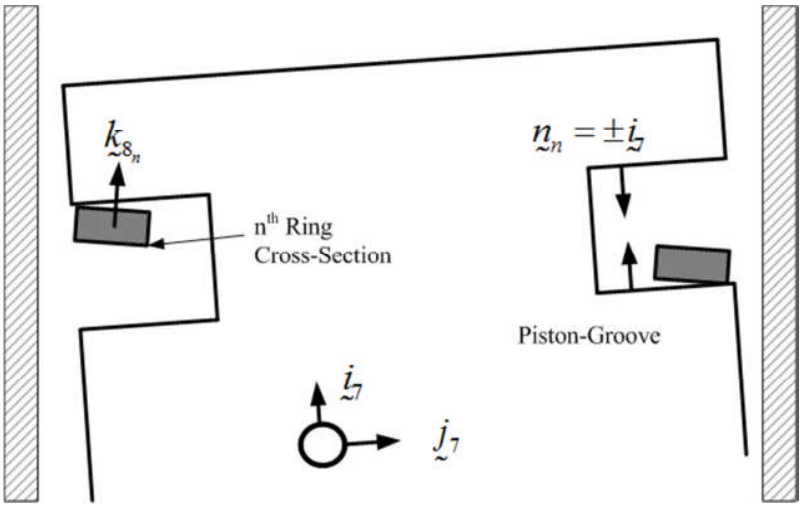

Fig. 2- 10 Schematic illustrating the normal vectors to the ring and the groove surfaces.

linear impulse and momentum along the $\bar{\underset{\sim}{n}}_n$ – direction on the n^{th} ring and the piston, one can write

$$m_{r_n} \dot{\underset{\sim}{r}}^*_{r_n}(t^+) \cdot \bar{\underset{\sim}{n}}_n = \left[m_{r_n} \dot{\underset{\sim}{r}}^*_{r_n}(t^-) + F^{imp}_{(P-R)_{n_j}} \bar{\underset{\sim}{n}}_n - P_{cyl} A^{top}_{r_n} \Delta t_{imp} \, \underset{\sim}{k}_8 \right] \cdot \bar{\underset{\sim}{n}}_n \qquad (2\text{-}26)$$

$$m_p \dot{\underset{\sim}{r}}^*_p(t^+) \cdot \bar{\underset{\sim}{n}}_n = \left[m_p \dot{\underset{\sim}{r}}^*_p(t^-) - F^{imp}_{(P-R)_{n_j}} \bar{\underset{\sim}{n}}_n - P_{cyl} A_p \Delta t_{imp} \, \underset{\sim}{i}_7 \right] \cdot \bar{\underset{\sim}{n}}_n \qquad (2\text{-}27)$$

where Δt_{imp} is the total duration of the impact during which P_{cyl} is considered to be constant. For the engine under consideration in this work, one has

$$\frac{A_{r_n}^{top}}{m_{r_n}} = 12.8\frac{A_p}{m_p} \tag{2-28}$$

Then, Eq. (2-27) can be simplified by neglecting the impulsive force, induced by the cylinder gas pressure, as follows

$$m_p \dot{\underset{\sim}{r}}_p^*(t^+)\cdot\bar{\underset{\sim}{n}}_n = \left[m_p \dot{\underset{\sim}{r}}_p^*(t^-) - F_{(P-R)_{n_j}}^{imp}\bar{\underset{\sim}{n}}_n \right]\cdot\bar{\underset{\sim}{n}}_n \tag{2-29}$$

Next, the definition of the coefficient of restitution, e, is applied on both the n^{th} ring and the piston. The resulting equations are then combined and the terms are rearranged in order to eliminate the velocity term of the contact point at the end of the compression period along the $\bar{\underset{\sim}{n}}_n$ – direction. This will yield to the following equation:

$$\left[\dot{\underset{\sim}{r}}_{p_j}^{(P-R)}(t^+) - \dot{\underset{\sim}{r}}_{r_{n_j}}^{*(P-R)}(t^+)\right]\cdot\bar{\underset{\sim}{n}}_n = \left\{ e\left[\dot{\underset{\sim}{r}}_{r_{n_j}}^{*(P-R)}(t^-) - \dot{\underset{\sim}{r}}_{p_j}^{(P-R)}(t^-)\right] + (1-e)P_{cyl}\frac{A_{r_n}^{top}}{m_{r_n}}\frac{\Delta t_{imp}}{2}\underset{\sim}{k}_8 \right\}\cdot\bar{\underset{\sim}{n}}_n \tag{2-30}$$

where the inertial velocities of the points of contact on the rings and the piston can be written as

$$\dot{\underset{\sim}{r}}_{r_{n_j}}^{*(P-R)}\Big|_{\{X,Y,Z\}} = \dot{\underset{\sim}{r}}_{r_n}^*\Big|_{\{X,Y,Z\}} + \left(\underset{\sim}{\omega}_{r_n}\times\underset{\sim}{r}_{O_{r_n}^* O_{j_n}^*}\right)\Big|_{\{x_8,y_8,z_8\}} \tag{2-31}$$

$$\dot{\underset{\sim}{r}}_{p_j}^{(P-R)}\Big|_{\{X,Y,Z\}} = \dot{\underset{\sim}{r}}_p^*\Big|_{\{X,Y,Z\}} + \left[\underset{\sim}{\omega}_p\times\left(\underset{\sim}{r}_{p_j}^{(P-R)} - \underset{\sim}{r}_p^*\right)\right]\Big|_{\{x_7,y_7,z_7\}} \tag{2-32}$$

Now the equations of angular impulse and momentum around the mass centers of the n^{th} ring and the piston can be written as

$$I_{r_n}\left[\underset{\sim}{\omega}_{r_n}(t^+)-\underset{\sim}{\omega}_{r_n}(t^-)\right]_{\{x_8,y_8,z_8\}}=\left(\underset{\sim}{r}_{O_{r_n}^{*}O_{j_n}^{*}}\right)_{\{x_8,y_8,z_8\}}\times F^{imp}_{(P-R)_{n_j}}\underset{\sim}{\bar{n}}_n \tag{2-33}$$

$$I_p\left[\underset{\sim}{\omega}_p(t^+)-\underset{\sim}{\omega}_p(t^-)\right]_{\{x_7,y_7,z_7\}}=\left(\underset{\sim}{r}^{(P-R)}_{p_j}-\underset{\sim}{r}^{*}_{p}\right)_{\{x_7,y_7,z_7\}}\times\left(-F^{imp}_{(P-R)_{n_j}}\underset{\sim}{\bar{n}}_n\right) \tag{2-34}$$

Note that the cylinder gas pressure is assumed to be uniform along the top surfaces of the n^{th} ring and the piston. This causes the moments due to P_{cyl}, around the mass centers of the n^{th} ring and the piston, to vanish. Also, one has

$$\begin{aligned}\underset{\sim}{\omega}_{r_n}&=-\dot{\phi}_n\sin(\psi_n)\underset{\sim}{I}+\dot{\phi}_n\cos(\psi_n)\underset{\sim}{J}+\dot{\psi}_n\underset{\sim}{K}\\&=(-\dot{\psi}_n\sin\phi_n)\underset{\sim}{i}_{8_n}+(\dot{\phi}_n)\underset{\sim}{j}_{8_n}+(\dot{\psi}_n\cos\phi_n)\underset{\sim}{k}_{8_n}\end{aligned} \tag{2-35}$$

$$\underset{\sim}{\omega}_p=(\dot{\theta}_{cs}+\dot{\beta}+\dot{\gamma})\underset{\sim}{k}_7=(\dot{\theta}_{cs}+\dot{\beta}+\dot{\gamma})\underset{\sim}{K} \tag{2-36}$$

Now, substitute Eqs. (2-26), (2-29), and (2-31) to (2-34) into Eq. (2-30) in order to eliminate all terms that need to be evaluated at t^+. Rearrange the terms and solve for the impulsive force. This will yield the following expression for $F^{imp}_{(P-R)_{n_j}}$

$$F^{imp}_{(P-R)_{n_j}}=\frac{(1+e)\left[\dot{\underset{\sim}{r}}^{(P-R)}_{p_j}(t^-)-\dot{\underset{\sim}{r}}^{*(P-R)}_{r_{n_j}}(t^-)\right]\cdot\underset{\sim}{\bar{n}}_n+0.5\,m_{r_n}^{-1}\Delta t_{imp}\,P_{cyl}\,A^{top}_{r_n}(e+1)\underset{\sim}{k}_{8_n}\cdot\underset{\sim}{\bar{n}}_n}{\left[m_p^{-1}+m_{r_n}^{-1}+I_p^{-1}\left\|\underset{\sim}{r}^{(P-R)}_{p_j}(t^-)\times\underset{\sim}{\bar{n}}_n\right\|^2+I_{r_n}^{-1}\left\|\underset{\sim}{r}^{*(P-R)}_{r_{n_j}}(t^-)\times\underset{\sim}{\bar{n}}_n\right\|^2\right]\Delta t_{imp}} \tag{2-37}$$

The above expression will then be used in Eqs. (2-6) and (2-21) in order to evaluate the virtual work expressions for the rings and the piston.

2.3 Summary

A detailed dynamic model for the crankshaft/connecting-rod/piston-assembly mechanism of a single cylinder IC engine has been presented in this Chapter. The focus has been restricted to the structural aspect of the problem whereby equations of motions governing the rigid body motion of the crank-slider mechanism and the rigid and flexible motions of the ring-pack have been derived. This model will be integrated with the solid-fluid model that will be discussed in the next Chapter in order to develop a tool that will be suitable to investigate the intricate dynamics of the piston-assembly along with its lubrication regimes.

CHAPTER 3

HYDRODYNAMIC AND ELASTO-HYDRODYNAMIC LUBRICATION REGIMES OF THE PISTON-ASSEMBLY

During an engine cycle, the piston-assembly is known to undergo boundary, mixed, and hydrodynamic lubrication regimes [66-74]. The current study focuses on the hydrodynamic lubrication regime of the piston-skirt and the elasto-hydrodynamic lubrication regime of the ring-pack. It considers the solid-fluid interaction between the piston-assembly and the oil film in a fully coupled manner. The structural component of the model affects the oil film by dictating its instantaneous thickness at any point and time along the piston-skirt and the ring-pack running surfaces. This is done herein by modeling the piston secondary motions, piston-slap and piston-tilting, along with the rigid and flexible motions of the rings. Moreover, the oil film will impact the motion of the piston-assembly through the instantaneous normal and tangential forces (friction forces) exerted on the running surfaces of the piston-assembly.

3.1 Assumptions of the Lubrication Regimes

In the current work, only hydrodynamic lubrication regime of the piston-skirt and the elasto-hydrodynamic lubrication regime of the ring-pack are considered. Boundary and mixed lubrication regimes have not been accounted for in this work. However, normal forces induced by metal-to-metal contact between the running surfaces of the rings and the liner, the rings and their respective piston grooves, the piston-skirt and the liner, have been accounted for through the constraint forces that are responsible for keeping the piston inside

the cylinder and confining the rings to their respective piston grooves. Moreover, since the formulation of the crank-slider mechanism treats the piston (without the ring-pack) as a rigid body then the lubrication regime between the piston-skirt and the liner is considered to be hydrodynamic. However, the rings in the current work have been considered to be independent deformable structures interacting with the piston grooves. This allows for the consideration of elasto-hydrodynamic lubrication regimes between the running surfaces of the ring-pack and the liner.

In deriving the oil film formulation, a 3-D and 1-D Reynolds' equations have been employed to model the hydrodynamic lubrication regime of the piston-skirt and the elasto-hydrodynamic lubrication regimes of the rings, respectively. Throughout these formulations, several assumptions were made that are in line with the work of Ref. [75]. The oil pressure across the oil film thickness is considered to be constant. The viscosity is assumed to be constant throughout the current work. The oil is assumed to be Newtonian undergoing fully-developed, steady, laminar flow. The oil particles at the solid-fluid interface are considered to move at the same speed as the solid surface. Furthermore, all body forces on the oil film are ignored.

3.2 Hydrodynamic Lubrication Regime of the Piston-Skirt

By applying the 3-D Reynolds' equation [75, 76] to the piston-skirt, one can write it with respect to polar coordinates as [58]:

$$3h^2\frac{\partial P_{ps}}{\partial x}\frac{\partial h}{\partial x}+h^3\frac{\partial^2 P_{ps}}{\partial x^2}+\frac{1}{R_P^2}\left(3h^2\frac{\partial h}{\partial \zeta}\frac{\partial P_{ps}}{\partial \zeta}+h^3\frac{\partial^2 P_{ps}}{\partial \zeta^2}\right)=6\eta V_P\frac{\partial h}{\partial x}+12\eta\frac{\partial h}{\partial t} \qquad (3-1)$$

where η is the dynamic viscosity of the fluid, h is the instantaneous oil film thickness defined by the clearance between the piston-skirt and the liner. V_P is the piston speed along the $\underset{\sim}{I}$ – direction. In addition, the last term in the above equation reflects the squeeze film effect.

The scheme used for solving Eq. (3-1) is exactly the same as the one used in Ref. [58]. It employs the finite difference method and considers both h and V_P to be known from the solution of the crank-slider mechanism equations of motion. The piston-skirt mesh is made up of 10 rows and 36 columns as shown in Figs. (3-1) and (3-2) [77]. The finite backward difference expression was used to approximate the squeeze film, $\frac{\partial h}{\partial t}$, term. Moreover, the finite central difference expression was used in the approximation of the spatial partial derivative terms. The reader is referred to Refs. [58, 77] for detailed discussions on the oil film formulation of the piston-skirt.

In the present work, the piston-skirt is considered to be fully flooded with oil with no occurrence of cavitation. The 3-D Reynolds' equation is then applied on all the nodes of the piston-skirt mesh by incorporating the above mentioned finite difference approximations. This resulted in 288 algebraic equations that had to be solved simultaneously in order to the compute the instantaneous oil film pressure distribution on the piston-skirt. The boundary conditions for the oil film are specified such that the nodal pressures at the first (top) and the last (tenth) rows of the mesh to be equal to that of the cylinder and crankcase gas pressures, respectively.

3.3 Elasto-Hydrodynamic Lubrication Regime of the Rings

The implementation of the 1-D Reynolds' equation [75, 76] to the n^{th} ring leads to the following equation:

$$3h_{r_n}^2 \frac{\partial P_{r_n}}{\partial x_{r_n}} \frac{\partial h_{r_n}}{\partial x_{r_n}} + h_{r_n}^3 \frac{\partial^2 P_{r_n}}{\partial x_{r_n}^2} = 6\eta V_{r_n} \frac{\partial h_{r_n}}{\partial x_{r_n}} + 12\eta \frac{\partial h_{r_n}}{\partial t} \qquad (3-2)$$

where h_{r_n} is the instantaneous oil film thickness defined by the clearance between the deformable configuration of the n^{th} ring and the liner. V_{r_n} is the speed of the n^{th} ring along the $\underset{\sim}{I}$ – direction. Note that the last term captures the squeeze film effect induced by the ring radial deformation.

Similar to the case of the piston-skirt, all rings are considered to be fully flooded with no cavitation formation in their oil films. Moreover, a mesh of 10 rows and 49 columns was defined for each ring of the ring-pack (see Fig. 3-2). The 1-D Reynolds' equation is applied on each node of the n^{th} ring mesh by implementing the finite central and backward difference expressions to approximate the spatial and temporal partial derivative terms, respectively. The resulting scalar algebraic equations can be written in the following general form:

$$\gamma_{r_{n_1}}(i,j)\, P_{r_n}(i,j)_t + \gamma_{r_{n_2}}(i,j)\, P_{r_n}(i+1,j)_t + \gamma_{r_{n_3}}(i,j)\; P_{r_n}(i-1,j)_t = \beta_{r_n}(i,j) \qquad (3-3)$$
$$for\ i = 2,\ldots,9 \ \ and \ \ \ j = 1,\ldots,49$$

where

$$\gamma_{r_{n_1}}(i,j) = \frac{-2}{\Delta x_{r_n}{}^2} h_{r_n}^3 (i,j)_t$$

$$\gamma_{r_{n_2}}(i,j) = 3\, h_{r_n}^2 (i,j)_t \frac{h_{r_n}(i+1,j)_t - h_{r_n}(i-1,j)_t}{4\left(\Delta x_{r_n}\right)^2} + h_{r_n}^3 (i,j)_t \frac{1}{\left(\Delta x_{r_n}\right)^2}$$

$$\gamma_{r_{n_3}}(i,j) = -3\, h_{r_n}^2 (i,j)_t \frac{h_{r_n}(i+1,j)_t - h_{r_n}(i-1,j)_t}{\left(2\,\Delta x_{r_n}\right)^2} + h_{r_n}^3 (i,j)_t \frac{1}{\left(\Delta x_{r_n}\right)^2}$$

$$\beta_{r_n}(i,j) = 6\eta \left(V_{r_n}\right)_t \frac{h_{r_n}(i+1,j)_t - h_{r_n}(i-1,j)_t}{2\,\Delta x_{r_n}} + 12\eta \frac{h_{r_n}(i,j)_t - h_{r_n}(i,j)_{t-1}}{\Delta t}$$

$$\Delta x_{r_n} = \frac{L_{r_n}}{Number\ of\ rows - 1}$$

Note that $i = 2, \ldots, 9$ and $j = 1, \ldots, 49$ because the boundary conditions for the oil film of the n^{th} ring are assigned such that the nodal pressures of the first (top) and the last (tenth) rows of the mesh are set to be equal to the pressures P_{1_n} and P_{2_n} of the control volumes surrounding the ring, respectively (see Fig. 3-3). These 392 algebraic equations per ring are solved simultaneously to yield the instantaneous oil film pressure distributions on the running-surfaces of the ring-pack.

3.4 Virtual Work of the Frictional and Normal Forces

The instantaneous oil film pressure distributions on the running-surfaces of the piston-skirt and the ring-pack are then used to compute the normal and the frictional losses exerted on the piston-assembly by the lubricating oil.

The local normal force applied on the (i,j) node of the piston-skirt, $\underset{\sim}{F}_{ij}^{ps}$, and the n^{th} ring, $\underset{\sim}{F}_{ij}^{r_n}$, are determined as follows [77]:

$$\underset{\sim}{F}_{ij}^{ps} = P_{ps}(i,j)\,S_{ps}(i,j)\,\underset{\sim}{\hat{n}}_{ij}^{ps} \tag{3-4}$$

$$\underset{\sim}{F}_{ij}^{r_n} = P_{r_n}(i,j)\,S_{r_n}(i,j)\,\underset{\sim}{\hat{n}}_{ij}^{r_n} \tag{3-5}$$

where $S_{ps}(i,j)$ and $S_{r_n}(i,j)$ are the piston-skirt and the n^{th} ring surface areas as defined in Ref. [77]. $\underset{\sim}{\hat{n}}_{ij}^{ps}$ is a unit vector normal to the piston-skirt surface at the $(i,j)^{\text{th}}$ node and pointing inward. It is also expressed with respect to the $\{x_7, y_7, z_7\}$ coordinate system. $\underset{\sim}{\hat{n}}_{ij}^{r_n}$ is a unit vector normal to the n^{th} ring surface at the $(i,j)^{\text{th}}$ node and pointing inward. It is defined with respect to the $\left\{x_{\bar{j}_n}', y_{\bar{j}_n}', z_{\bar{j}_n}'\right\}$ coordinate system.

The local friction force at the (i,j) node of the piston-skirt, $\underset{\sim}{f}_{ij}^{ps}$, and the n^{th} ring, $\underset{\sim}{f}_{ij}^{r_n}$, are computed from:

$$\underset{\sim}{f}_{ij}^{ps} = \tau_{ps}(i,j)\,S_{ps}(i,j)\,\underset{\sim}{i}_7 \tag{3-6}$$

$$\underset{\sim}{f}_{ij}^{r_n} = \tau_{r_n}(i,j)\,S_{r_n}(i,j)\,\underset{\sim}{\bar{k}}_n' \tag{3-7}$$

where $\tau_{ps}(i,j)$ and $\tau_{r_n}(i,j)$ are the shear stresses at the $(i,j)^{th}$ node on the piston-skirt and the n^{th} ring surfaces, respectively. They are determined by employing the Newton's law of viscous flow [58].

The virtual work done by the normal and friction nodal forces on both the piston-skirt and the n^{th} ring can be obtained from

$$\delta W_p^{Oil} = \sum_{j=1}^{36}\sum_{i=1}^{10} R_{\{X,Y,Z\}}^{\{x_7,y_7,z_7\}} \left(\underset{\sim}{F}_{ij}^{ps} + \underset{\sim}{f}_{ij}^{ps} \right).\delta \underset{\sim}{r}_{p_{ij}} \tag{3-8}$$

$$\delta W_{r_n}^{Oil} = \sum_{j=1}^{49}\sum_{i=1}^{10} R_{\{X,Y,Z\}}^{\left\{x_{\bar{j}_n'}, y_{\bar{j}_n'}, z_{\bar{j}_n'}\right\}} \left(\underset{\sim}{F}_{ij}^{r_n} + \underset{\sim}{f}_{ij}^{r_n} \right).\delta \underset{\sim}{r}_{r_{n_{ij}}} \tag{3-9}$$

where $\underset{\sim}{r}_{p_{ij}}$ and $\underset{\sim}{r}_{r_{n_{ij}}}$ are expressed with respect to the inertial frame. δW_p^{Oil} and $\delta W_{r_n}^{Oil}$ are used in Eqs. (2-6) and (2-21), respectively, in order to capture the effects of the lubricating oil film on the intricate dynamics of the piston-assembly.

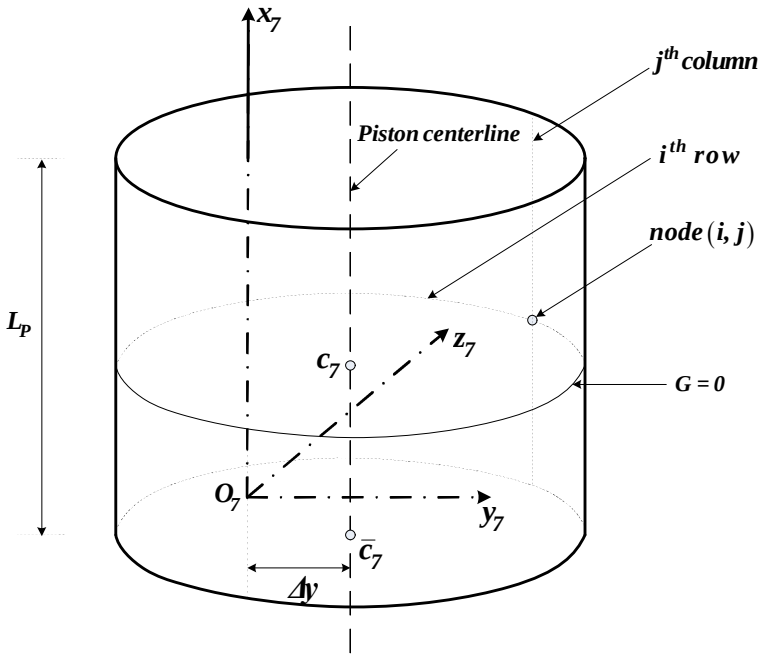

Fig. 3- 1 Piston-skirt and its local coordinates. (Adopted from Ref.[77])

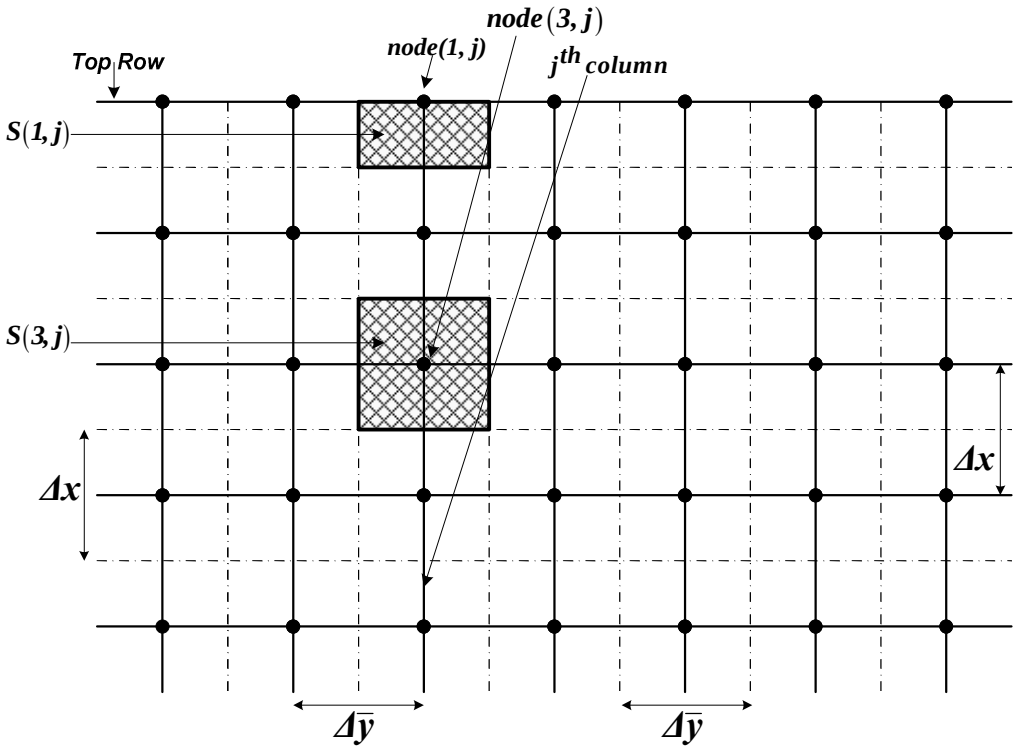

Fig. 3- 2 Mesh of an unrolled piston-skirt. Adopted from Ref.[77]

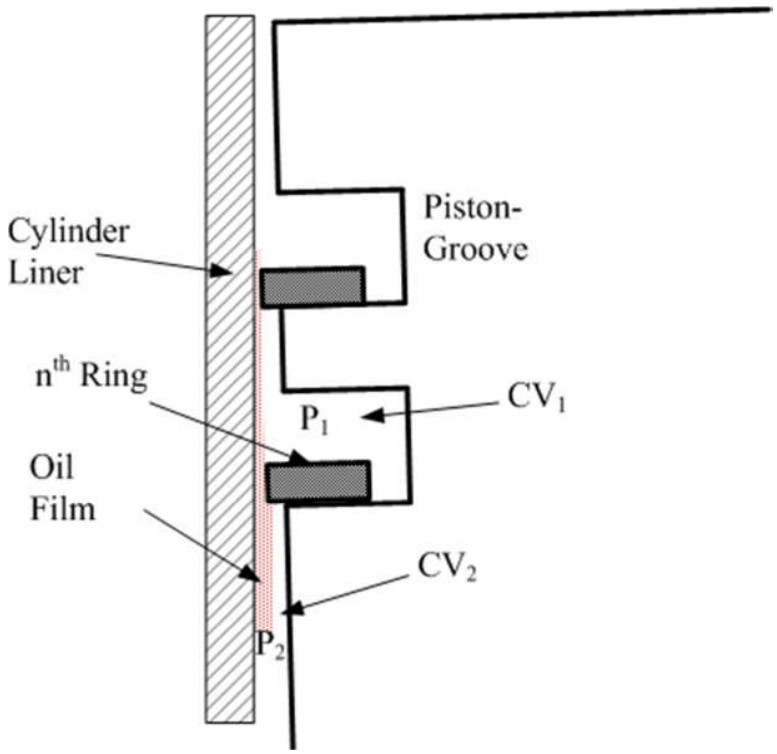

Fig. 3- 3 Schematic of the control volumes surrounding the n^{th} ring.

3.5 Summary

Only the hydrodynamic lubrication regime of the piston-skirt and the elasto-hydrodynamic lubrication regime of the ring-pack have been considered in this study. A 3-D Reynolds' equation has been employed for determining the oil film pressure distribution on the piston-skirt. Moreover, a 1-D Reynolds' equation has been used to compute the oil film pressure distribution on the running surfaces of the rings. In both cases, the Reynolds equations have been solved by using the finite difference method. Newton's law of viscous flow has been implemented to determine the shear stresses at the interface between the piston-assembly and the oil film. These stresses were used in the calculation of the hydrodynamic and elasto-hydrodynamic frictional forces on the piston-skirt and the running surfaces of the rings, respectively. The virtual work done on the piston-assembly by the normal and frictional forces of the oil film will then be combined with the formulation of Chapter 2 in order to consider the effects of the oil film on the intricate dynamics of the piston-assembly.

In the next Chapter, the simulation results, generated based on the model developed in Chapters 2 and 3, will be presented and analyzed.

CHAPTER 4
DIGITAL SIMULATION RESULTS

The formulations of Chapters 2 and 3 are fully integrated in this Chapter in order to carry out the digital simulations. The numerical results accounts for the coupled dynamics of the crankshaft/connecting-rod/piston mechanism, the ring-pack, and the solid-fluid interactions at the interface between the lubricating oil film and the running surfaces of the piston-skirt and rings. The simulation results serve to demonstrate the capability of the current tool in predicting the piston primary and secondary motions, the dynamic behavior of the rings within their respective grooves, the oil film pressure distribution along the running surfaces of the piston-skirt and the rings, the hydrodynamic and elasto-hydrodynamic frictional losses of the skirt and the rings, respectively.

4.1 Integrated Model of the Crankshaft/Connecting-rod/Piston-Assembly

In Chapter 2, the equations governing the rigid body motion of the crankshaft/connecting-rod/piston mechanism and the rigid and flexible motions of the rings are covered in details. Moreover, the formulation accounts for the piston-liner, ring-liner, and ring-groove interactions. Therefore, the formulation of Chapter 2 is mostly concerned with the structural dynamics aspect of the problem. In order to account for the oil film effect on the structural dynamics of the crank-slider mechanism, two terms, δW_p^{Oil} and $\delta W_{r_n}^{Oil}$, were introduced in the virtual work expressions of the piston and the rings in Eqs. (2-6) and (2-21), respectively. These terms reflect the virtual work performed by the normal (induced by the oil film pressure) and friction forces on the skirt and the rings. To

account for the effect of structural dynamics of the system on the oil film pressure distribution, the oil film thickness between the skirt and the liner is determined from the instantaneous location and orientation of the piston within the cylinder. Similarly, the instantaneous locations and orientations of the deformed rings within their respective grooves are used in the calculation of the thicknesses of the oil films between the rings and the liner. Note that the ring-groove interaction in this study ignores the presence of any oil film.

Moreover, the frictional losses, associated with the loaded bearings, auxiliaries and unloaded bearings along with the valve train, are included in this work by implementing the formulation in Ref. [78]. The equations for determining the frictional losses are presented in Tables 4-1 and 4-2.

4.2 Simulation Results

The capability of the model, in predicting the intricate dynamics of the crankshaft/connecting-rod/piston mechanism, the piston secondary motions, the translational and rotational motions of the rings within their respective grooves, the longitudinal and in-plane transverse deformations of the ring, the hydrodynamic frictional losses of the piston-skirt, and elasto-hydrodynamic frictional losses of the deformable rings, will be demonstrated herein through digital simulations. The theoretical results were generated based on the material properties and geometric dimensions of the crankshaft, connecting-rod, piston, and ring-pack that are listed in Tables 4-3 to 4-6. These dimensions are obtained from a research engine whose cylinder and piston were modified in-house [79]. The initial speed of the crankshaft was selected to be 3500 rpm. The profiles of

the cylinder gas pressure under engine firing conditions, the inter-ring clearance pressure, and the crankcase pressure are shown in Fig. 4-1. Note that the cylinder gas pressure trace represents experimental data that was generated on another engine. Moreover, the initial profile of the ring in-plane transverse deformation is illustrated in Fig. 4-2. This profile was determined from the steady-state solution of a simulation that only considered the ring dynamic response to the liner constraint forces with the initial ring profile being the free-shape or un-deformed configuration of the ring.

Valve train	$F_{vt} = 0.26 n_{valve} SL / \sqrt{\dot{\theta}}$
Auxiliaries and unloaded bearings	$T_a = 9.6 \eta \dot{\theta}$
Loaded bearings	$T_{lb} = 0.5(\pi/4) D^2 P_{cyl} \lvert\cos\theta\rvert (d_1/2) / \sqrt{\dot{\theta}}$

Table 4-1 Frictional losses of various engine components [78].

Main journal bearing diameter	$d_1 = 0.0319m$
Valve spring load	$SL = 225N$
Number of valves used	$n_{valve} = 2$
Viscosity of the oil	10.35 mPa.s

Table 4-2 Parameters used in calculating frictional losses of engine components.

Crankshaft Beam Element	Length, L_i (m)	Area, A_i (m^2)	Mass Moment of Inertia $(Kg.m^2)$
1	157.34×10^{-3}	7.99×10^{-4}	1.76×10^{-4}
2	44×10^{-3}	16.67×10^{-4}	7.615×10^{-4}
3	28.46×10^{-3}	8.71×10^{-4}	4.01×10^{-4}
4	44×10^{-3}	16.67×10^{-4}	7.615×10^{-4}
5	172×10^{-3}	5.84×10^{-4}	0.834×10^{-4}
Connecting-Rod	167×10^{-3}	7.5×10^{-4}	17.87×10^{-4}

Table 4-3 Geometric dimensions and mass moments of inertia for the crankshaft elements and the connecting-rod.

Piston	
Piston length	*47.8 mm*
Piston diameter	*59.72 mm*
Piston groove height	*3 mm*
Piston pin offset	*0.446 mm*
Bore diameter	*59.96 mm*
Rings	
Un-deformed radius	30.53 *mm*
Rectangular cross section (width x height)	*2.49 mm ×2.38 mm*
Gap angle (ring free shape)	*16.16°*
Crank-Slider Mechanism	
Crank radius	*44 mm*
Connecting-rod length	*167.34 mm*

Table 4-4 Geometric dimensions of the crank-slider mechanism.

Crankshaft density	$\rho_{cs} = 7800\, Kg/m^3$
Connecting-rod density	$\rho_{cr} = 2710\, Kg/m^3$
Ring Modulus of elasticity	$E_r = 131\times10^9\, N/m^2$
Shear Modulus of elasticity	$G_r = 52.4\times10^9\, N/m^2$
Density	$\rho_r = 7469\ \mathrm{Kg}/\ m^3$

Table 4-5 Material properties of the crankshaft, the connecting-rod, and the ring.

	Mass (Kg)	**Center of mass offset** (m)	**Mass moment of inertia** $(Kg.m^2)$
Flywheel	$m_f = 12.5$	0	0.1478
Counterweights 1 and 2	$m_{cw1} = m_{cw2} = 0.82$	0.041530	0.002
Crankgear	$m_{cw1} = m_{cw2} = 0.82$	0	0.062
Piston	$m_p = 0.6368$	0.0126300	3.27×10^{-4}

Table 4-6 Mass, offsets, and mass moment of inertia of various engine components.

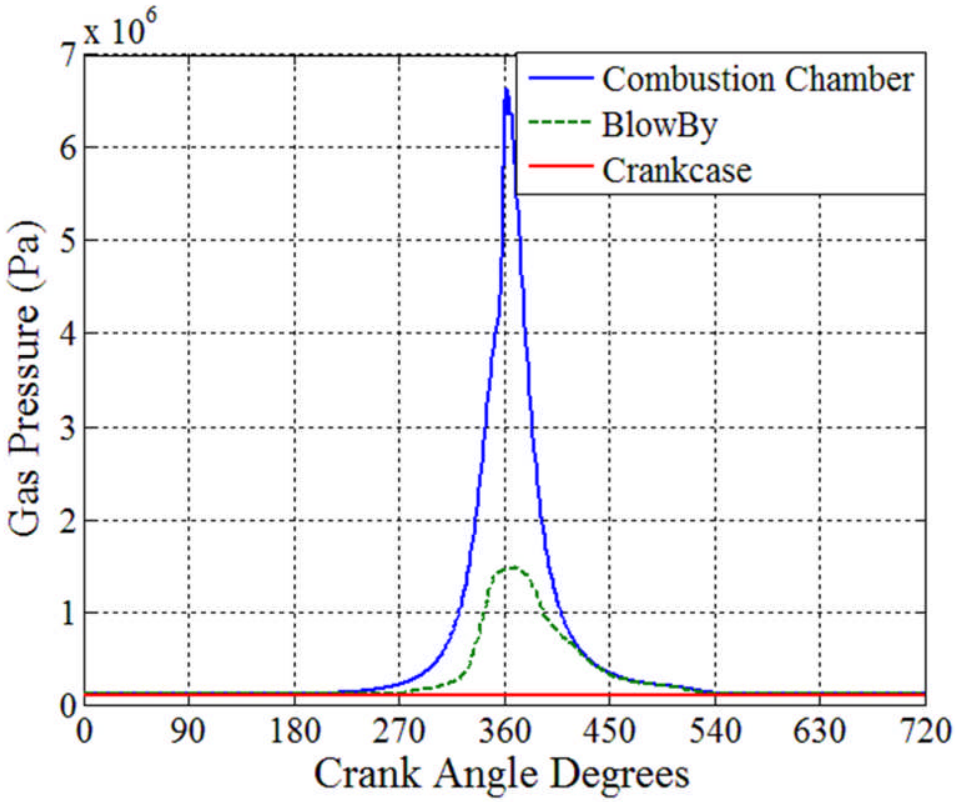

Fig. 4- 1 Pressure traces of the combustion chamber, the inter-ring clearance, and the crankcase.

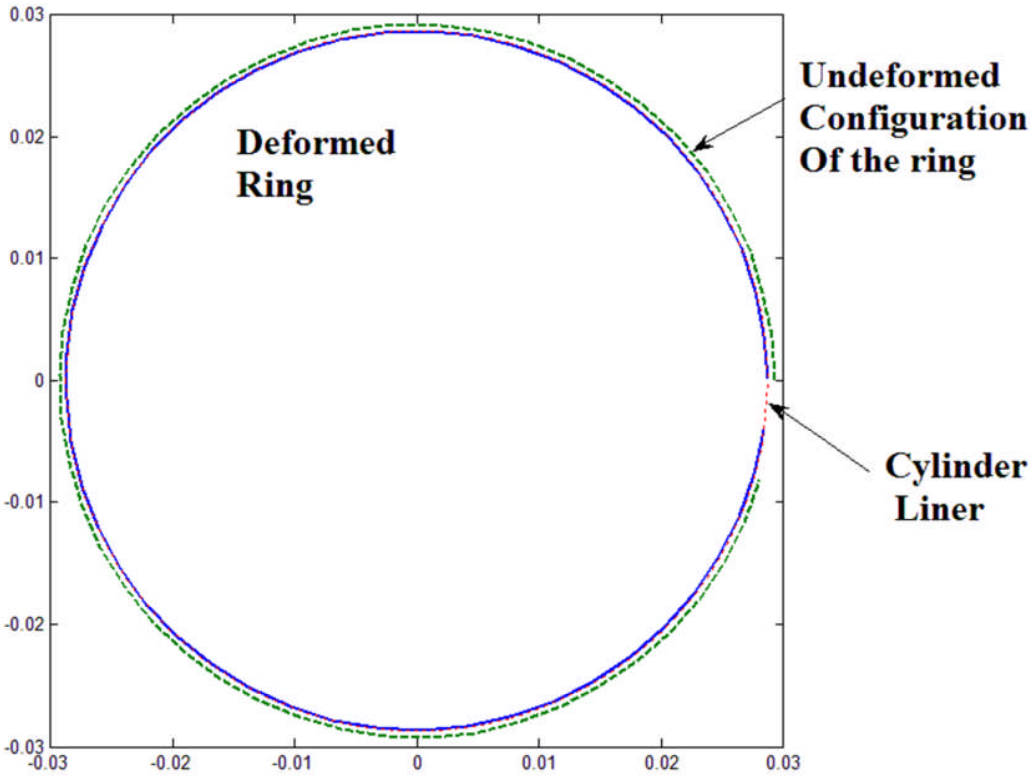

Fig. 4- 2 Initial deformed configuration of the ring.

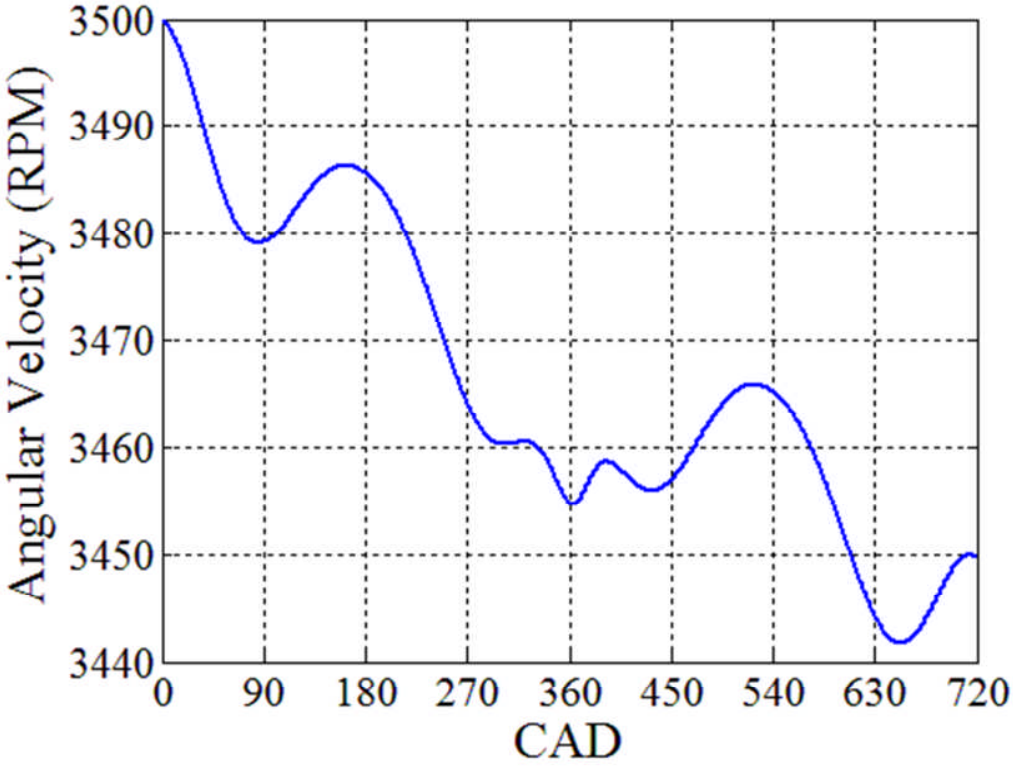

Fig. 4- 3 Angular velocity of the crankshaft.

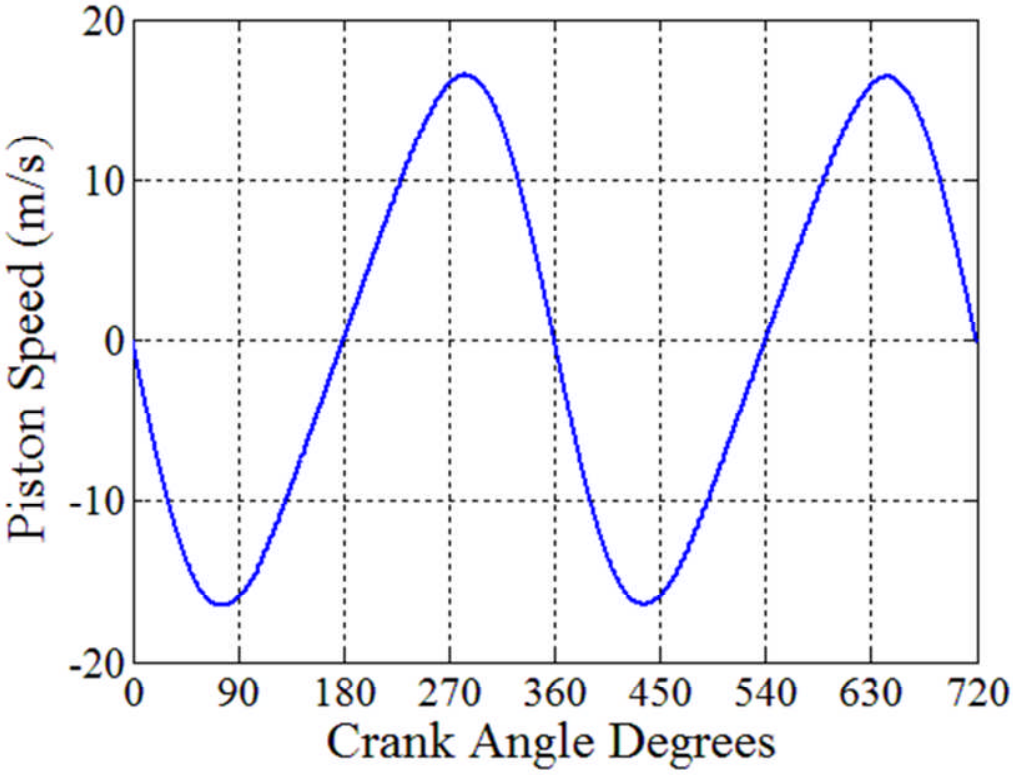

Fig. 4- 4 Piston speed.

The angular velocity of the crankshaft and the piston speed are shown in Figs. 4-3 and 4-4, respectively. Figure 4-3 reveals that the results pertain to a transient case where the engine is in a decelerating mode.

The piston tilting angle and the locations of its four corners are illustrated in Figs. 4-5 and 4-6. Note that a negative value of the tilt angle reflects a rotation of the piston toward the anti-thrust side (left side). Figure 4-5 reveals that the piston undergoes gradual, rather than abrupt, decrease and increase in its tilting angle during the compression and expansion strokes, respectively. This is in sharp contrast to the piston tilt pattern obtained when only the first compression ring was considered and the oil film effect was ignored (see discussion in the next section). Therefore, the gradual variations in the piston tilt angle can be attributed to the piston support provided by the rings through the ring-groove interactions as well as to the viscous damping effect provided by the oil film along the running surfaces of the skirt and the ring-pack. The significant difference in the tilt angle profiles observed in Fig. 4-5 and Fig. 4-31 of the next Section serves to highlight the importance of the effects of ring dynamics on the dynamic behavior of the piston secondary motions. Such an effect has been overlooked by previous research studies.

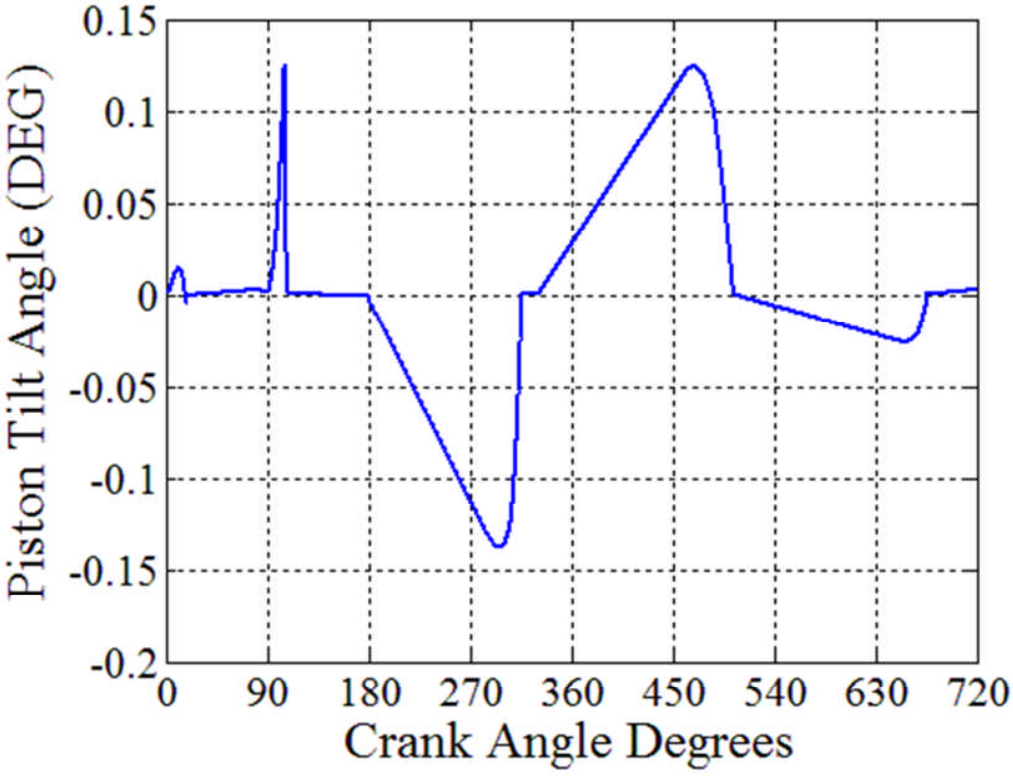

Fig. 4- 5 Piston tilt angle.

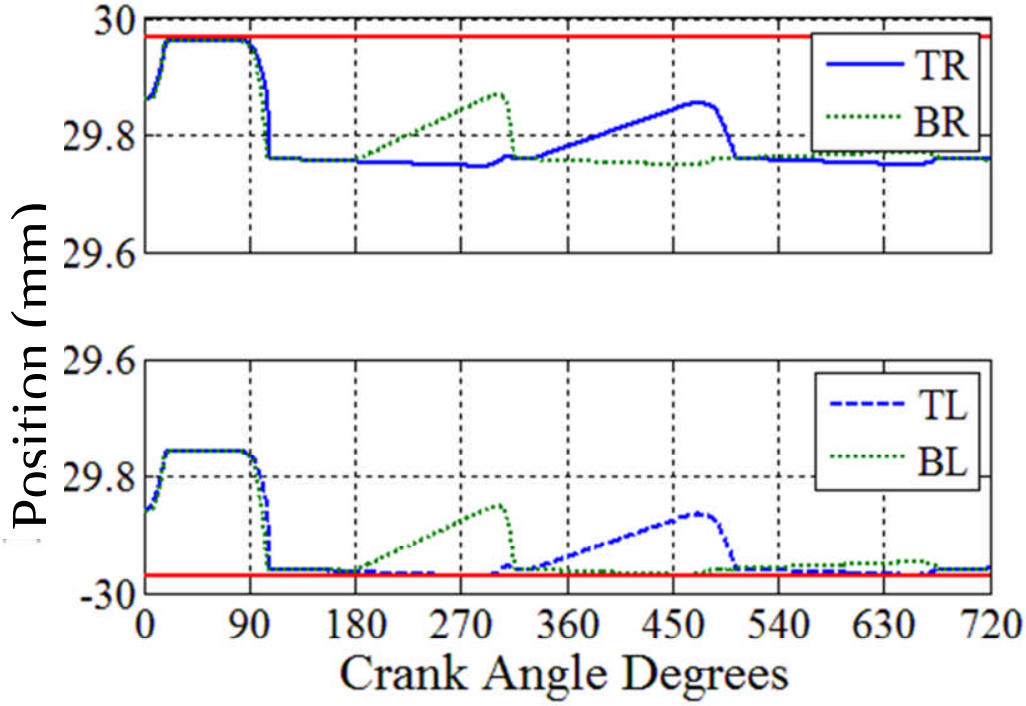

Fig. 4- 6 Piston lateral motion at top right (TR), top left (TL), bottom right (BR), and bottom left corners.

The tilting angles of the rings relative to the piston orientation around the $\underset{\sim}{K}-$ direction are shown in Figs. 4-7 to 4-9, while the absolute tilting angle of the rings around the $\underset{\sim}{J}-$ direction are shown in Figs. 4-10 to 4-12. These figures reveal that the tilting angle of the rings around the $\underset{\sim}{J}-$ direction, commonly ignored in research studies, are as significant as the tilting angle of the ring around the $\underset{\sim}{K}-$ direction.

Figures 4-13 to 4-15 show the axial motions of the rings within their respective grooves. The initial axial locations of the rings within their respective grooves are different. They are selected so that none of the rings are in touch with their grooves. Each figure exhibits the locations of the highest and lowest points on the ring in the axial direction during the entire engine cycle. To analyze the results, consider the axial motions of the first and second compression rings (see Figs. 4-13 and 4-14). As the piston moves downward during the intake stroke, the upper surfaces of the grooves collide with the rings and drag them downward with the piston for a certain period of the intake stroke. Note that each ring has a different period. The rings remain in contact with the upper surfaces of the grooves as long as the piston speed keeps on increasing. As the piston reaches its maximum speed and starts decelerating, the rings will separate from the surfaces of their respective grooves at different moments. This is because the rings have different inertial forces, gas pressures, normal and friction forces induced by their respective oil films. The momentums and the gas pressure differentials between the top and bottom surfaces enable the rings to reach the lower surfaces of the grooves and stick to them for the remainder of the intake

stroke. This configuration persists throughout the compression and expansion strokes where the dominant loads on the rings are due to gas pressure differentials between their top and bottom surfaces. This configuration remains till the exhaust valve opens and causes the cylinder gas pressure to drop to a level where the role of the inertial forces becomes significant; thus, causing the rings to separate from the lower surfaces of their respective grooves (see Figs. 4-13 and 4-14).

However, this trend of ring axial motion becomes significantly different in the case of the oil control ring (see Fig. 4-15). This is because the gas pressures for both top and bottom surfaces of the ring have been set to the crankcase pressure. Thus, the inertial forces become the dominant factor that governs the dynamic behavior of the oil control ring.

Figures 4-16 to 4-19 illustrate the hydrodynamic friction force on the piston-skirt and the elasto-hydrodynamic friction forces associated with the rings. The hydrodynamic friction force of the piston-skirt is consistent with what has been observed in the literature. During the intake and exhaust strokes, the friction force increases in magnitude as the piston speed increases and vice versa (see Fig. 4-16). The notch observed after 90 CAD is induced by an abrupt change in the piston tilt angle. However, the trend of the friction force becomes different in the later portion of the compression stroke and early portion of the power stoke due to the dominant role played by the cylinder gas pressure.

Figure 4-17 reveals that the elasto-hydrodynamic friction force of the first compression ring is dominated by the back gas pressure, which is considered to

be that of the combustion chamber. This is the reason for its highest values occurring near TDC under a firing engine condition. However, the inertial forces effects seem to be more pronounced in the elasto-hydrodynamic friction force of the second compression

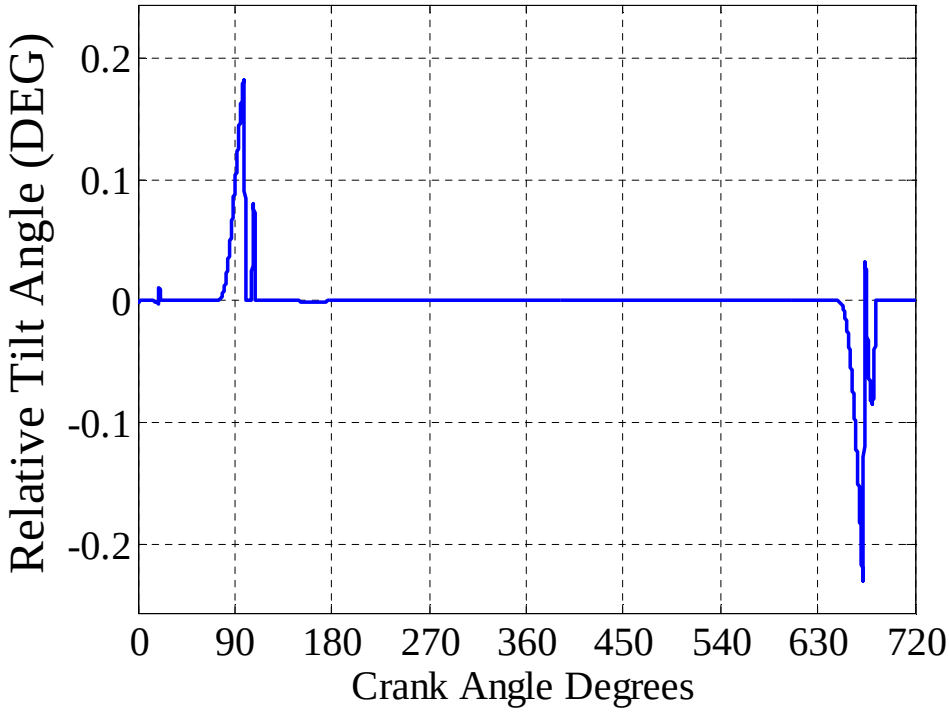

Fig. 4- 7 Relative tilt angle of the first compression ring with respect to the piston around the $\underset{\sim}{K}$ – direction.

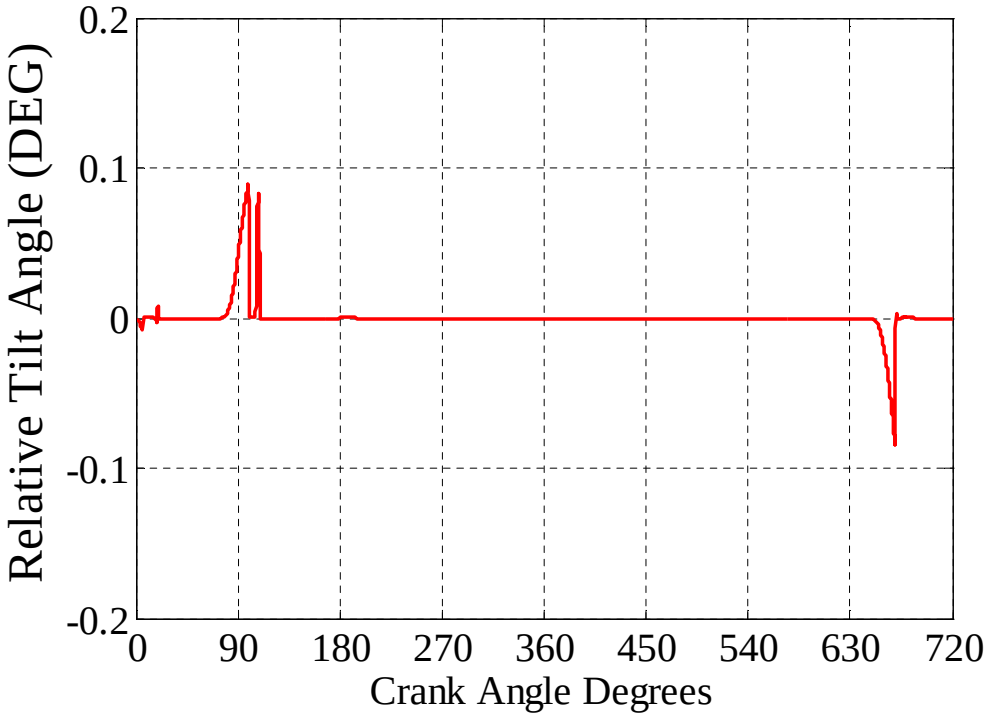

Fig. 4- 8 Relative tilt angle of the second compression ring with respect to the piston around the $\underset{\sim}{K}$ – direction.

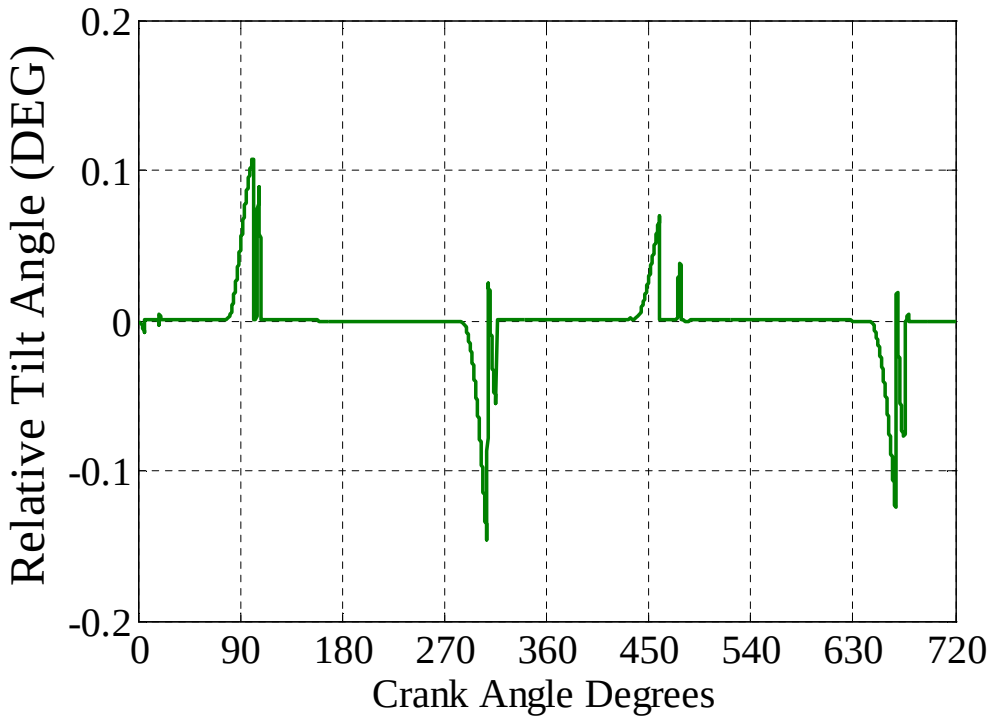

Fig. 4- 9 Relative tilt angle of the oil control ring with respect to the piston around the $\underset{\sim}{K}$ – direction.

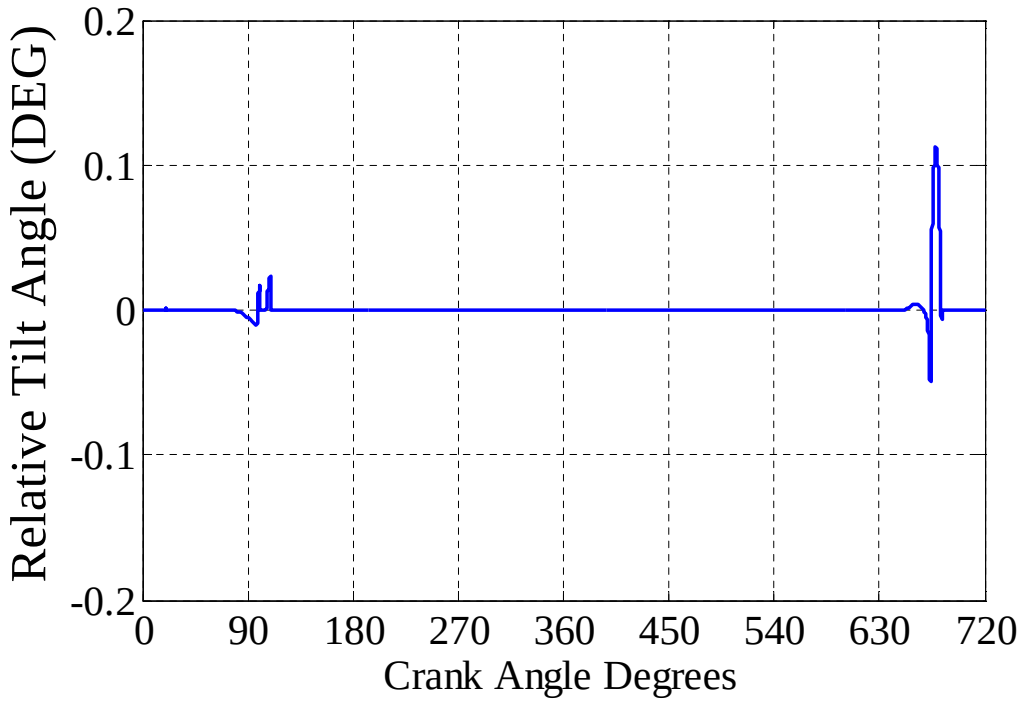

Fig. 4- 10 Tilt angle of the first compression ring around the $\underset{\sim}{J}$ – direction

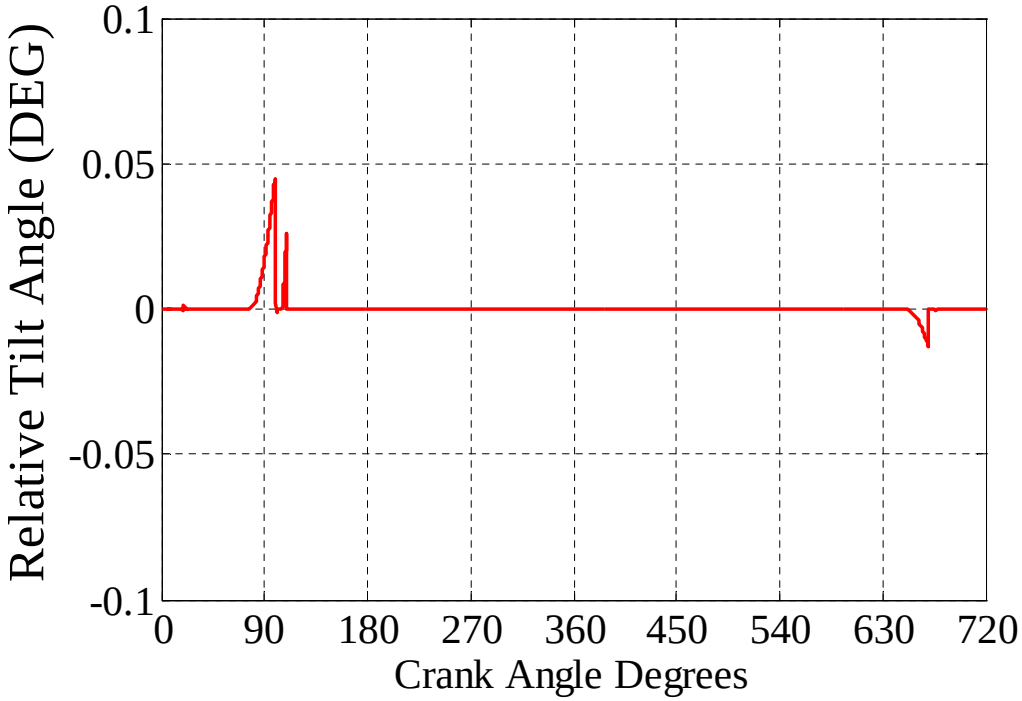

Fig. 4- 11 Tilt angle of the second compression ring around the $\underset{\sim}{J}$ – direction.

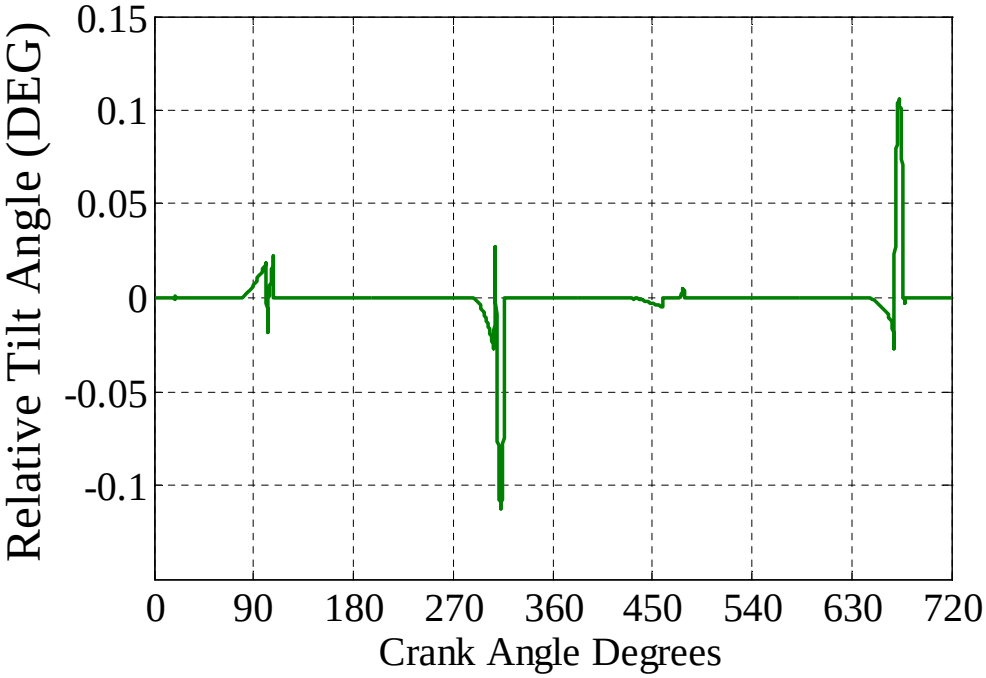

Fig. 4- 12 Tilt angle of the oil control ring around the $\tilde{J}$ – direction.

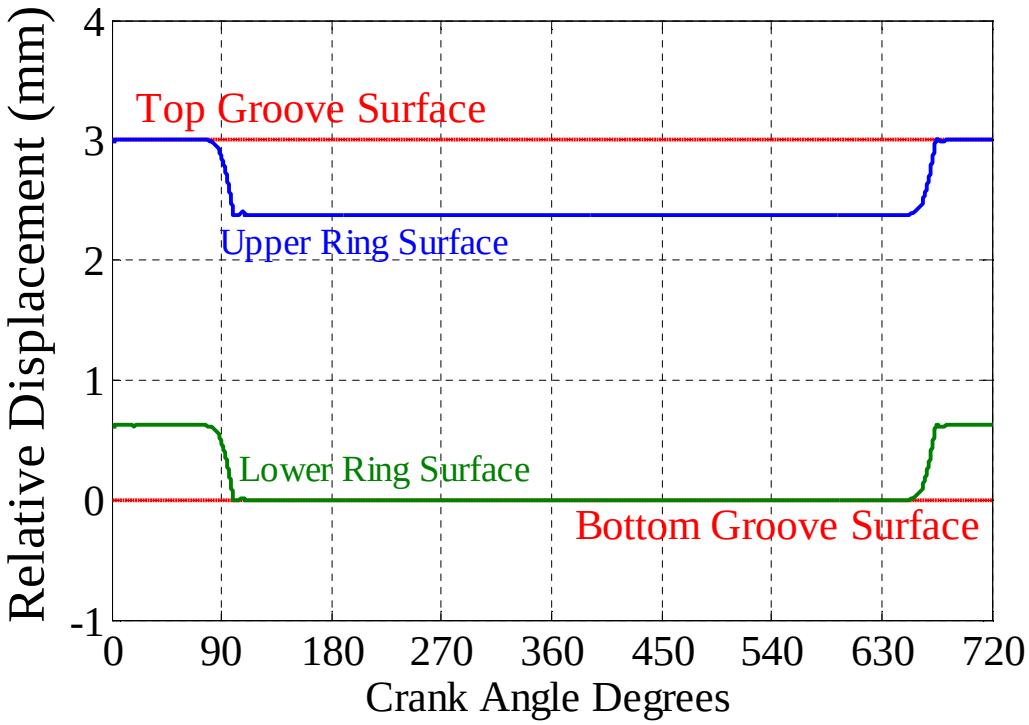

Fig. 4- 13 Axial motion of the first compression ring within the groove.

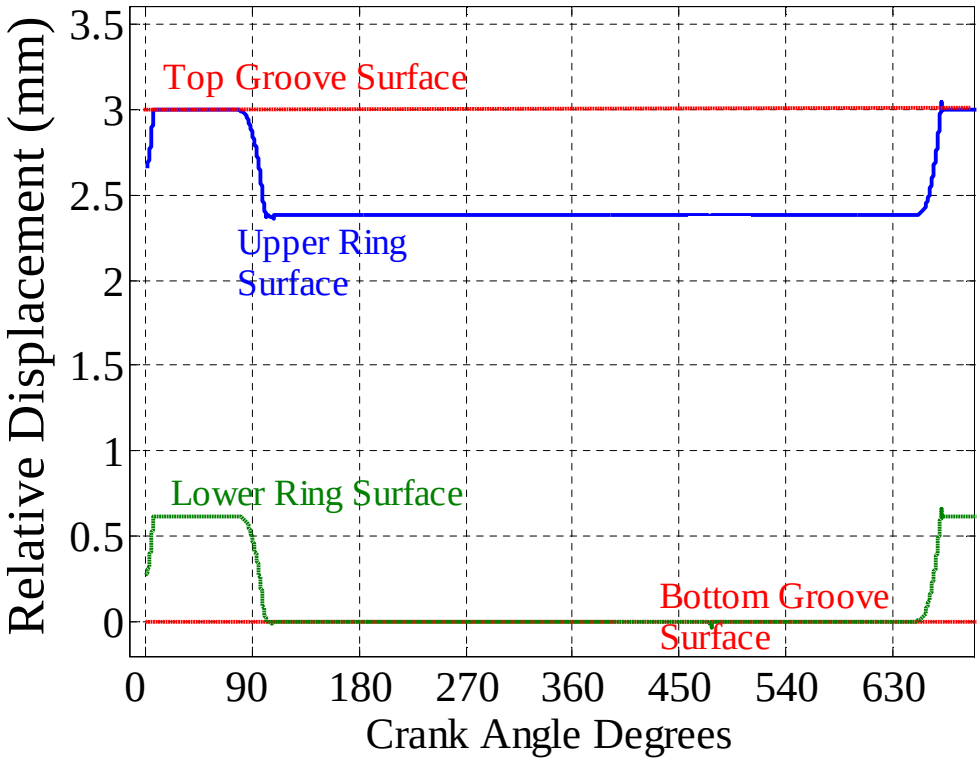

Fig. 4- 14 Axial motion of the seond compression ring within the groove.

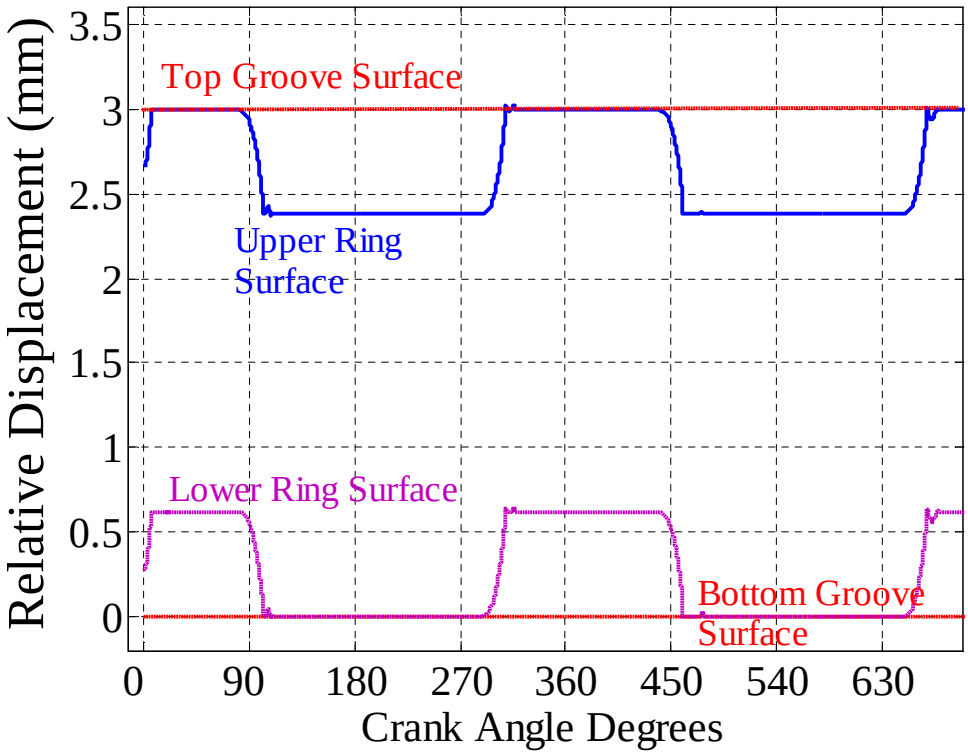

Fig. 4- 15 Axial motion of the oil control ring within the groove.

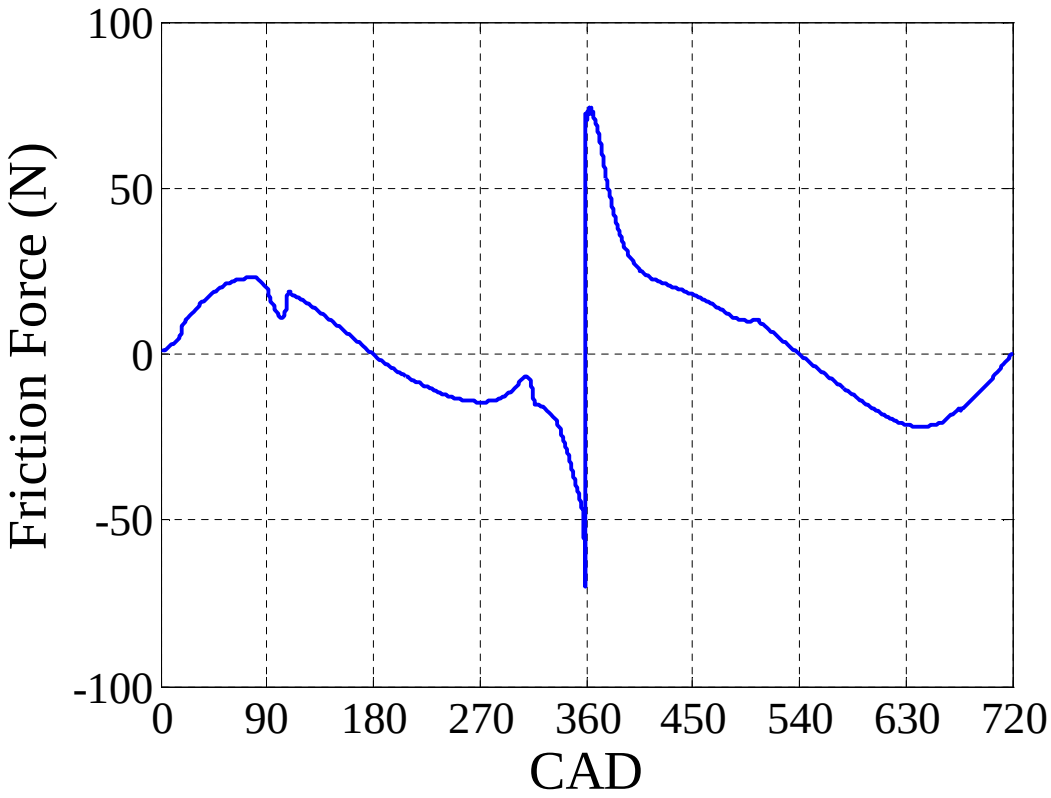

Fig. 4- 16 Hydrodynamic friction force of the piston-skirt.

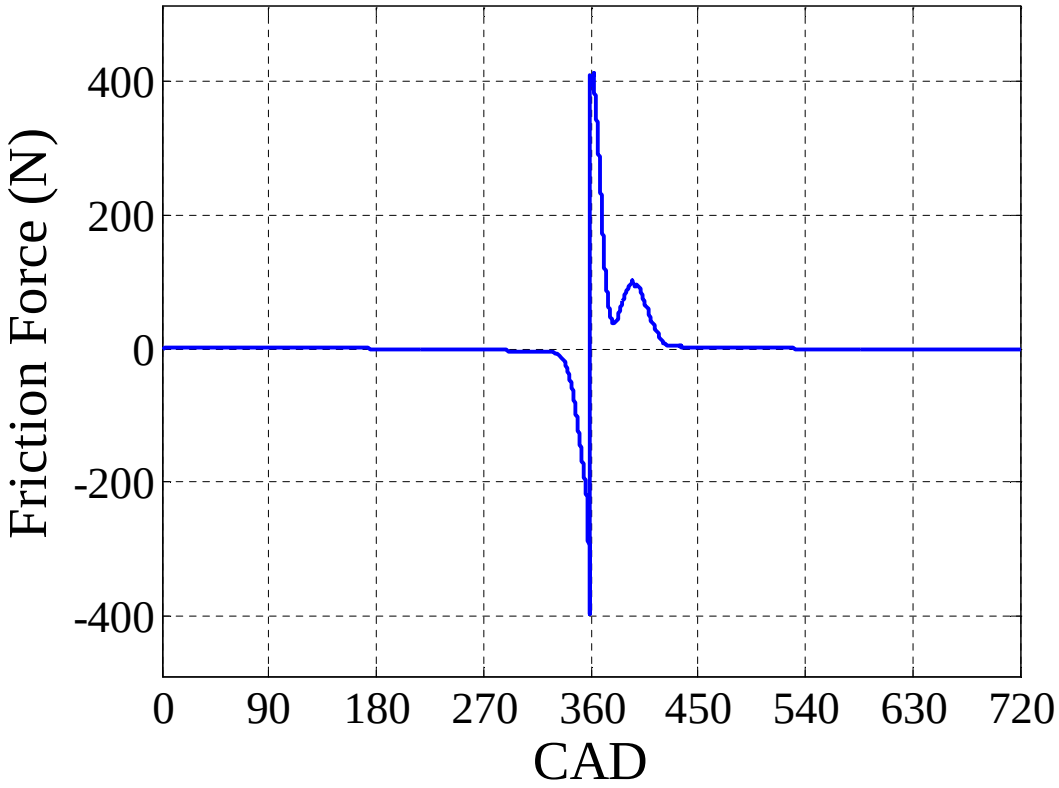

Fig. 4- 17 Elasto-hydrodynamic friction force of the first compression ring.

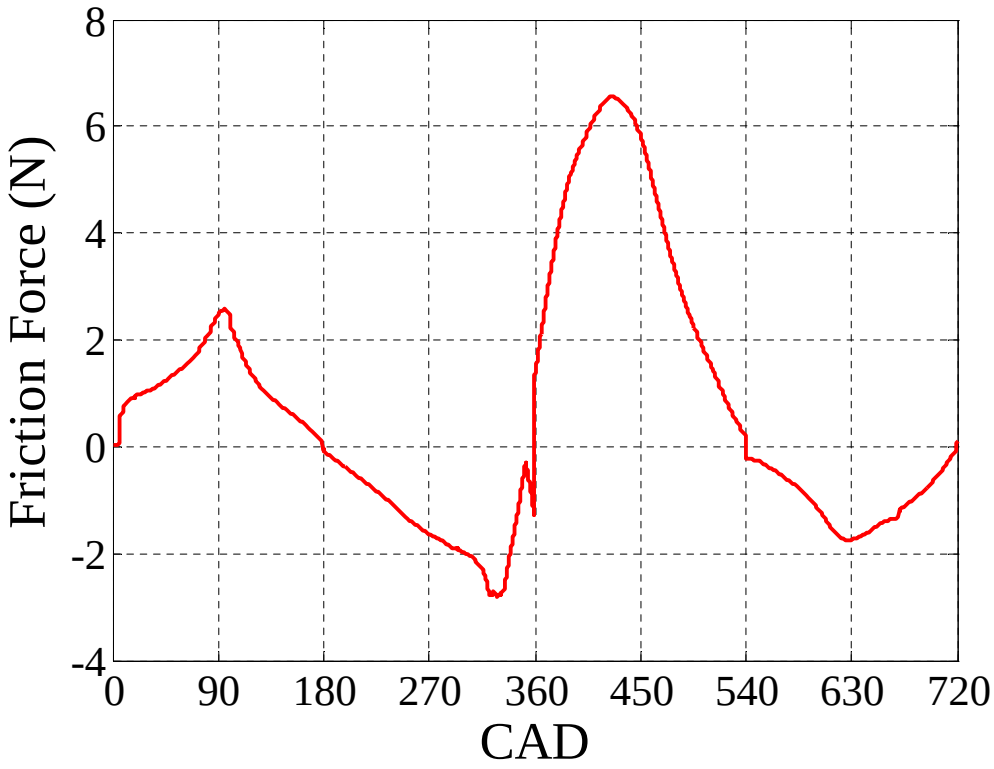

Fig. 4- 18 Elasto-hydrodynamic friction force of the second compression ring.

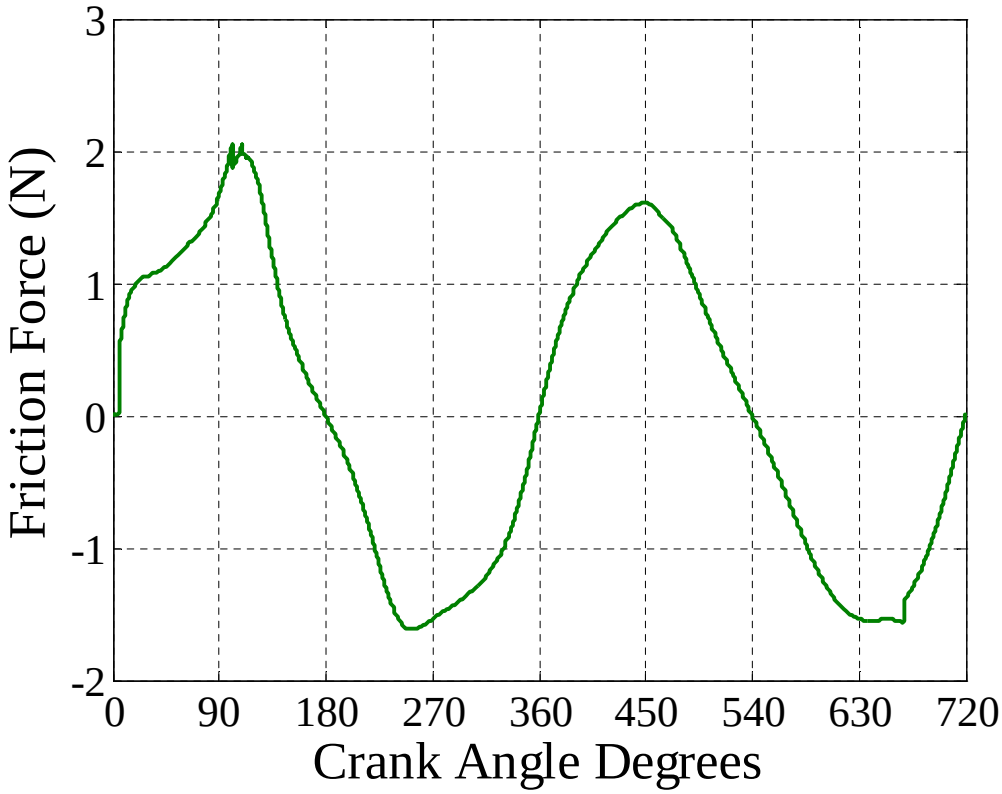

Fig. 4- 19 Elasto-hydrodynamic friction force of the oil control ring.

ring, which has a significantly less back gas pressure (see Fig. 4-18). In the case of the oil control ring (see Fig. 4-19), the elasto-hydrodynamic friction force is completely dominated by inertial forces since its back gas pressure is set to be atmospheric.

By considering the simulation results at 295^{o} CAD, the piston tilting angle was found to be -0.15^{o}, which reflects a case where the piston is leaning toward the anti-thrust side of the liner. The thickness and pressure distribution of the piston-skirt oil film are shown in Figs. 4-20 and 4-21. It should be noted that the piston-skirt is considered to be fully flooded with no cavitation. In addition, the nodal pressures on the top and bottom rows of the piston-skirt mesh were set to the combustion chamber and crankcase pressures, respectively (see Fig. 4-21). At the anti-thrust side corresponding to column 18 in the mesh, Fig. 4-20 illustrates thicker oil film at the bottom end than at the top end of the piston. This is consistent with the piston tilting angle at 295^{o} CAD.

The in-plane transverse deformation and the oil film thickness of the first compression ring are shown in Figs. 4-22 and 4-23, respectively. Note that the plot in Figs. 4-22 starts from the ring-gap. In addition, the pressures above and below the first compression ring were defined to be the combustion chamber and the inter-ring clearance gas pressures, respectively. One can easily notice that the oil film thickness profile closely follows that of the in-plane transverse deformation of the ring. Similar patterns have also been observed for the cases of the second compression ring and the oil control ring (see Figs. (4-24) to (4-27). It should be pointed out that the pressures above and below the second

compression ring were specified to be the inter-ring clearance and crankcase gas pressures, respectively. Whereas, the pressures above and below the oil control ring were considered to be equal to the crankcase gas pressure.

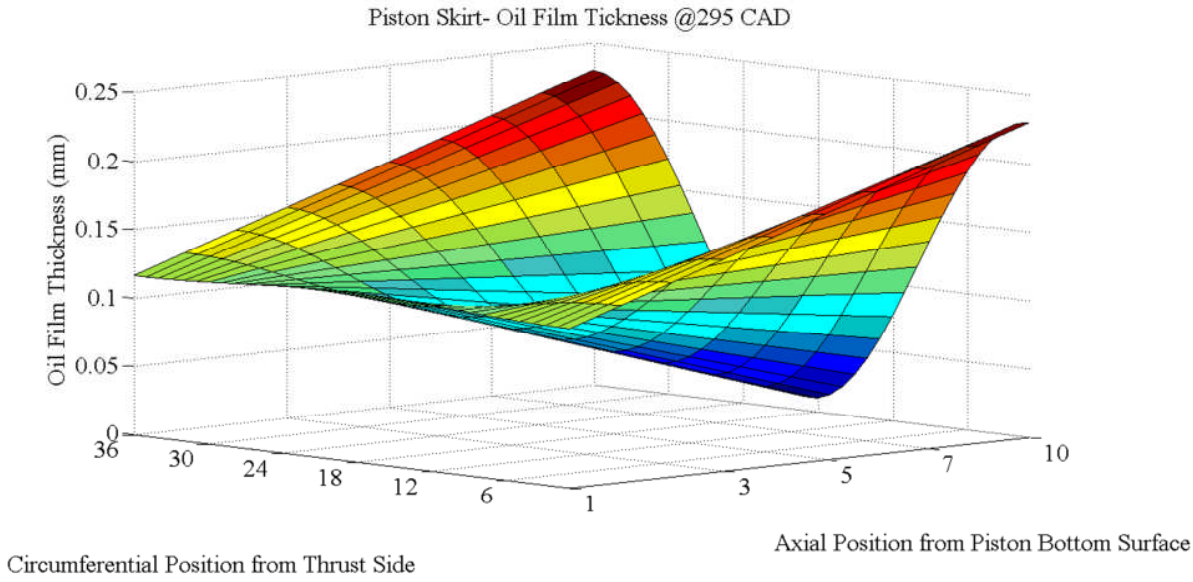

Fig. 4- 20 Piston-skirt oil film thickness at 295^{o} CAD.

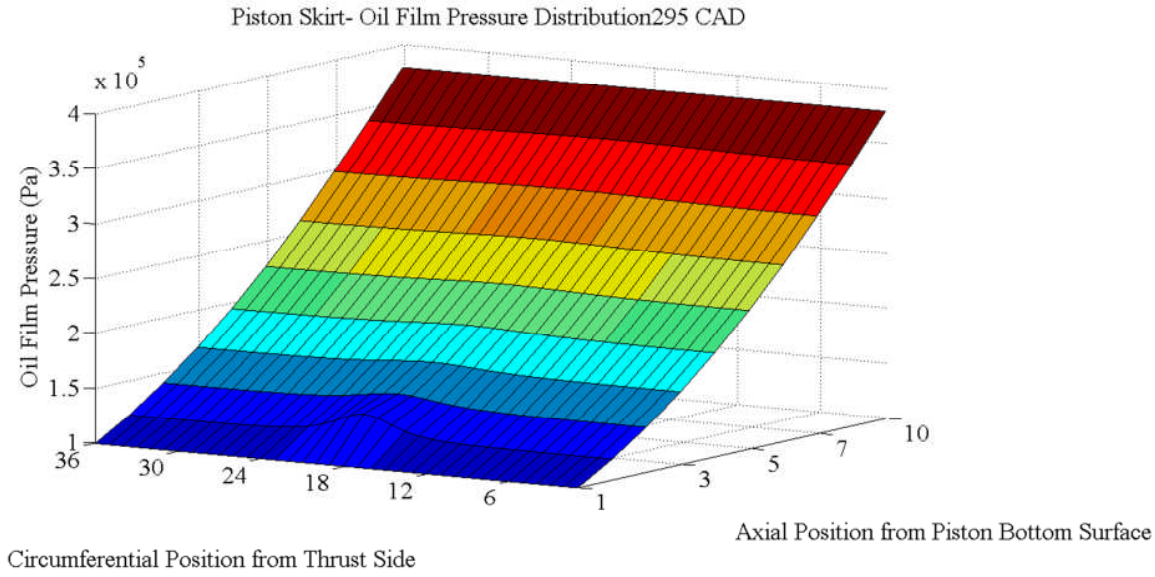

Fig. 4- 21 Piston-skirt oil film pressure distribution at 295^{o} CAD.

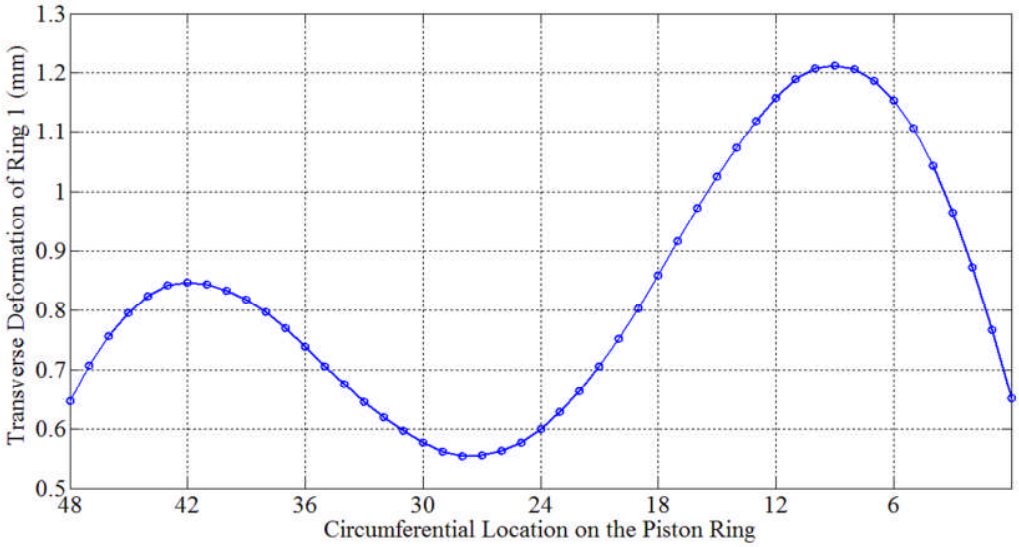

Fig. 4- 22 In-plane transverse deformation of the first compression ring at 295^{o} CAD.

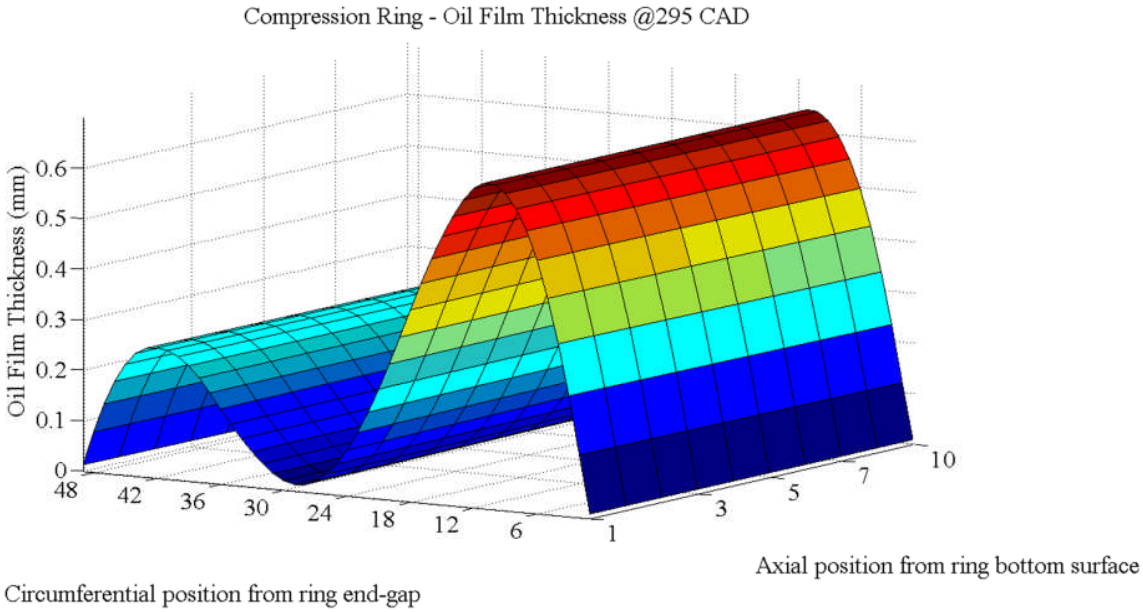

Fig. 4- 23 Oil film thickness of the first compression ring at 295^{o} CAD.

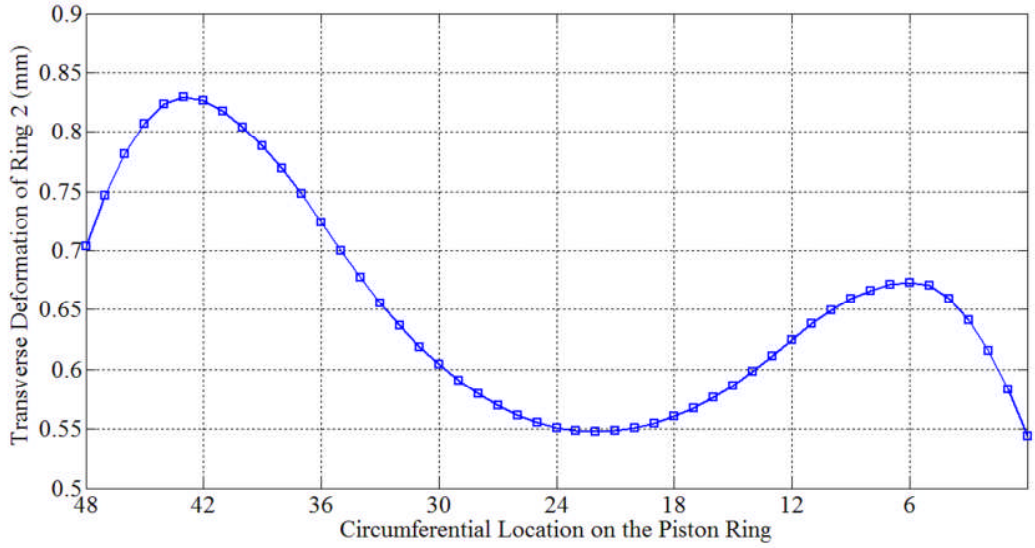

Fig. 4- 24 In-plane transverse deformation of the second compression ring at 295^{o} CAD.

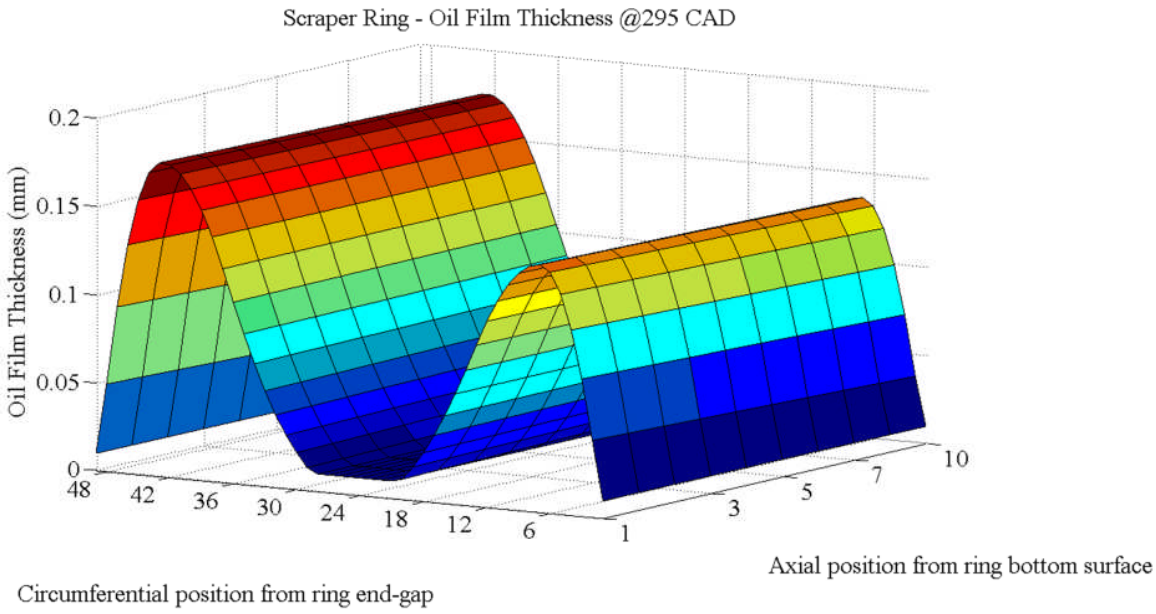

Fig. 4- 25 Oil film thickness of the second compression ring at 295^{o} CAD.

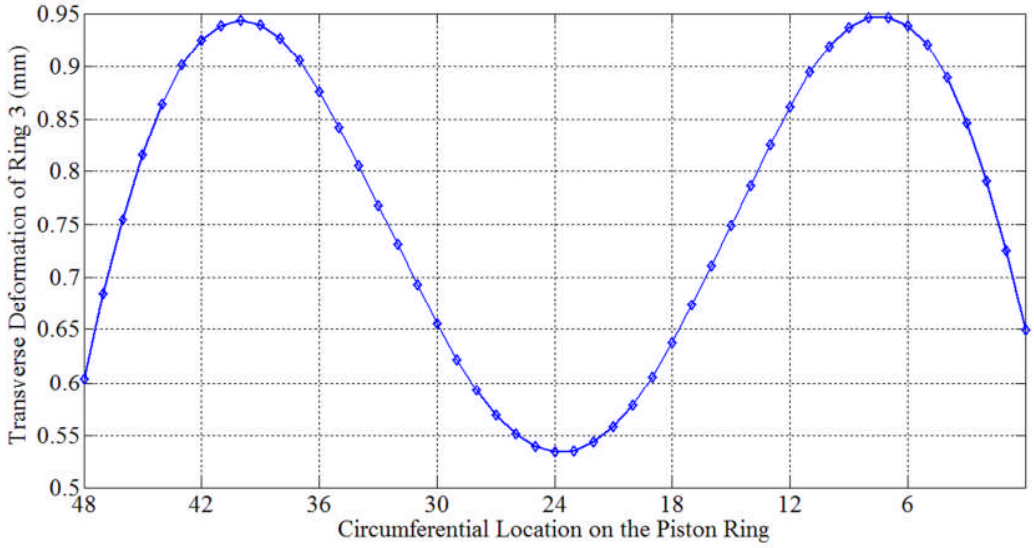

Fig. 4- 26 In-plane transverse deformation of the third compression ring at 295^{o} CAD

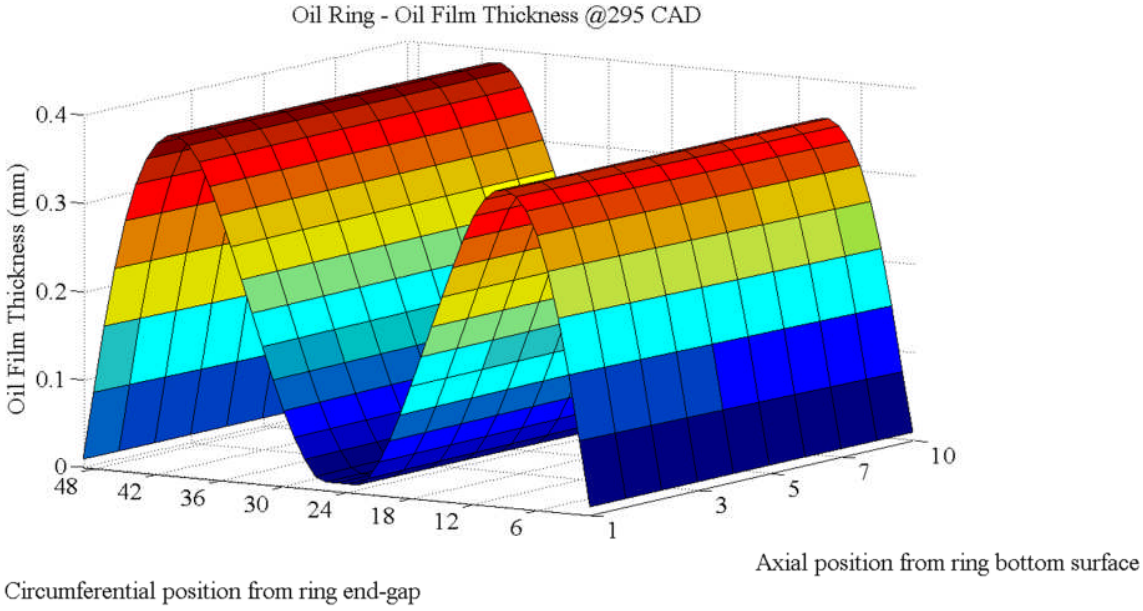

Fig. 4- 27 Oil film thickness of the third compression ring at 295^{o} CAD.

4.3 Special Case

In this case, only the first compression ring is considered [80]. The dynamics of the second compression ring and the oil control ring are ignored. Moreover, the lubricating oil film and the hydrodynamic frictional losses have been neglected in this case. The focus is mainly on examining the piston-liner, ring-grrove, and ring-liner interactions.

The simulation results are generated based on an initial engine speed of 3500 rpm. The cylinder gas pressure under engine firing conditions is shown in Fig. 4-28. In addition, the crankcase pressure is assumed to be atmospheric. Moreover, the material properties and geometric dimensions of the crank-slider mechanism are included in Table 4-7.

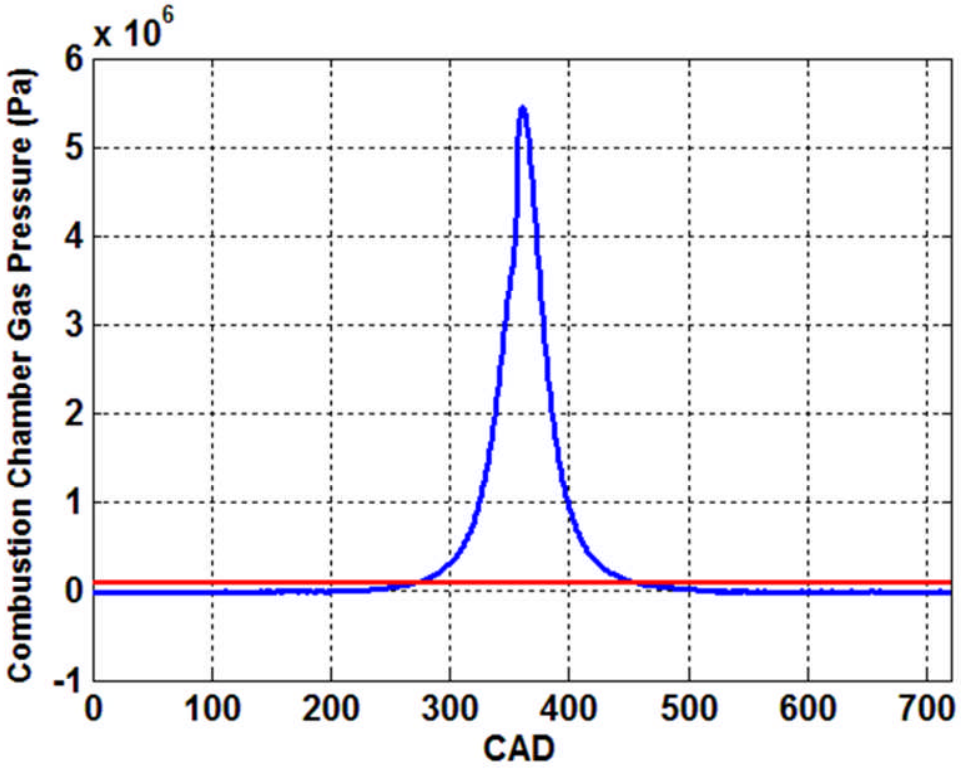

Fig. 4- 28 Pressure traces of the combustion chamber and the crankcase used in the special case.

Crank-Slider Mechanism	
Piston length	*47.8 mm*
Piston diameter	*59.72 mm*
Bore diameter	*59.96 mm*
Piston pin offset	*0.446 mm*
Crank radius	*44 mm*
Connecting rod length	*167.34 mm*
Ring	
Modulus of elasticity	E= 131×10^9 N/m^2
Poisson's ratio	*0.25*
Density	ρ= 7469 Kg/ m^3
Undeformed radius	R= 30.53 *mm*
Cross section (width x height)	*2.49 mm ×2.38 mm*
Gap angle	*16.16°*

Table 4-7 Geometric and material properties of the crank-slider mechanism for the special case.

The simulation results are shown in Figs. 4-29 to 4-33. They reveal the clearance between the deformable configuration of the ring and the liner at a specific crank angle degree. Note that the plot in Fig. 4-29 starts from the ring gap. The tilting angles of the piston and the rings have been generated under two different cylinder gas pressure profiles. The first one corresponds to the engine firing condition while the second one assumes an atmospheric pressure. The latter simulates the case of an engine without the cylinder head. The tilting angles of the piston during the entire engine cycle for both cylinder gas pressure profiles are shown in Fig. 4-30. Both curves are similar except for the later portion of the compression stroke and for most of the power stroke. This is because the high cylinder gas pressure under engine firing condition has forced the piston to maintain a specific tilting angle during this period.

The tilting angles of the ring relative to the piston orientation around the $\underset{\sim}{J}-$ and $\underset{\sim}{K}-$directions are shown in Figs. 4-31 and 4-32, respectively. They demonstrate that the tilting angle of the ring around the $\underset{\sim}{J}$ direction, which is commonly neglected in research studies, to be as significant as the tilting angle of the ring around the $\underset{\sim}{K}$ direction.

Figure 4-33 focuses on the axial motion of the ring within the piston groove. It shows the locations of two points on the top and bottom surfaces of the ring as the piston goes through the entire engine cycle. For both profiles of the cylinder gas pressure, the initial position of the ring is considered to be in the middle of the groove. In the case of an atmospheric cylinder gas pressure, the piston moves downward during the intake stroke causing the ring to collide with the top

surface of the groove. The ring remains in contact with the groove as long as the piston speed keeps on increasing. As the piston reaches its maximum speed at around 76 CAD and starts decelerating, the ring will separate from the groove. Its momentum enables it to reach the lower surface of the groove and stick to it for the remainder of the intake stroke. This configuration is retained during the portion of the compression stroke where the piston speed is increasing. Beyond the point of maximum speed, the piston slows down and the ring separate from the lower surface and moves on to collide and maintain contact with the upper surface of the groove. This trend is repeated again in the power and exhaust strokes.

A significantly different pattern of response was obtained for the ring under engine firing conditions (see Fig. 4-33). As the piston moves downward during the intake stroke, the upper surface of the groove collides with the ring. The latter will then be dragged downward with the piston for the remainder of the intake stroke and for the onset portion of the compression stroke. The reason for the ring to be stuck to the upper surface of the groove during this period of the engine cycle stems from the fact that the cylinder gas pressure is smaller than the atmospheric pressure of the crankcase. However, as the cylinder gas pressure starts to build up during the compression stroke, a point will be reached where the cylinder pressure becomes greater than that of the crankcase and the ring separates from the upper surface and comes in contact with the lower surface of the groove. Due to the large cylinder pressure in the later portion of the compression stroke and for most part of the power stroke, the ring remains in

contact with the lower surface of the grove. This configuration remains till the exhaust valve opens and causes the cylinder gas pressure to drop below that of the crankcase; thus, causing the ring to separate from the lower surface of the groove (see Fig. 4-33).

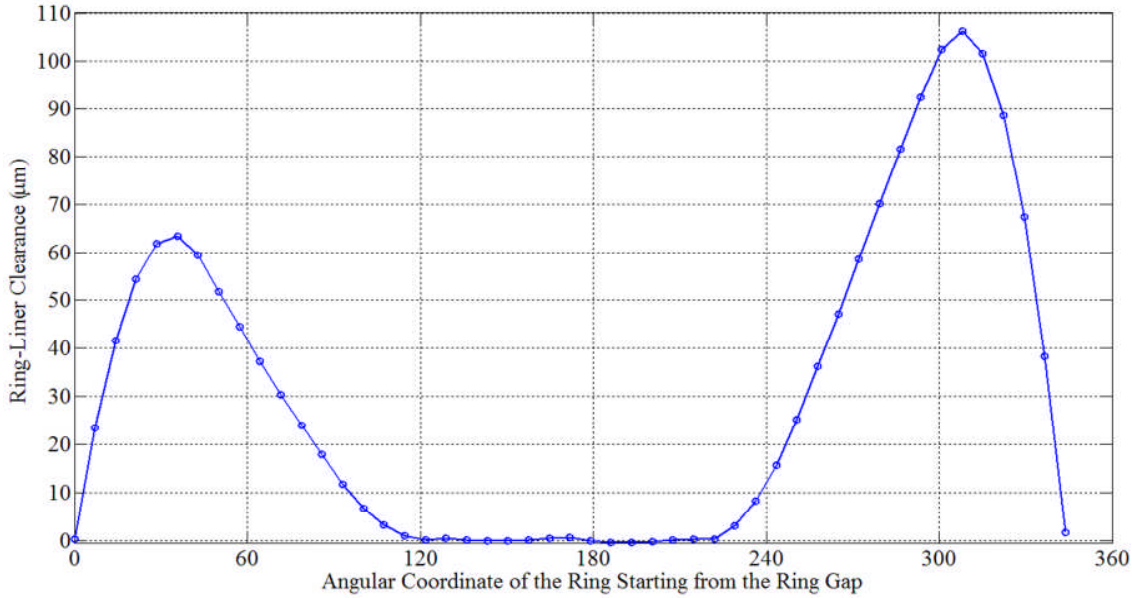

Fig. 4- 29 Clearance between the deformable configuration of the ring and the liner.

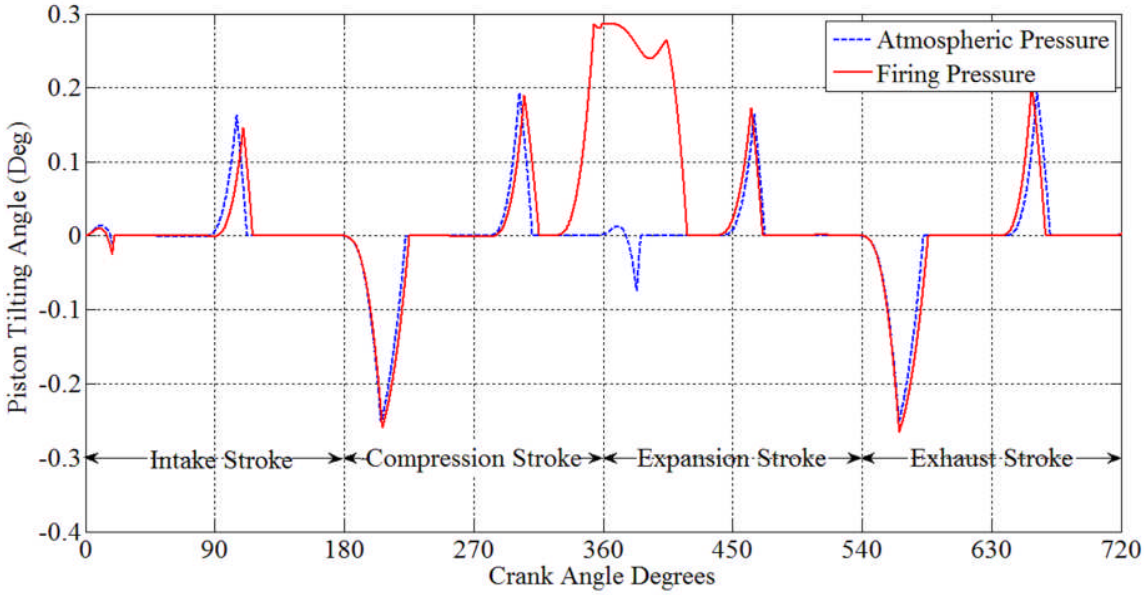

Fig. 4- 30 Tilting angle of the piston.

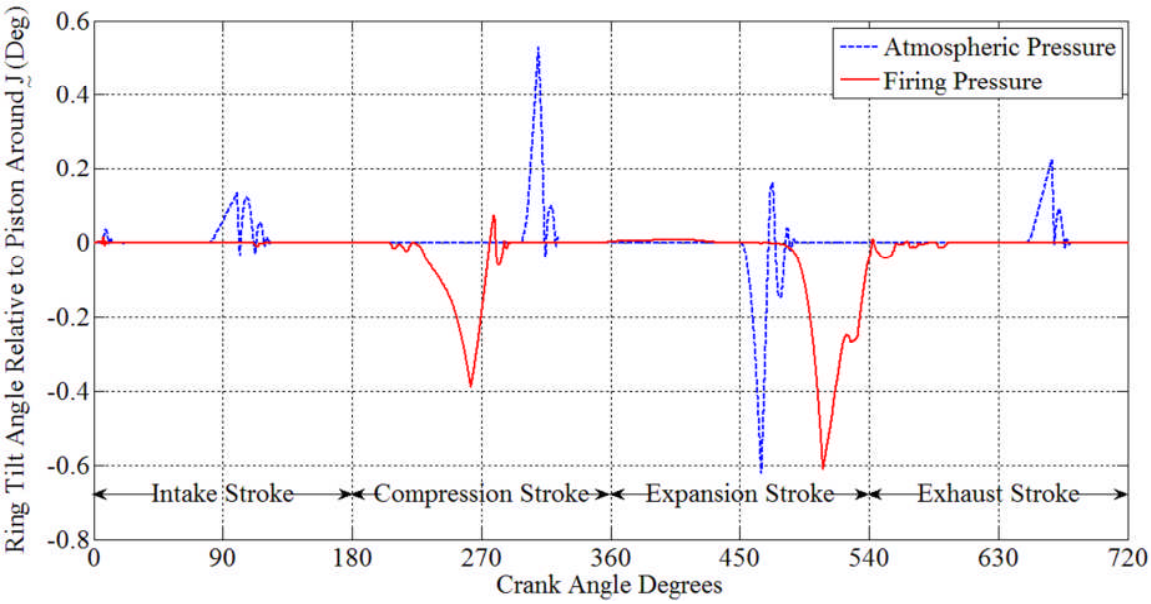

Fig. 4- 31 Tilt angle of the ring with respect to the piston around the $\underset{\sim}{J}$ direction.

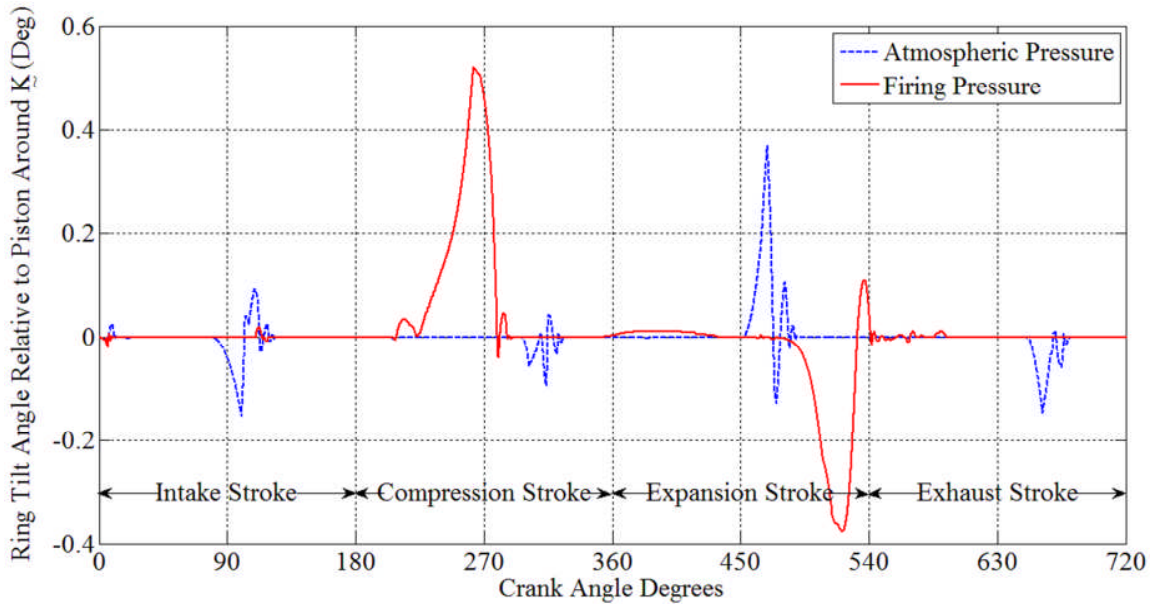

Fig. 4- 32 Tilt angle of the ring with respect to the piston around the $\underset{\sim}{K}$ direction.

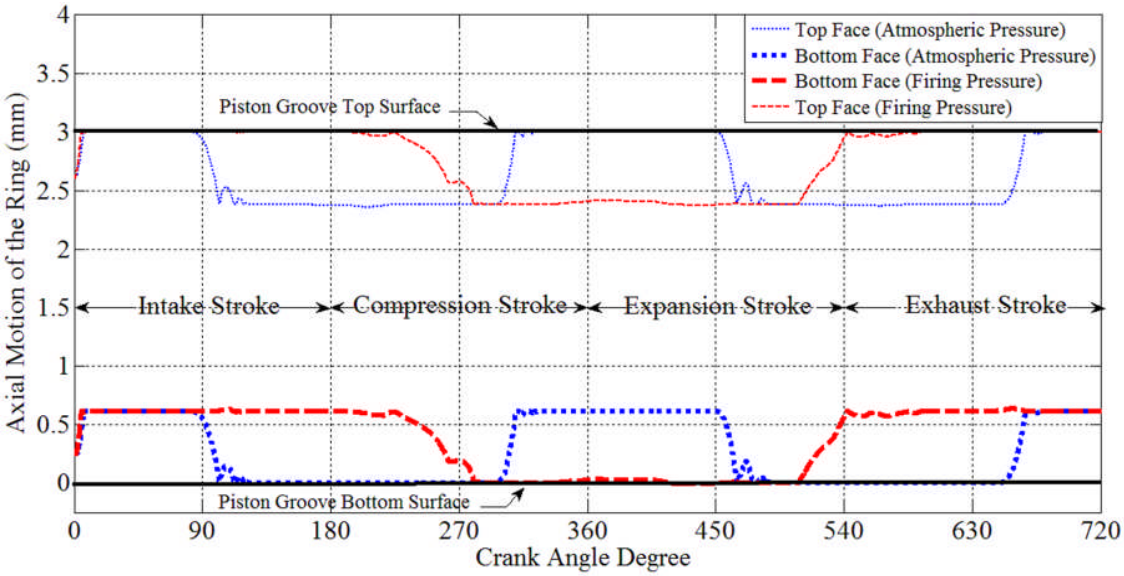

Fig. 4- 33 Ring axial position within the piston groove.

4.4 Summary

The theoretical results demonstrate the unique capabilities of the current tool, in predicting the intricate and coupled dynamics of the crankshaft/connecting-rod/piston mechanism, the ring-pack, and the solid-fluid interactions at the interface between the lubricating oil film and the running surfaces of the piston-skirt and rings, under realistic engine operating conditions. The results revealed the importance of the effect of ring-pack dynamics on the piston secondary motions as well as the important roles of the tilt angles of the rings around the $\underset{\sim}{J}-$direction, which are ignored in previous research studies. They show the hydrodynamic friction force of the piston-skirt, the elasto-hydrodynamic friction forces of the rings, the structural deformations of the rings, the piston secondary motions. These results are generated in a fully integrated system, which is one of the main feature of the current work.

CHAPTER 5
SUMMARY AND CONCLUSIONS

The current work is summarized and the main contributions are listed in this Chapter. Moreover, prospective research topics are suggested.

5.1 Brief Overview of the Current Work

The present study addresses the challenging research issue of predicting the intricate dynamics and instantaneous hydrodynamic frictional losses of the piston-assembly of high power density Diesel engines during the entire engine cycle under various operating conditions. This topic has been considered due to the fact that piston-assembly dynamics have a direct effect on the performance of internal combustion (IC) engines. It is widely recognized that the piston-assembly is a major contributor to frictional losses, which have a significant and adverse effect on the engine fuel economy. Furthermore, during the engine cycle, the piston-assembly may experience boundary, mixed, and hydrodynamic lubrication regimes. The lubrication regimes involving metal-to-metal contact lead to wear, which ultimately affect the engine durability.

Moreover, the ring-pack main function is to serve as a dynamic seal preventing the cylinder gases from leaking into the crankcase and vice versa. This is done in order to improve the engine thermal efficiency by reducing the blow-by gases, which can occur through the ring end gaps, ring-groove dynamic clearance, and ring-bore dynamic conformability. The sealing capability of the rings is dictated by their intricate dynamics and the pressure differentials between the control volumes that are formed by the ring-groove-liner clearances.

Furthermore, the elasticity of the rings strongly influences the ring-liner conformability, which can worsen the blowby problem. Moreover, the interaction between the rings and the gas flows can cause the rings to flutter in the axial direction and/or collapse in the radial direction, which can create more opening through which gases can leak into the crankcase.

Furthermore, the ring-pack serves to control the oil film along the cylinder liner. Forty to eighty percent of the engine oil consumption has been attributed to ring-pack dynamics. It should be noted that any reduction in the oil consumption will ultimately result in lowering the tail-pipe emissions.

In addition, a reasonable prediction of the piston secondary motions can provide important design insights into the reduction of piston-slap, and ultimately, engine noise [9, 10].

The objective of the current work is to develop a reliable tool that can predict, with a reasonable accuracy, the intricate dynamics and hydrodynamic frictional losses of the piston-assembly for a single cylinder four strokes, internal combustion engine. Such a tool will provide engine designers and manufacturers with valuable insights into the dynamic behavior of the piston-assembly, which can be instrumental for optimizing the design of the piston-assembly and assessing the impact of their design refinement on the overall engine performance.

In the current work, the proposed tool has been developed in modular form with three main modules. The first one provides the rigid body motion of the crankshaft/connecting-rod/piston mechanism excluding the ring-pack. It treats

the crank-slider mechanism as an open-kinematic chain consisting of multi-rigid bodies connected in series with the piston whose motion is confined to the bounding wall of the cylinder. This module accounts for all the coupling terms between the crankshaft, connecting-rod, and the piston. In addition, it captures the piston secondary motions, namely, piston-slap and piston-tilting.

The open-kinematic chain modeling approach for the crank-slider mechanism enables the piston to undergo free or constrained motions whereby the piston may have a single-point, double-point, or surface contact with the liner. The various piston configurations during an engine cycle cause the number of constraint equations to vary with the instantaneous position and orientation of the piston within the cylinder. Thus, the present model will have a variable structure in order to handle the piston-liner interaction.

The second module focuses on the intricate dynamics of the ring-pack, which is considered herein to be made up of two compression rings and one oil control ring. Each ring has been modeled as a shear deformable structure undergoing two angular and one translational (axial) rigid body degrees of freedom within its respective piston groove. The longitudinal and in-plane transverse deformations of the ring are handled by employing two-node shear deformable curved beam elements, which are derived based on the Timoshenko beam theory and account for the inherent coupling between the longitudinal and transverse deformations of curved structures [55, 57]. Eight curved beam elements were employed to approximate the structural deformations of the ring. Both ring-liner and ring-groove interactions are considered in this work.

Depending on its location and orientation within the piston groove, the ring may have single-point, two-point, or surface contact with the top and/or bottom surfaces of the piston groove. In the event of no contact between the ring and the groove, the ring motion is considered to be free.

The ring-liner interaction has been handled by concentrated constraint forces applied at seven equally spaced points along the curved beam element. They assume non-zero values whenever the radial distance between the point of application of the constraint force on the ring and the liner becomes smaller than a certain threshold. The constraint force is considered to increase linearly with the reduction of the radial distance between the ring and the liner.

The ring-groove interaction is first handled by impulsive forces induced by the collision between the ring and its respective groove surfaces. The impact problem was formulated based on the collision between two rigid bodies, which involved the implementation of both linear and angular impulse and momentum equations. Moreover, the surfaces of the colliding rigid bodies are assumed to be smooth. Once the collision phase is over, the ring-groove interaction will be handled by constraint forces based on the nature of contact between the ring and its respective groove.

The third module aims at predicting the normal and friction forces exerted on the piston-assembly by the lubricating oil film. It accounts for the hydrodynamic lubrication regime of the piston-skirt and the elasto-hydrodynamic lubrication regime of the ring-pack. Boundary and mixed lubrication regimes have not been accounted for in this work. However, normal forces induced by

metal-to-metal contact between the running surfaces of the rings and the liner, the rings and their respective piston grooves, the piston-skirt and the liner, have been accounted for through constraint forces that are responsible for keeping the piston inside the cylinder and confining the rings to their respective piston grooves.

The third module captures the solid-fluid interaction between the piston-assembly and the oil film. This is done by having the piston secondary motions dictate the instantaneous oil film thickness along the piston-skirt and the ring-pack running surfaces. While the effects of the lubricating oil film on the dynamics of the piston-assembly are accounted for through the instantaneous normal and tangential friction forces exerted on the running surfaces of the piston-assembly. A 3-D and 1-D Reynolds' equations have been implemented to determine the oil film pressure distributions along the running surfaces of the piston-skirt and the ring-pack, respectively. The shear stresses, used in the computation of the friction forces, were calculated based on the Newton's law of viscous flow.

The three modules are then fully integrated to perform the digital simulations. The results predict the intricate dynamics and the hydrodynamic frictional losses of the piston-assembly under different operating conditions. The advantage of this tool stems from its ability to provide detailed information regarding the piston tilting angle, the relative tilting angles between the rings and the piston, the oil film pressure distributions on the running surfaces of the piston-assembly and many other details.

5.2 Main Contributions

The main contributions of the current work are:

- Development of a detailed dynamic model capable of predicting the rigid and flexible motions of the rings within their respective piston grooves.
- Implementation of two-node shear deformable curved beam elements, based on the Timoshenko beam theory, to model the inherently coupled longitudinal and in-plane transverse deformations of the ring.
- Formulation of a detailed impact problem between two rigid bodies in order to determine the impulsive forces associated with the collision between the ring and its respective groove.
- Formulation of the elasto-hydrodynamic lubrication regime that accounts for the longitudinal and in-plane transverse deformations of the ring-pack.
- Development of a fully-integrated dynamic model that is capable of predicting the rigid body motion of the crankshaft/connecting-rod/piston mechanism, the secondary motions of the piston, the intricate motions of the rings within their respective grooves, the hydrodynamic frictional loss of the piston-skirt, the elasto-hydrodynamic frictional losses of the rings, the thickness of the oil films between the piston-skirt and the liner as well as between the rings and the liner.
- Demonstration of the significant effect of the ring-pack dynamics on the piston secondary motions as well as the important roles of the tilting angles of the rings around the $\underset{\sim}{J}-$ direction. These effects are ignored in previous research studies.

- Only qualitative validation on the frictional losses has been made in this study.

5.3 Limitations

The proposed model predicts the hydrodynamic lubrication regime of the piston skirt and the elasto-hydrodynamic lubrication regime of the ring-pack. However, both boundary and mixed lubrication regimes have been ignored in this work. Only fully-flooded inlet oil film condition was considered. This assumption has to be relaxed in future studies in order to account for both oil transport and oil starvation phenomena; thus, allowing the code to be more representative of real engine conditions, particularly, near TDC in the compression and power strokes. Moreover, the effect the effect of thermal distortion on the ring, liner, and piston was neglected. The thermal effect on the oil film can be currently considered by changing the numerical value of the viscosity according to different temperature conditions.

5.4 Future Work

Prospective research work may include the following research issues:

- Inclusion of the torsional (twist) and out-of-plane transverse deformations in the dynamic model of the ring.
- Expand the capability of the model to consider the interaction between the dynamic behavior of the piston-assembly and gas flows induced by blowby.
- Perform experimental validation of the proposed tool.

REFERENCES

1. 2004 Federal Mogul Piston Ring Handbook. 2004; Available [online] from: http://www.federalmogul.com/korihandbook/en/index.htm.
2. Tian, T.,2002. "Dynamic behaviours of piston rings and their practical impact. Part 1: ring flutter and ring collapse and their effects on gas flow and oil transport", *Proceedings of the Institution of Mechanical Engineers Part J-Journal of Engineering Tribology*, **216**, 209-227.
3. Tian, T., 2002. "Dynamic behaviours of piston rings and their practical impact. Part 2: oil transport, friction and wear of ring/liner interface and the effects of piston and ring dynamics", *Proceedings of the Institution of Mechanical Engineers Part J-Journal of Engineering Tribology*, **216**, 229-247.
4. Hronza, J. and Bell, D., 2007, "A Lubrication and Oil Transport Model for Piston Rings Using a Navier-Stokes Equation with Surface Tension", SAE Paper No. 2007-01-1053.
5. Ariga, S., 1996, "Observation of transient oil consumption with in-cylinder variables", SAE Paper No. 961910.
6. Kobayashi H., S.A., Yoshida H., Tani M.,1998. "Effect of negative twist second ring on oil consumption for light duty diesel engines". JSAE Paper No. 9839083.
7. Jackson, M.A., 1996. "Assessment of a sulfur dioxide based diagnostic system in characterizing real time oil consumption in a diesel engine". *MS Thesis, MIT*, 1996.

8. Harigaya, Y., Suzuki, M., Toda, F. and Takiguchi, M., 2006. "Analysis of oil film thickness and heat transfer on a piston ring of a diesel engine: Effect of lubricant viscosity", *Journal of engineering for gas turbines and power*, **128**, 685.

9. Ungar, E. and Ross, D., 1965. "Vibrations and noise due to piston-slap in reciprocating machinery". *Journal of Sound and Vibration*, **2**(2),132-146.

10. Fielding, B. and Skorecki, J., 1969. "Identification of mechanical sources of noise in a diesel engine: sound originating from piston slap", *Proceedings of the Institution of Mechanical Engineers, Part 1 ,* **184**(46), 859-874.

11. Andersson, P., Tamminen, J. and Sandström, C.E., 2002, "Piston ring tribology: A literature survey". *VTT Research Notes*, **2178**, 1-105.

12. Ruddy, B., Dowson, D. and Economou, P.,1982, "A review of studies of piston ring lubrication", *Proceedings of the 9th Leeds-Lyon Symposium on Tribology: Tribology of Reciprocating Engines*, paper V(i), 109-121.

13. Ting, L., 1985, "A review of present information on piston ring tribology". SAE Paper No. 852355.

14. Jeng, Y.R., 1992, "Friction and Lubrication Analysis of a Piston-Ring Pack". SAE Paper No. 920492.

15. Jeng, Y., 1992, "Theoretical Analysis of Piston Ring Lubrication Part I-Fully Flooded Lubrication", *Tribology transactions*, **35**, 696-706.

16. Jeng, Y., 1992, "Theoretical Analysis of Piston Ring Lubrication Part II- Starved Lubrication and Its Application to a Complete Ring Pack". *Tribology transactions*, **35**, 707-714.

17. Herbst, H.M. and Priebsch, H.H., 1999, "Simulation of Effects of piston ring parameters on Ring Movement, Friction, Blowby, and LOC"; Available [online]: https://online.tugraz.at/tug_online/voe_main2.getVollText?pDocumentNr=42425&pCurrPk=23354.

18. Herbst, H.M. and Priebsch, H.H., 2000, "Simulation of piston ring dynamics and their effect on oil consumption", SAE Paper No. 2000-01-0919.

19. Hu, Y., Cheng, H.S., Arai, T., Kobayashi, Y. and Aoyama, S., 1994, "Numerical simulation of piston ring in mixed lubrication—a nonaxisymmetrical analysis", *Journal of tribology*, 1994, **116**, 470-478.

20. Priest, M., Dowson, D. and Taylor, C., 2000, "Theoretical modelling of cavitation in piston ring lubrication", *Proceedings of the Institution of Mechanical Engineers, Part C: Journal of Mechanical Engineering Science*, **214** (3), 435-447.

21. Greenwood, J. and Tripp, J., 1970. "The contact of two nominally flat rough surfaces". *Proceedings of the Institution of Mechanical Engineers,* **185,** 625-634.

22. Rohde, S.M., 1980, "A mixed friction model for dynamically loaded contacts with application to piston ring lubrication", Winter Annual Meeting of ASME Chicago, IL.

23. Ruddy, B., Dowson, D. and Economou, P., 1981. "A theoretical analysis of the twin land type of oil control piston ring". *Journal of Mechanical Engineering Science* ,**23**(2), 51-62.

24. Patir, N. and Cheng, H.,1978, " An average flow model for determining effects of three-dimensional roughness on partial hydrodynamic lubrication"*, ASME Journal of Lubrication Technology*, **100**, 12-17.

25. Keribar, R., Dursunkaya, Z. and Flemming, M.F., 1991, " An integrated model of ring pack performance"*. Journal of engineering for gas turbines and power*, **113**, 382-389.

26. Tian, T., Wong, V.W. and Heywood, J.B., 1996, "A piston ring-pack film thickness and friction model for multigrade oils and rough surfaces", SAE Paper No. 962032.

27. Tian, T., Noordzij, L.B., Wong, V.W. and Heywood, J.B., 1998, " Modeling piston-ring dynamics, blowby, and ring-twist effects". *Journal of Engineering for Gas Turbines and Power-Transactions of the Asme*, 1998. **120**(4), 843-854.

28. Iijima, N., Miyamoto, T., Takiguchi, M., Kai, R. and Sato, M. 2002, "An experimental study on phenomena of piston ring collapse", SAE Paper No. 2002-01-0483.

29. Ejakov, M.A., Schock, H.J. and Brombolich, L.J. 1998, "Modeling of ring twist for an IC engine", SAE Paper No. 982693.

30. Rabute, R. and Tian, T., 2001, "Challenges involved in piston top ring designs for modern SI engines". *Journal of Engineering for Gas Turbines and Power-Transactions of the ASME*, 2001. **123**(2), 448-459.

31. Furuhama, S., Hiruma, M., and Tsuzita, M., 1979, "Piston ring motion and its influence on engine tribology", SAE Paper No. 790860.

32. Dowson, D., Economou, P., Ruddy, B., Strachan, P. and Baker, A.,1979, "Piston ring lubrication. Part II: theoretical analysis of a single ring and a complete ring pack". *Energy conservation through fluid film lubrication technology*, 23-52.

33. Ruddy, B., Dowson, D., Economou, P. and Baker, A., 1979, "Piston ring lubrication–Part III: the influence of ring dynamics and ring twist". *Energy conservation through fluid film lubrication technology,* ASME Winter Annual Meeting, 191-215.

34. Liu, L., Tian, T. and Rabuté, R., 2003, "Development and applications of an analytical tool for piston ring design", SAE Paper No. 2003-01-3112.

35. Liu, L. and Tian, T.,2004, "A Three-Dimensional Model for Piston Ring-Pack Dynamics and Blow-By Gas Flow", *ASME Internal Combustion Engine Division Fall Technical Conference (ICEF2004),* Oct 24–27, 2004 , Long Beach, California, USA

36. Liu, L. and Tian, T., 2005, "Modelling Piston Ring-Pack Lubrication With Consideration of Ring Structural Response", SAE Paper No. 2005-01-1641.

37. Timoshenko, S. and Lessels, J.M., 1925, *Applied Elasticity*,Westinghouse Press, Pittsburgh, PA.

38. Feodosyev, V.I., 1977. *Selected Problems and Questions in Strength of Materials*, 1977: Mir Publishers.

39. Dunaevsky, V.V. and Alexandrov, S., 2002, "Development of conformability model of piston rings with consideration of their three-dimensional torsional distortions and Fourier series representation of cylinder bore geometry", SAE Paper No. 2002-01-3131.

40. Dunaevsky, V., Alexandrov, S. and Barlat, F., 2001, "The effect of contact pressure on piston ring twist", SAE Paper No. 2001-01-2720.

41. Dunaevsky, V.V., Alexandrov, S. and Barlat, F., 2000, "Analysis of three-dimensional distortions of the piston rings with arbitrary cross-section", SAE Paper No. 2000-01-3453.

42. Sun, D., 1991, "A thermal elastica theory of piston-ring and cylinder-bore contact", *Journal of Applied Mechanics*, 1991, **58**(1), 141-153.

43. Mittler, R., Mierbach, A. and Richardson, D., 2009, "Understanding the fundamentals of piston ring axial motion and twist and the effects on blow-by", *Proceedings of the ASME Internal Combustion Engine Division 2009 Spring Technical Conference*, May 3-6 2009, Milwaukee, Wisconsin, USA.

44. Dursunkaya, Z. and Keribar, R., 1992, "Simulation of Secondary Dynamics Of Articulated and Conventional Piston Assemblies", SAE Paper No. 920484.

45. Dursunkaya, Z., Keribar, R. and Ganapathy, V., 1994, "A model of piston secondary motion and elastohydrodynamic skirt lubrication", *Journal of tribology*, **116**, 777-785.

46. Duyar, M., Bell, D. and Perchanok, M. 2005, "A Comprehensive Piston Skirt Lubrication Model Using a Mass Conserving Ehl Algorithm", SAE Paper No. 2005-01-1640.

47. Duyar, M. 2007," Mass Conserving Elastohydrodynamic Piston Lubrication Model With Incorporated Crown Lands", *ASME Internal Combustion Engine Division Fall Technical Conference, ICEF2007, Oct 14-17, 2007, Charleston, South Carolina,USA.*

48. Elrod, H.,1981, "A cavitation algorithm", *ASME Journal of Lubrication Technology,* **103**(3), 350–354.

49. Perchanok, M., 2000, "Modeling of piston-cylinder lubrication with a flexible skirt and cylinder wall". SAE Paper No. 2000-01-2804.

50. Stanley, R., Taraza, D., Henein, N. and Bryzik, W., 1999, "A simplified friction model of the piston ring assembly", SAE Paper No. 1999-01-0974.

51. Ting, L. and Mayer J., 1974, "Piston Ring Lubrication and Cylinder Bore Wear Analysis: Part 1- Theory", *Journal of Lubrication Technology ,* **96**(3), 305-314.

52. Ting, L. and Mayer, J., 1974, "Piston Ring Lubrication and Cylinder Bore Wear Analyses: Part 2-Theory Verification". *Journal of Lubrication Technology,* **96**(2), 258-266.

53. Furuhama, S. and Tada, T.,1961. "On the Flow of Gas Through the Piston-Rings: 1st Report, The Discharge Coefficient and Temperature of Leakage Gas", *Bulletin of JSME*, **4**(16), 684-690.

54. Furuhama, S. and Tada, T.,1961, "On the flow of gas through the piston-rings: 2nd Report, The character of gas leakage", *Bulletin of JSME*, **4**(16), 691-698.

55. Friedman, Z. and Kosmatka, J.,1998, "An accurate two node finite element for shear deformable curved beams", *International journal for numerical methods in engineering*, **41**(3), 473-498.

56. Friedman, Z. and Kosmatka, J, 1993, " An improved two-node Timoshenko beam finite element", *Computers & structures*, **47**(3), 473-481.

57. Yang, F., Sedaghati, R. and Esmailzadeh, E., 2008, "Free in-plane vibration of general curved beams using finite element method", *Journal of Sound and Vibration*, **318** (4-5), 850-867.

58. Chalhoub, N.G. and Edelby, W., 2008, "Piston Secondary Motions and Hydrodynamic Lubrication Regime in a Single Cylinder Internal Combustion Engine", *Proceedings of DSCC2008, 2008 ASME Dynamic Systems and Control Conference,* Ann Arbor, Michigan, USA.

59. Nehme, H., Chalhoub, N. and Henein, N.,1998, "Development of a dynamic model for predicting the rigid and flexible motions of the crank slider mechanism", *Journal of engineering for gas turbines and power*, **120**, 678.

60. Baraff, D.1994, "Fast contact force computation for nonpenetrating rigid bodies", *SIGGRAPH '94 Proceedings of the 21st annual conference on Computer graphics and interactive techniques,* July 24-29,1994, Orlando, Florida, USA.

61. Brach, R.M., 1991, *Mechanical impact dynamics: rigid body collisions*, New York: John Wiley and sons. Chap. 5.

62. Glocker, C. and Pfeiffer, F., 1992, "Dynamical systems with unilateral contacts"*, Nonlinear Dynamics*, **3**(4), 245-259.

63. Glocker, C. and Pfeiffer, F., 1995, "Multiple impacts with friction in rigid multibody systems"*, Nonlinear Dynamics*, **7**(4), 471-497.

64. Chalhoub, N. and Chen, L., 1998, "A structural flexibility transformation matrix for modelling open-kinematic chains with revolute and prismatic joints", *Journal of Sound and Vibration*, **218**(1), 45-63.

65. Gear, C.W., 1971, *Numerical initial value problems in ordinary differential equations*, Prentice Hall, Englewood Cliffs, NJ, USA.

66. Furuhama, S., Sasaki, S., 1983, "New device for the measurement of piston frictional forces in small engines". SAE Paper No. 831284.

67. Furuhama, S., Takiguchi, M., 1979, "Measurement of piston frictional force in actual operating diesel engine". SAE Paper No. 790855.

68. Takiguchi, M., Machida, K. and Furuhama, S.,1988, "Piston friction force of a small high speed gasoline engine", *Journal of tribology*, **110**(1), 112-118.

69. Rosenberg, R.C., 1982, "General friction considerations for engine design", SAE Paper No. 821576.

70. McGeehan, J.A., 1978, "A literature review of the effects of piston and ring friction and lubricating oil viscosity on fuel economy", SAE Paper No. 780673.

71. Fadel, C., Chalhoub, N., Kfoury, G. and Henein, N., 2008, "Direct Measurement of the Piston-Assembly Friction Force in a Single Cylinder Engine Under Motoring Conditions". *ASME 2008 Dynamic Systems and Control Conference (DSCC2008)*, October 20–22, 2008 , Ann Arbor, Michigan, USA.

72. Rogowski, A., 1961, " Method of Measuring the Instantaneous Friction of Piston Rings in a Firing Engine", SAE Paper No. 610263.

73. Ha, K., Kim, J., Cho, M. and Oh, D., 2002. "Development of Piston Friction Force Measurement System". SAE Paper No. 2002-01-2902.

74. Cho, S.W., Choi, S.M. and Bae, C.S., 2000, "Frictional modes of barrel shaped piston rings under flooded lubrication". *Tribology International*, **33**(8), 545-551.

75. Cameron, A., 1966, *The Principles of Lubrication*, Wiley, New York.

76. Dowson, D., Higginson, G.R., Archard, J.F., Crook, A.W., 1977. *Elasto-Hydrodynamic Lubrication*, Pergamon Press, New York.

77. Edelby, W., 2008, "Piston secondary motions and hydrodynamic lubrication regime in a single cylinder internal combustion engine". MS thesis, Wayne State University.

78. Rezeka, S.F. and Henein, N.A., 1984, "A new approach to evaluate instantaneous friction and its components in internal combustion engines", SAE Paper No. 840179.

79. Fadel, C., 2007, "An experimental Study for a Direct Measurement of the Piston-Assembly Frictional Losses in a Single Cylinder Test Rig". MS thesis, Wayne State University.

80. Hakeem, M., Chalhoub, N., and Schihl, P., 2011, “Dynamic Model of the Piston-Ring Assembly Using Curved Beam Finite Elements”. *ASME 2011 Dynamic Systems and Control Conference (DSCC2011)*, Oct 31st –Nov. 2nd, 2011 , Arlington, Virginia, USA.

ABSTRACT

INTRICATE DYNAMICS AND HYDRODYNAMIC FRICTIONAL LOSSES OF THE PISTON-RING ASSEMBLY IN INTERNAL COMBUSTION ENGINES

by

MOHANNAD ABDULLAH HAKEEM

DECEMBER 2011

Advisor: Dr. Nabil Chalhoub

Major: Mechanical Engineering

Degree: Doctor of Philosophy

Frictional losses in internal combustion engines approximately account for 10% of the expended fuel energy. Moreover, forty percent of these losses are attributed to the reciprocating motion of the piston-assembly. Besides the adverse effect of friction on fuel economy, the intricate dynamics of the piston-assembly tend to significantly influence the thermal efficiency through blow-by, the engine durability through wear, and the engine noise through piston-slap. Moreover, 40 to 80% of the lubricant oil consumption has been attributed to the ring-pack dynamics.

In this dissertation, a reliable tool has been developed using MATLAB/SIMULINK and embedded C-S Functions that predicts the intricate dynamics and lubrication regimes of the piston-assembly under various engine operating conditions. The current formulation considers the interconnected motions of the crankshaft, the connecting-rod, the piston (both primary and secondary

motions), and the ring-pack using a multi-body dynamic approach. Curved beam Finite Element method for Timoshenko beams was used to account for the longitudinal and in-plane transverse deformations of the rings. Furthermore, the interaction between piston skirt, ring running surface, and the lubricating oil film was included in order to predict hydrodynamic and elasto-hydrodynamic lubrication regimes.

AUTOBIOGRAPHICAL STATEMENT

Mohannad Hakeem graduated from the American University of Beirut in Beirut, Lebanon, with a Bachelor of Mechanical Engineering in 2002. He started working as a part-time HVAC and pump-station design engineer while pursuing his Master's degree in Mechanical Engineering at the American University of Beirut. He obtained his MS in 2005, and the subject of his Master's thesis was the development of a demand-driven controller for a variable speed chilled water pump.

In 2005, he moved to Detroit, MI to pursue a Ph.D. degree in Mechanical Engineering at Wayne State University. He worked as a graduate research and teaching assistant at the Center of Automotive Research at WSU. His coursework focused on linear and nonlinear control theory, in addition to fundamental understanding of diesel engine performance and emissions mechanisms. His research work included thermodynamic modeling of diesel engine in-cylinder processes, common rail injection modeling, diesel droplet evaporation modeling, and friction estimation in engines. He is married to Ghina Ghazzawi Hakeem and has two kids: Salah-Eddine and Maryam Hakeem.